EXCITATION WAVE DYNAMICS AND THEIR INTERACTION WITH EXTERNAL FIELDS
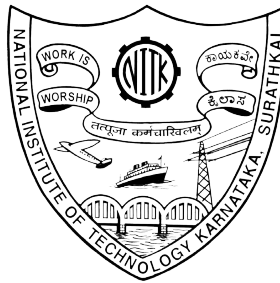
Thesis

submitted in partial fulfillment of the requirements for the degree of

DOCTOR OF PHILOSOPHY

by

SHREYAS

DEPARTMENT OF PHYSICS

NATIONAL INSTITUTE OF TECHNOLOGY KARNATAKA (NITK),

SURATHKAL, MANGALORE - 575 025

October 22, 2021

DECLARATION

By the Ph.D Research Scholar

I hereby *declare* that the Research Thesis entitled **"Excitation Wave Dynamics And Their Interaction With External Fields"**, which is being submitted to the ***National Institute of Technology Karnataka, Surathkal*** in partial fulfillment of the requirements for the award of the Degree of ***Doctor of Philosophy*** in ***Physics*** is a *bonafide report of the research work carried out by me*. The material contained in this thesis has not been submitted to any University or Institution for the award of any degree.

Shreyas
Register No.: 155105 PH15F04
Department of Physics
National Institute of Technology Karnataka
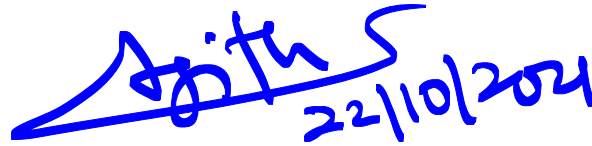Surathkal.

Place: NITK - Surathkal

Date: October 22, 2021

CERTIFICATE

This is to *certify* that the Research Thesis entitled **"Excitation Wave Dynamics And Their Interaction With External Fields"**, submitted by **Shreyas** (Register Number: 155105 PH15F04) as the record of the research work carried out by him, is *accepted* as the *Research Thesis submission* in partial fulfillment of the requirements for the award of degree of ***Doctor of Philosophy***.

Dr. T K Shajahan
Research Guide
Assistant Professor
Department of Physics
NITK Surathkal - 575025

Chairman - DRPC
(Signature with Date and Seal)

Statement of Contribution

1. This thesis is written based on the following published articles.

   - **Shreyas Punacha**, Sebastian Berg, Anupama Sebastian, Valentin I Krinski, Stefan Luther and T. K. Shajahan (2019). " Spiral wave unpinning facilitated by wave emitting sites in cardiac monolayers". *Proceedings of Royal Society A, 475 (2230): 20190420, 2019.*
   DOI:10.1098/rspa.2019.0420.

   - **Shreyas Punacha**, Naveena Kumara A and T. K. Shajahan (2020). " A theory of unpinning of spiral waves using circularly polarized electric fields in mathematical models of excitable media." *Physical Review E, 102(3), 032411. 2020.*
   DOI:10.1103/PhysRevE.102.032411.

   - **Shreyas Punacha**, M. Abhishek and T. K. Shajahan. (2019). " Unpinning spiral wave anchored to two obstacle". *Indian Academy of Sciences Conference Series, 2, 2019.*
   DOI:10.29195/iascs.02.01.0001.

2. All the experimental details included in this thesis are performed by Dr. T. K. Shajahan and Dr. Sebastian Berg in Max Planck Institute for Dynamics and Self-Organization, Göttingen, Germany. It is included in the thesis for the reason of continuity only.

3. The publications that are not included in the thesis are listed at the end of the thesis under the section titled publications.

Dedication

To my family, who encouraged me to go ahead with this adventure.

ACKNOWLEDGEMENT

Shreyas

ABSTRACT

Rotating spiral waves of excitation are common in many physical, chemical and biological systems. In physiological systems like the heart, such waves anchor to unexcitable tissue (an obstacle), become stable pinned waves and cause life-threatening cardiac arrhythmias. The traditional high voltage defibrillation techniques used to treat arrhythmias are known to have pro-arrhythmic effects. Therefore, it is crucial to develop low energy methods to unpin and eliminate them.

This thesis investigates two kinds of low voltage electric fields to unpin the pinned spiral waves. In the first method using pulsed electric fields, the spiral wave will be unpinned only when the pulse is delivered inside a narrow time interval called the unpinning window of the spiral. In experiments with cardiac monolayers, we found that other obstacles situated near the spiral's pinning centre can facilitate unpinning. In numerical simulations, we found that the unpinning window can change depending on the location, orientation and distance between the pinning centre and the obstacle. The second method involves unpinning the spiral using circularly polarised electric fields (CPEF). Here, we show that the spiral can always be unpinned below a threshold time period of CPEF for a given obstacle size. Our analytical formulation accurately predicts the threshold and explains the absence of the traditional unpinning window. We also show that the unpinning always happens within the first rotation of the electric field.

Previous unpinning studies using two-dimensional experimental and numerical models show that the width of the unpinning window is very narrow. This could be due to the presence of multiple obstacles as our results suggests. The absence of unpinning window with CPEF eliminates the problem of timing the pulses and guarantees unpinning of the spiral below a certain threshold time period. We hope that the results discussed in this thesis regarding the spatial arrangement of the obstacles and its interactions with the electric fields will open new ways towards low-energy therapies of the cardiac arrhythmias.

Keywords: Spiral waves; Cardiac arrhythmias; Unpinning; Low-voltage defibrillation.

Contents

List of Figures

List of Tables

Nomenclature

1D	One Dimensional
2D	Two Dimensional
3D	Three Dimensional
etc.	Et cetera
ATP	Adenosine Triphosphate
AV Node	Atrioventricular Node
CPEF	Circularly Polarised Electric Field
FFP	Far Field Pacing
ICD	Implantable Caridoverter Defibrillator
KCL	Kirchhoff's Current Law
LEAP	Low Energy Anti-fibrillation Pacing
SA Node	Sianoatrial Node
UW	Unpinning Window
VF	Ventricular Fibrillation
VT	Ventricular Tachycardia
WEH	Wave Emission From Heterogeneity

Chapter 1

Introduction

This chapter gives a brief introduction to the excitable media with the focus on the control of spiral waves in the heart. It includes a detailed literature survey, scope and objectives of the research. In the end, an organization of the thesis is also presented.

The modern-day introductory Physics textbooks are filled with examples of swinging pendulums, spinning tops and billiard-ball collisions to construct a mental picture of fundamental concepts like momentum, energy, spin *etc*. Similarly, a typical Biology course would begin with the study of cells, evolution *etc*. However, real-world problems rarely have disciplinary boundaries. This thesis presents one such problem that lies on the borderline between Physics and Biology; it describes how the tools from different disciplines can be used to solve a contemporary public-health issue.

The modern roots of Biophysics can be traced down to the 18th century when the role of electricity was established in biological cells (Galvani (1792)). Today, all the biological tissues that support electrical waves are classified along with other media that show similar waves of excitation. Together they are known as excitable media. Every excitable media is made up of many excitable cells that interact with each other using a diffusion like coupling. The general properties of the excitable cell are the following:

1. It has a stable *resting state*.

2. It shows a characteristic response to external stimulus.

3. It has a *excitation threshold*. The cell can only be activated if the stimulus is supra-threshold.

4. It has a property of refractoriness. It takes a certain amount of time for the cell to be ready for a second stimulus following an excitation. During this time interval, another stimulus, no matter how strong, will not be able to generate a second activation. This interval is called the *refractory period*.

The presence of a threshold of excitation means that the medium has no memory of the stimulus used to initiate the excitation after the initial transients. The refractoriness property gives rise to wave annihilation, analogous to the colliding fire-fronts in a forest fire. Depending on the physiological context, the waves of excitation behave differently. In a 1D cable of excitable cells such as an axon, the excitation travels as pulses without attenuation, whereas in a 2D medium such as Belousov-Zhabotinsky chemical reaction (see Fig. 1.1 (a)), they show patterns like spiral or target waves. In a 3D excitable medium such as the ventricles of a heart, scroll waves can be formed. The spatiotemporal pattern formation seen in different types of excitable media is shown in Fig. 1.1. Examples include spiral waves on the surface of a rabbit heart (Fig. 1.1 (b)), colonies of starving slime mold Dictyostelium discoideum bacteria (Fig. 1.1 (c)) and a condition called Geographic tongue where spiral waves are seen on human tongue (Fig. 1.1 (d)).

The study done in this thesis primarily focuses on the dynamics and elimination of spiral waves in the heart. Therefore, before presenting the problems and the hypotheses of this study, we briefly describe the anatomy and physiology of the heart.

1.1   Anatomy And Physiology Of Heart

The human heart (see Fig. 1.2) is a muscular organ that pumps blood through the circulatory system. A normal human heart is divided into four chambers, with two atria and
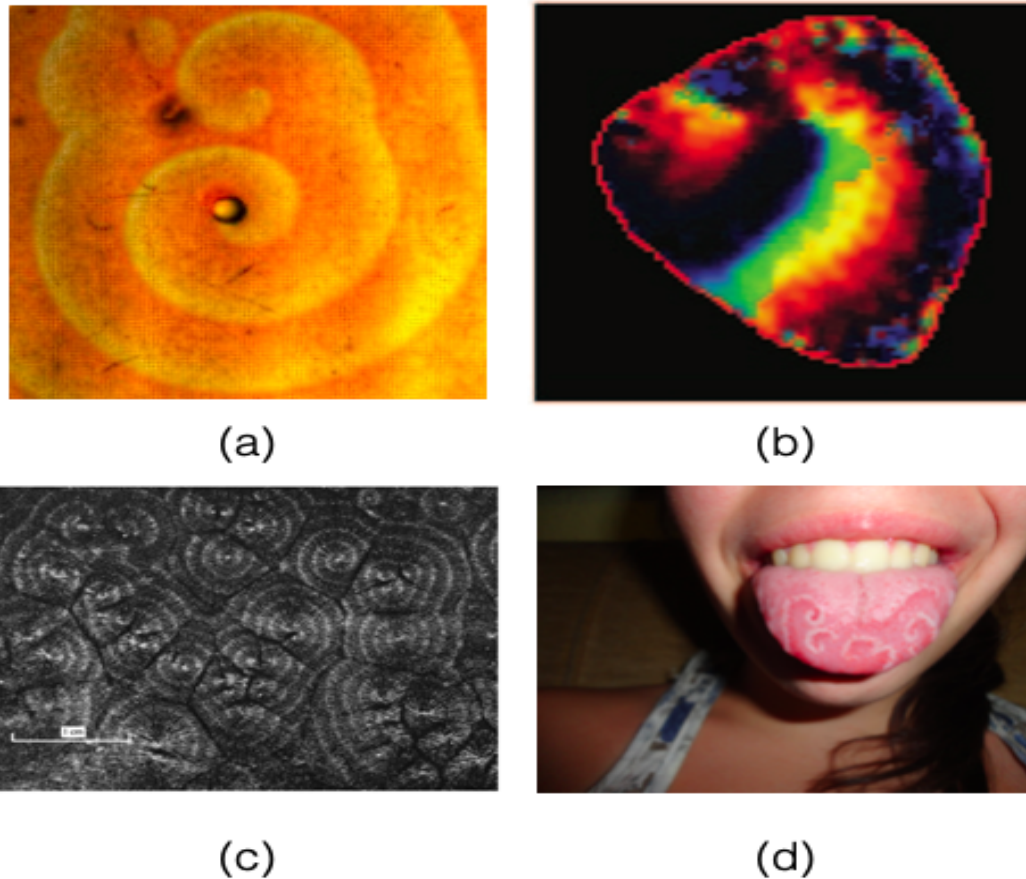
Figure 1.1: **Patterns in biological excitable media. (a)** Chemical waves in two dimensional Belousov-Zhabotinsky reaction (Experiments by Amrutha S V and Sibeesh PP). **(b)** Spiral waves in the surface of rabbit heart (Weiss et al. (2005)). **(c)** Spiral waves in colonies of starving slime mold Dictyostelium discoideum bacteria (Alcantara and Monk (1974)). **(d)** Geographic tongue - spiral waves on human tongue (Seiden and Curland (2015)).

two ventricles. The atria are the upper receiving chambers of the heart. The ventricles are the heart's pumping chambers, which lie below the atria and comprise most of the heart's volume. The entire heart can be seen as two separate pumps, one on the left and the other on the right (Fig. 1.2 (a)). The right atria receive deoxygenated blood from the superior and inferior vena cava, which then releases it to the lungs through the right ventricles and pulmonary artery. The oxygenated blood from the lung enters the left atria and is circulated to different parts of the body through the most prominent artery, called the aorta, connected to the left ventricle. During one heartbeat, different heart chambers undergo contractions (systole) and relaxation (diastole). This involves the

blood being pumped into the heart from the veins and pushed back to the body through arteries. A healthy heart allows the blood to flow in only one direction with several valves, which prevent the backflow of blood. The heart wall comprises three layers, the inner endocardium, the middle myocardium and the outer epicardium (Guyton and Hall (2006)). Like any other tissue in the body, the heart tissue needs some mechanism for its maintenance, such as the supply of oxygen and removal of the wastes. This is achieved by coronary circulation. It is a network of veins and arteries surrounding the heart muscle. The coronary arteries supply blood to the myocardium and other parts of the heart. The coronary veins remove the deoxygenated blood from the heart muscle.
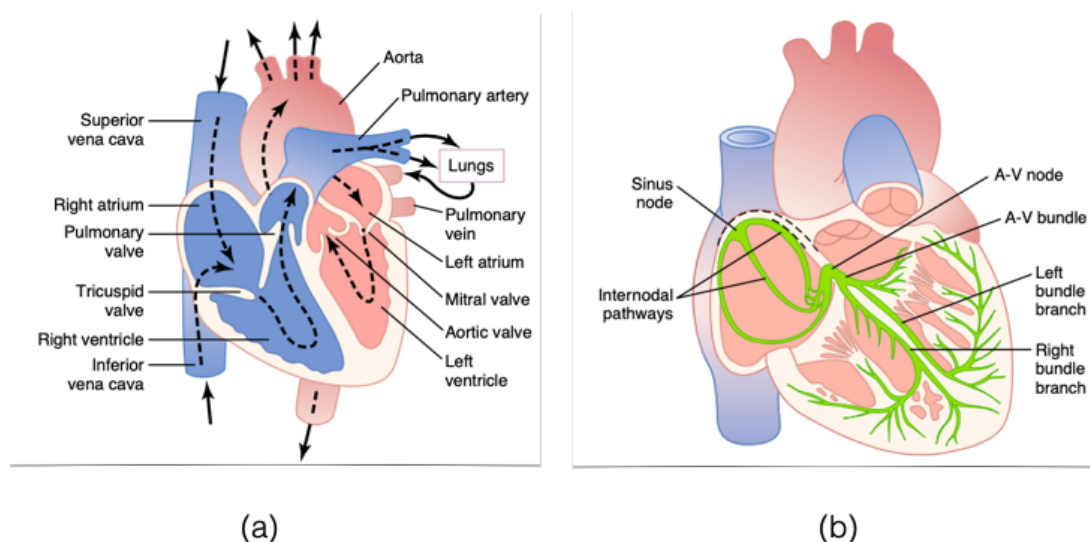
Figure 1.2: **Anatomy and physciology of human heart (a)** Anatomy of human heart. Four chambers of the heart, the right atrium the left atrium and the right and left ventricles are shown (Guyton and Hall (2006)). **(b)** Physciology of human heart showing the conduction pathway of the heart (Guyton and Hall (2006)).

The lub-dub symphony of the cardiac cycle described above is controlled by the electrical signals generated by a specialized group of cells in the right atrium of the heart called the sinoatrial node (SA node). SA nodal cells (see Fig. 1.2 (b)) are oscillatory; they generate periodic electrical signals that can drive the surrounding tissue. The electrical impulses generated by the SA node stimulate the atria to contract. Simultaneously they travel to the Atrioventricular Node (AV Node) through a conduction pathway called Inter Nodal Pathway. Atria and ventricles are electrically isolated from each other by a layer of fibrous tissue. So, the AV node acts as an electrical window

between the two. The AV node holds the electrical signals for some time, allowing the atria to contract. Once the atrial contraction is complete and the ventricles are filled with blood, the signals are released through the Bundle of His and Purkinje fibers to every corner of the ventricles. This is followed by ventricular contraction. The delay induced by the AV node prevents the atria and ventricles from contracting together. The SA node, AV node, Bundle of His and Purkinje fibers constitute the conduction pathway of the heart.

The heart muscle fibres are made up of cardiac cells coupled with each other through gap junctions. However, due to the elongated shape of the cells, the coupling is anisotropic. The fiber axis continuously rotates by about $180°$ from the innermost endocardium to the outer epicardium. In addition to this, other properties such as the action potential duration and polarization are also known to be different across different parts of the cardiac muscle (Szentadrassy et al. (2005)). The heart muscle contains naturally occurring heterogeneities such as scars, fibrotic tissue *etc.*, which change the behaviour of the muscle (Kakkar and Lee (2010)). The electrical impulses that SA Node gives out are called action potentials. The mechanism of action potential generation is described in the next section.

1.2 The Cardiac Action Potential

The cardiac muscle is made up of cells called cardiomyocytes. Each cardiomyocyte is enclosed by a cell membrane embedded with specialized proteins called ion channels as shown in Fig. 1.3 (a). They permit the selective passage of ions (such as K^+ ions, Na^+ *etc.*) in and out of the cell and help in maintaining a potential difference across the cell membrane. This potential difference is called transmembrane potential. The ion channels are also voltage-gated, meaning that they open only if the transmembrane potential hits a certain threshold voltage. Initially, the extracellular space contains a large number of Na^+ ions and a very small amount of K^+ ions. So, in the resting state, the interior of the cell is negatively polarized as marked by ④ in Fig. 1.3 (b).

When the cells around the ventricular cardiomyocyte get excited, the transmembrane potential shoots up from the resting state of -90 mV. If the stimulus is high
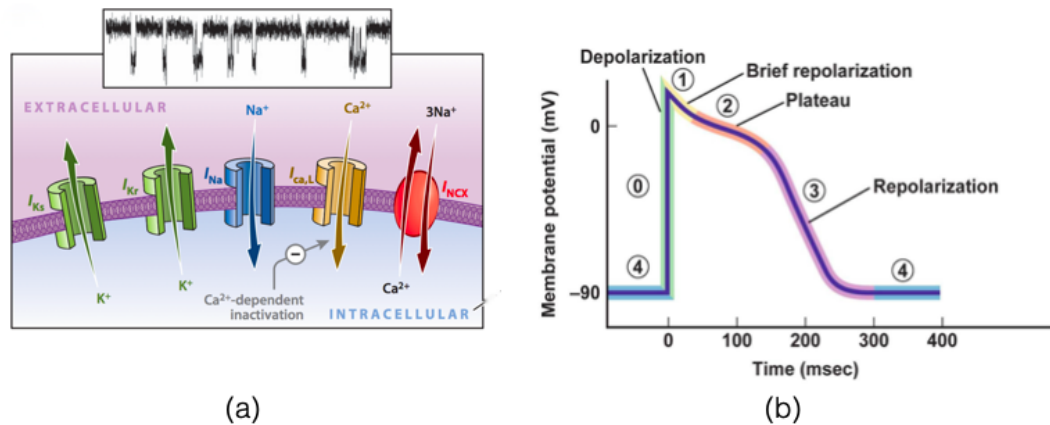
Figure 1.3: **Structure of cell membrane and action potential. (a)** Schematic representation of the outer membrane of the ventricular cell incorporating ion channels with selective permeabilities to different ions. **(b)** Cardiac action potential representing the time course of transmembrane voltage in response to a suprathreshold electrical stimulus (Karma (2013)).

enough, the transmembrane potential raises to about +20 mV due to the diffusion of Na$^+$ ions down the gradient into the cell. As a result of this, the cell's interior loses its negative polarization and becomes more positive. This phase is called the depolarization phase (marked by ⓪ in Fig. 1.3 (b)). Once the action potential peaks (indicated by ① in Fig. 1.3 (b)) the sodium channels begin to close in succession and the potential begins to fall. Now the calcium channel gates are released. This bring in positive Ca^{2+} ions, but the potassium channels simultaneously open which compensates for the addition of Ca^{2+} ions, maintaining the potential intact. This process leads to the plateau region in the action potential curve (indicated by ② in Fig. 1.3 (b)). At the end of the plateau, all the calcium ion channels would have already closed and the k$^+$ ions continues leaving the cell until the transmembrane potential drops to resting state. This state is called the repolarisation state (shown as ③ in Fig. 1.3 (b)).

Meanwhile, the sodium-potassium pump transports three sodium ions outside the cell to bring two potassium ions inside at the expense of an ATP. These processes make the inside of the cell more negative. This increases the potassium concentration inside the cell. The outside of the cell remains at the same concentration as it is an infinite bath of ions. In this way, the action potential generated in a single cell can propagate to the neighbouring cells through gap junctions and cause contractions of the muscle.

In the next section we discuss how the excitation waves in the heart muscle can form rotating waves and cause cardiac arrhythmia.

1.2.1 Scope

Any deviation from the normal sinus rhythm of the heart is called Cardiac Arrhythmia. In a normal heart, the electrical waves given out by the SA node will spread across the heart and excite the entire muscle. After the excitation, the muscle recovers and waits for another wave. However, the waves that cannot fully excite the whole tissue in their first attempt can re-enter the unexcited parts of the tissue due to the property of refractoriness and form spiral-shaped rotating patterns (Winfree (1989), Davidenko et al. (1992)). These rotating spiral waves in heterogeneous excitable media tend to attach to heterogeneities (also called obstacles) and form stable pinned waves (Davidenko et al. (1992), Valderrábano et al. (2001), Bub et al. (2002)). Once pinned, they rotate with very high frequency around the boundary of the obstacle. In an excitable medium, if there are two wave sources with different frequencies, the region of influence of a higher frequency source will continue to expand due to the phenomenon of wave annihilation. Ultimately, the entire tissue will be controlled by the higher frequency source (Krinsky and Agladze (1983)). Therefore, a spiral wave can override the natural rhythm set by the heart's pacemaking cells leading to cardiac arrhythmia. A healthy human heart beats between 60 to 100 times per minute. During the initial stages of arrhythmia, the number of beats may increase above 100. This condition is called Tachycardia which causes irregularity in the blood pumping ability of the heart. If left untreated, Tachycardia can lead to a potentially life-threatening condition called fibrillation, where the rotating wave breaks up into multiple spiral waves (Gray et al. (1998)). When this happens in the heart's ventricles, it is called Ventricular Tachycardia (VT) and Ventricular Fibrillation (VF), respectively.

Antiarrhythmic drugs are a group of pharmaceuticals used to treat the abnormal rhythms of the heart. Different drugs have a different mechanism of action - some slow down impulse initiation, while others keep the tissue refractory for an extended time (Rosen and hoffman (1973)), *etc*. Several efforts have been made to classify the an-

tiarrhythmic drugs in the literature (Lei et al. (2018)). However, since these drugs have several modes of action, classifying them has always been a problem. The major disadvantage of these medications is that nearly all of them are pro-arrhythmic, meaning that a drug given to terminate one kind of arrhythmia can cause arrhythmia of another kind (Roden (1998), Frommeyer and Eckardt (2016)). Another well-known method used in treating cardiac arrhythmia is called catheter ablation (Glass (1996)). Here, a catheter is inserted into desired locations in the patient's heart and using a radio frequency of 40-50 watts; the abnormal tissue is either ablated or dissociated from the rest of the healthy tissue (Terasawa et al. (2009)).

Ventricular fibrillation is usually treated by applying high voltage counter shocks (∼1kV, 12ms, 30A) delivered to the whole heart muscle (Otani et al. (2019)) either using a high voltage defibrillator or an implantable cardioverter-defibrillator (ICDs). It is presumed that this shock resets all the excitation waves in the cardiac muscle and resets the rhythm. Even though this technique is reliable and life-saving, the physical pain and the psychological distress caused to the patient are immense (Matchett et al. (2009), Tung (1996)). It can also damage the tissue causing scars, leading to the dysfunction of the myocardium (Godemann et al. (2004)). Since all the methods presented above have demerits, there is an immediate need for alternatives.

Wiener and Rosenblueth were the first to hypothesize that the spiral waves could be the reason behind the rapid heart beats during fibrillation (Weiner and Rosenblunth (1946)). Later, the similarities between the spiral waves in excitable media and inside a fibrillating heart were pointed out by physicists such as Moe and Krinsky (Krinskii (1966), Moe et al. (1964)) in mathematical models. Zhabotinsky was the first to describe spiral waves in experiments in a 1970 Russian report. In 1972, Art Winfree re-discovered the spiral waves in Belusov-Zhabotinsky reaction (Winfree (1972)). However, the connection between the spiral waves occurring in chemical medium like Belusov-Zhabotinsky reaction to the one occurring in the heart was not known. It was Art winfree who made that connection. To understand the dynamics of the rotating spiral waves, Winfree initiated several numerical and experimental studies in excitable media. The properties such as meander (Winfree (1992)) and breakup (Courtemanche

and Winfree (1991)) of spiral waves were the results of these careful observations. Following these dynamical studies, several pioneering works have been conducted for understanding the mechanisms of electrical defibrillation and termination of the spiral waves. The notable one was a proposal to use low voltage electric fields to drift the freely rotating spiral away to the boundary of the medium by Biktashev's group (Biktashev and Holden (1998)). Other methods of control include applying current through a lattice of electrodes (Rappel et al. (1999)) and limiting the size of the tissue using low voltage electric pulses (Sinha et al. (2001)). The techniques described above involves an electrical stimulus applied to a large area of tissue. Such global applications of electrical fields have limited clinical applications. Keeping this in mind, techniques using localized low energy electric pulses were proposed as an alternative to the high voltage shocks as they are below the pain threshold and do not damage the tissue.

To control the spiral waves inside the heart, one has to understand the factors affecting their initiation and interactions with the obstacles and the external electric fields. For this purpose, excitation waves have been studied in intact hearts using voltage-sensitive dyes (Luther et al. (2011), Davidenko et al. (1992)), in chemical medium such as Belousov - Zhabotansiky reactions and in mathematical models of excitable media (Shajahan et al. (2007, 2016), Ten Tusscher and Panfilov (2003), Fenton et al. (2002)). All these work aim to address either of the following problems: (1) Initiation of spiral waves, (2) dynamics of spiral waves and (3) elimination of spiral waves. This thesis specifically concerns about the elimination of pinned spiral waves from the medium. This involves understanding the dynamics of waves interacting with the obstacles in the presence of different kinds of electric fields.

When the spiral wave is pinned to the obstacle, it becomes necessary to apply the stimulus close to the core wave to unpin it (Bittihn et al. (2008)). By applying a sequence of far-field pulses, it was shown that the fibrillation could be controlled with 80% less energy compared to standard defibrillation. Here the low voltage electric field pulses recruit tissue heterogeneities as wave emitting sites, and this may be helping to unpin and remove even the waves pinned to small scale obstacles in the tissue.

1.2.2 Objectives

To unpin a spiral from the obstacle, one has to apply a stimulus close to the spiral's core in a narrow spatial and temporal window called the unpinning window. (Bittihn et al. (2008)). To solve the problem of spatial location, a method called Far Field Pacing (FFP) was suggested (Bittihn et al. (2008)). In this method, electric pulses are applied to the tissue using a pair of electrodes, which generates secondary excitations from the heterogeneities. Since these heterogeneities are the pinning centres themselves, the emitted excitations appear close to the pinned spiral's core. However, the problem of timing the pulse so that it falls into the unpinning window persists.

Recently, many groups have started using periodic field pulses to increase the chances of unpinning. The idea is to fire multiple pulses at the pinned spiral with the hope of one of the pulses falling into the unpinning window. The technique is called Low-Energy Antifibrillation Pacing (LEAP) and is found to be very effective (Li et al. (2009), Luther et al. (2011)). However, these studies also revealed that unpinning window is relatively narrow in mathematical models of excitable media and experiments with cardiac monolayer compared to the experimental studies in the intact heart (Luther et al. (2011), Shajahan et al. (2016)). Despite their critical importance in low- energy antifibrillation techniques, this problem has not received much attention. We study how these additional obstacles can alter the unpinning of a single spiral.

The technique of LEAP hypothesizes that multiple periodic pulses can unpin spiral waves by firing the stimulus into the unpinning window of the spiral. However, the technique's success critically depends on the pacing frequency and the width of the unpinning window. If the pacing frequency is not optimal or if the unpinning window is too narrow, the technique could potentially fail. Therefore, as an alternative to LEAP, we use a circularly polarized electric field to unpin the spirals.

Circularly polarised electric fields (CPEF) was first introduced by Jiang-Xing Chen et al. to study the drift of spiral waves (Chen et al. (2006)). Later, in a simulation study, it was used to terminate the pinned spirals by Feng et al. (Feng et al. (2014)). In this study, they compared the circularly polarized electric field's efficiency to that of the pulsed electric field and found a significant increase in the success rate with much

lower voltage strength than pulsed electric fields. The subsequent study showed that the higher frequency circular wave trains generated by the CPEF could successfully terminate spiral turbulence (Feng et al. (2015)). Recently, the effect of CPEF on an irregularly shaped obstacle was also performed (Feng and Gao (2019)). In addition to these studies, the ability of CPEF to control the turbulence has been shown experimentally in the Belousov-Zhabotinsky reaction (Ji et al. (2013)). Despite its success in terminating the spirals, the factors and parameters determining the success remain elusive. Therefore, we try to provide a theory and mechanism of unpinning using circularly polarized electric fields.

Thus, the objectives of this study are as follows:

1. To study how the additional obstacles can alter the unpinning window of a single pinned spiral.

2. To provide a theory and mechanism for the unpinning of spiral waves using circularly polarized electric fields.

1.3   Organization of the thesis

The work presented in this thesis concerns with the study of dynamics and control of rotating excitation waves via electric field pulses in excitable media. The study is carried out with the hope of opening new and efficient pathways in low voltage defibrillation therapies of the heart. Such a study requires a sound understanding of the dynamics of the excitation waves causing the arrhythmias. Moreover, the control strategies to be devised must be supported by sufficient mathematical and theoretical background.

The thesis consists of five chapters. To make it self-contained, Chapter 1, gives a brief introduction to the excitable media in general with the focus on control of spiral waves in the heart using available techniques. This chapter also includes the relevant literature survey, the scope of the research carried out, and the research objectives. At the end of this chapter, an organization of the thesis is also presented.

Chapter 2 presents the experimental techniques and the mathematical foundations necessary for this study. This includes brief details about the mathematical models and

numerical techniques used in this work.

Chapter 3 and chapter 4 are centred around the question of how the unpinning window of the single obstacle is affected by the presence of an additional obstacle nearby. Here, we systematically investigate the process of unpinning numerically by introducing an additional obstacle and calculate the unpinning window of the spiral wave using a pulsed electric field. The numerical result is consolidated with experiments performed using cardiac monolayers. (All the experimental work in this thesis is carried out by the co-authors Dr. T. K. Shajahan and Dr. Sebastian Berg in Max Planck Institute of Dynamics and Self Organization, Göttingen, Germany.)

Chapter 5 is dedicated to unpinning spiral waves using the circularly polarized electric field (CPEF). Here, we present separate mechanism of unpinning spiral waves having different chirality and propose a robust theory to validate the findings of the numerical simulations.

Chapter 6 contains the summary of the research work presented in this thesis. It also includes concluding remarks and the scope for future research in these areas.

Chapter 2

Methods

This chapter briefly describes the experimental techniques, mathematical foundations and numerical modelling details necessary to understand the concepts presented in this thesis.

2.0.1 Experimental Methods

Cardiac monolayers have been used as an experimental tool to study conduction and electrophysiology as early as the 1970s (DeHaan and Gottlieb (1968)). The development of high-resolution optical techniques has made it possible to map the dynamics of cardiac waves (Bub et al. (1998)) in monolayers. Unlike the intact heart, the monolayer is isotropic and mostly homogeneous which makes it an ideal system to study the excitation waves. In the past, monolayers have been used to study the mechanisms of formation of reentry (Bub et al. (2005)), unidirectional block (Rohr et al. (1997)) , calcium instabilities (Chang et al. (2012)), and the effects of fibroblast on conduction (Zlochiver et al. (2008)), to name a few.

2.0.2 Real-time optical mapping

High-resolution optical mapping allows to observe reentrant wave dynamics in the cardiac monolayer. Activity in the monolayer will be mapped using a macroscope (Olympus MVX10) and a CCD camera (Photometrics Cascade). The imaging system can record from a field of view of up to 3×3 cm2 with spatial 2 resolution starting from 16 $\times$ 16 μm. The camera can record fluorescent activity optimally from an area of 1 cm2 at about 40 Hz, which is sufficient to capture electrical waves in the monolayer. Since the fluorescent signals from a monolayer are small compared to that from intact hearts, usually calcium signals are mapped. Calcium gives a much larger fluorescent signal, and it closely follows the voltage in most slow pacing applications (Tung and Zhang (2006)). Usually, a calcium-sensitive dye Ca-green from Invitrogen is used since this dye is suitable for capturing even small changes in the intracellular calcium concentration. Waves in embryonic chicken monolayers are sufficiently slow (1 cm/sec) to allow electrical and pharmacological intervention. This will help one to control the dynamics as it evolves and study the transition.

2.0.3 Mathematical Background

One of the most outstanding achievements of 20th-century biophysics is the mathematical framework developed by Sir Alan Hodgkin and Sir Andrew Huxley for explaining the initiation and propagation of action potentials (Hodgkin and Huxley (1952d,b), Hodgkin et al. (1952), Hodgkin and Huxley (1952c,a)). After the end of the Second World War, Hodgkin and Huxley learned about the voltage clamp technique during one of their visits to K. S Cole's lab and later used it to understand the action potentials in an axon (Huxley (1996)). Hodgkin and Huxley's work laid the mathematical foundation for modern biophysical research.

The Hodkin-Huxley model was developed based on a series of experiments performed on a giant squid axon. Using experiments, they demonstrated that the ionic currents could be understood in terms of changes in the Na^+ and K^+ conductances in the membrane. Using the Voltage-clamp method, they developed a mathematical

model that explains the voltage and time-dependent properties of the Na⁺ and K⁺ conductances. D. Noble applied this model to explain the cardiac action potentials for the first time in 1962 (Noble (1962)).

In the sections below, we present a brief mathematical background used in modelling the excitable media in general. Following the mathematical background, the models and techniques used in this work are described in detail.

2.1   Cable Equations
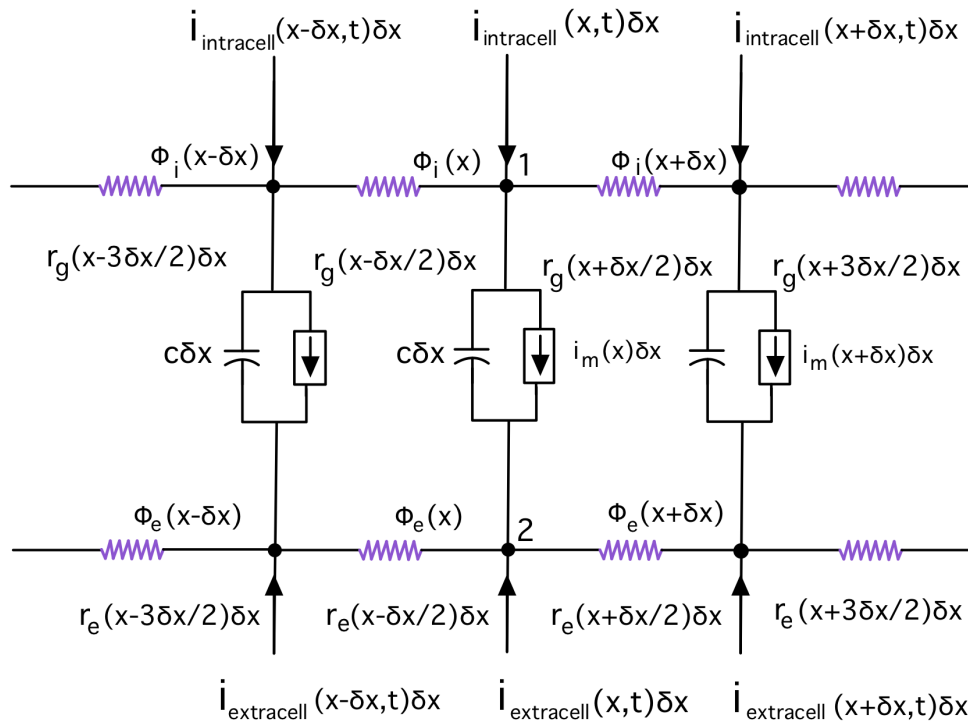
Figure 2.1: **Electrical circuit modelling a series of excitable cells.** The top part of the circuit is the intracellular space and the bottom part is the extracellular space. The arrows at the top and bottom parts of the circuit correspond to the intracellular and extracellular stimulation respectively.

We begin by building an electronic circuit model to explain the one-dimensional description of action potential propagation in cardiac cells (see Fig. 2.1). The excitable

tissue is thought of as a series of biological cells lying along a one-dimensional cable. The cells are connected via a series of gap junctions which can be modelled as resistors with r_g as the value of resistance per unit length of the chain. Let x be the center of the coordinate system and if the length of the cell in x-direction is δx, then the value of each gap junction resistor located between the cells x and $x + \delta x$ can be given as $r_g(x + \delta x/2)\delta x$. Every cell in the cable can interact with the extracellular space through the cell membrane and the ion channels embedded in the membrane. Each cell membrane can be modelled as a capacitor with capacitance $c\delta x$, where c is the membrane's capacitance per unit length. The ion channel is represented as a little box in the circuit, assuming that it has complicated dynamics. The extracellular fluid, a resistive medium, can also be modelled as a series of resistors. Although their resistance values must be lower than the gap junction resistors since the extracellular space is vast and continuous, the current must flow without much trouble instead of the gap junctions that are narrow in shape. Let $r_e\delta x$ be the value of extracellular resistance per unit length.

The voltage at different nodes can be identified by their locations: the intracellular potential of the cell located at x is $\phi_i(x)$ and the corresponding extracellular potential is $\phi_e(x)$.

Applying Kirchhoff's current law (KCL) at node "1", we get,

$$c\frac{\partial(\phi_i(x) - \phi_e(x))}{\partial t} + i_m(x) + \frac{(\phi_i(x) - \phi_i(x - \delta x))}{r_g\delta x^2} + \frac{(\phi_i(x) - \phi_i(x + \delta x))}{r_g\delta x^2} - i_{intracell}(x) = 0$$
(2.1)

For simplicity, we assume that the gap junction resistance $r_g(x - \delta x/2) = r_g(x + \delta x/2) = r_g$ a constant.

If the cell size δx is small we can use Taylor expansion to simplify the expression as follows(The third and fourth terms),

$$c\frac{\partial V_m(x,t)}{\partial t} + i_m(x,t) - \frac{1}{r_g}\frac{\partial^2\phi_i(x,t)}{\partial x^2} - i_{intracell}(x,t) = 0$$
(2.2)

where the membrane potential $V_m(x) = \phi_i(x) - \phi_e(x)$ is the potential difference between inside and outside of the cell.

Applying KCL to node 2 will give us the following equation,

$$c\frac{\partial(-V_m(x,t))}{\partial t} - i_m(x,t) - \frac{1}{r_e}\frac{\partial^2\phi_e(x,t)}{\partial x^2} - i_{extracell}(x,t) = 0 \qquad (2.3)$$

The final form of 2.2 and 2.3 are given below,

$$\frac{\partial V_m}{\partial t} = \frac{-i_m}{c} + D_g\frac{\partial^2 V_m}{\partial x^2} + D_g\frac{\partial^2\phi_e}{\partial x^2} + \frac{i_{intracel}}{c} \qquad (2.4)$$

$$(D_e + D_g)\frac{\partial^2\phi_e}{\partial x^2} = -D_g\frac{\partial^2 V_m}{\partial x^2} - \frac{i_{intracell}}{c} - \frac{i_{extracell}}{c} \qquad (2.5)$$

The Eq. 2.5 is constructed using $c\frac{\partial V_m}{\partial t} + i_m$ from Eq. 2.4. $D_g = \frac{1}{r_g c}$ and $D_e = \frac{1}{r_e c}$. Eqs. 2.4 and 2.5 are called cable equations.

2.2 Bidomain model

Bidomain model is a generalization of the cable equations described in section 2.1. In deriving the cable equations in the last section, we made several assumptions regarding the isotropy and homogeneity of the tissue. The cardiac tissue is a three-dimensional structure and not one-dimensional. The assumption that the resistance per unit length to be the same in any direction is not valid (the tissue is not isotropic). Moreover, the gap junction and extracellular resistances are not the same everywhere (the tissue is not homogeneous).

The bidomain model considers both the extracellular and intracellular spaces while describing the cardiac tissue. Here, we assume that both the intracellular and extracellular spaces occupy the entire geometric space. These two spaces are connected through ion channels on the cell membrane. Let us assume that the extracellular space is a heterogeneous anisotropic medium. The equivalent three dimensional circuit is shown in Fig. 2.2 (a). Let δx, δy and δz be the distance between the nodes in x, y and z directions. To obtain a continuous medium we let δx, δy and $\delta z \to 0$.

In an anisotropic medium, the resistor's value is proportional to the resistor's length and inversely proportional to its area of cross-section, but the constant of proportion-
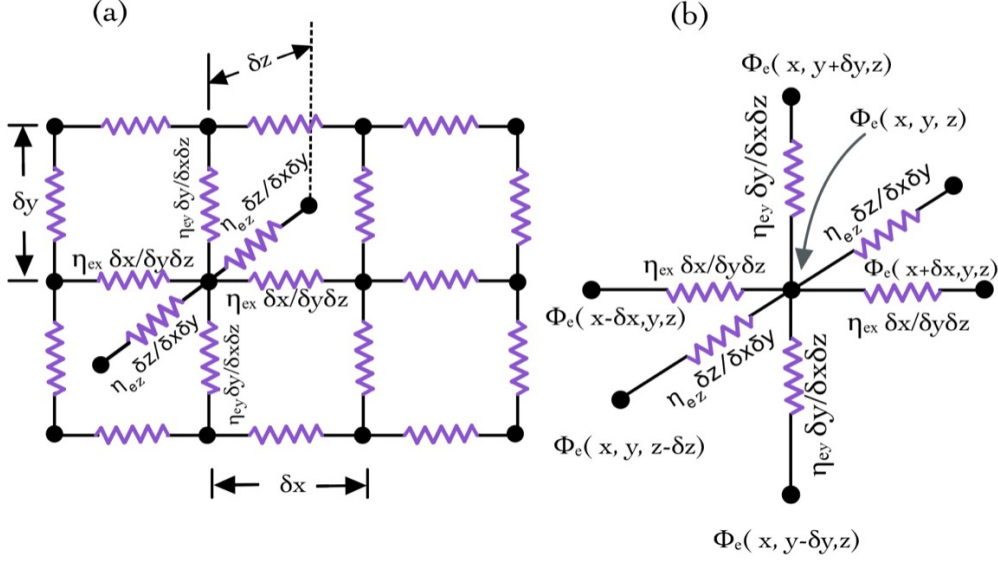
Figure 2.2: **(a)** A part from the 3D lattice of extracellular network of resistors. **(b)** The voltages and resistors used to compute KCL at node (x,y,z).

ality, known as resistivity, is different in different directions. Let $\eta_{ex}, \eta_{ey}, \eta_{ez}$ be the resistivities of the medium. Therefore, the value of resistor along x-direction (for example) would be $\eta_{ex}\delta x/\delta y\delta z$.

Applying KCL at node (x, y, z) (see Fig. 2.2 (b)), dividing by $-\delta x, \delta y, \delta z$ and expanding each of the six terms using Taylor series we obtain,

$$\frac{\partial}{\partial x}\left(\frac{1}{\eta_{ex}}\frac{\partial \phi_e}{\partial x}\right) + \frac{\partial}{\partial y}\left(\frac{1}{\eta_{ey}}\frac{\partial \phi_e}{\partial y}\right) + \frac{\partial}{\partial z}\left(\frac{1}{\eta_{ez}}\frac{\partial \phi_e}{\partial z}\right) = 0 \qquad (2.6)$$

Now we connect the extracellular space with the intracellular at a single node (x, y, z) as shown in Fig. 2.3. Let j_m be the current per unit volume coming from the intracellular space. Then the current flowing into any node in the extracellular space will be $j_m\delta x\delta y\delta z$ where $\delta x\delta y\delta z$ is the volume associated with the node. We also add the possibility of a stimulus being applied to the extracellular space by a current of magnitude $i_{extracell}$ per unit volume. Doing a similar analysis as above, we obtain

$$\frac{\partial}{\partial x}\left(\frac{1}{\eta_{ex}}\frac{\partial \phi_e}{\partial x}\right) + \frac{\partial}{\partial y}\left(\frac{1}{\eta_{ey}}\frac{\partial \phi_e}{\partial y}\right) + \frac{\partial}{\partial z}\left(\frac{1}{\eta_{ez}}\frac{\partial \phi_e}{\partial z}\right) = -j_m - i_{extracell} \qquad (2.7)$$
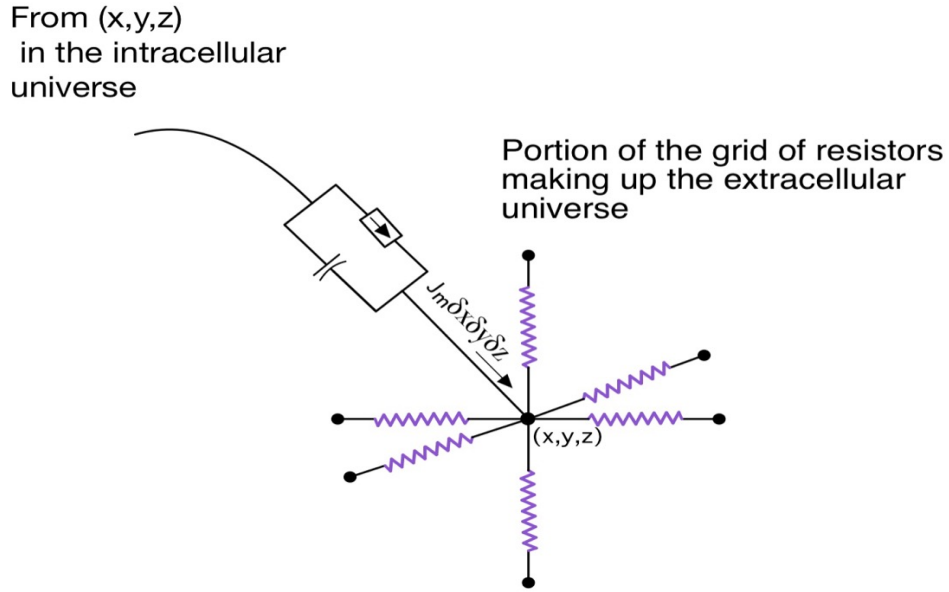
Figure 2.3: A part of the circuit required to apply KCL at the point (x,y,z) when linked to the intracellular universe.

We now relate j_m to the currents flowing through the capacitors and the ion channels explicitly. Then the total current flowing out of the intracellular space in a volume $\delta x, \delta y, \delta z$ containing the point (x, y, z) is

$$j_m = c\frac{\partial V_m}{\partial t} + i_m \tag{2.8}$$

where j_m, c and i_m are the total current through the membrane, capacitance and ion channel current per unit volume of the tissue. Substituting Eq. 2.8 in Eq. 2.7 we obtain

$$\frac{\partial}{\partial x}(D_{ex}\frac{\partial \phi_e}{\partial x}) + \frac{\partial}{\partial y}(D_{ey}\frac{\partial \phi_e}{\partial y}) + \frac{\partial}{\partial z}(D_{ez}\frac{\partial \phi_e}{\partial z}) = -\frac{\partial V_m}{\partial t} - \frac{i_m}{c} - \frac{i_{extracell}}{c} \tag{2.9}$$

where the components of D_e are $D_{ex} = 1/(c\eta_{ex}), D_{ey} = 1/(c\eta_{ey})$ and $D_{ez} = 1/(c\eta_{ez})$. The RHS of Eq. 2.9 can be written as

$$\nabla \cdot D_e \cdot \nabla \phi_e = \frac{\partial}{\partial x}(D_{ex}\frac{\partial \phi_e}{\partial x}) + \frac{\partial}{\partial y}(D_{ey}\frac{\partial \phi_e}{\partial y}) + \frac{\partial}{\partial z}(D_{ez}\frac{\partial \phi_e}{\partial z}) \tag{2.10}$$

Where, the quantity D_e is defined to contain the scalar quantities D_{ex}, D_{ey} and D_{ez}. In the matrix form it can be written as,

$$\begin{bmatrix} D_{ex} & 0 & 0 \\ 0 & D_{ey} & 0 \\ 0 & 0 & D_{ez} \end{bmatrix}$$

Now, Eq. 2.9 can be written compactly as

$$\nabla \cdot D_e \cdot \nabla \phi_e = -\frac{\partial V_m}{\partial t} - \frac{i_m}{c} - \frac{i_{extracell}}{c} \tag{2.11}$$

where the components of D_e are $D_{ex} = 1/(c\eta_{ex})$, $D_{ey} = 1/(c\eta_{ey})$ and $D_{ez} = 1/(c\eta_{ez})$.

Similarly, the equations for 3D anisotropic heterogeneous versions of cable equations can be derived. For the sake of simplicity, we write the bidomain equations directly below.

$$\frac{\partial V_m}{\partial t} = \frac{-i_m}{c} + \nabla \cdot D_g \cdot \nabla V_m + \nabla \cdot D_g \cdot \nabla \phi_e + \frac{i_{intracell}}{c} \tag{2.12}$$

$$\nabla \cdot (D_e + D_g) \cdot \nabla \phi_e = -\nabla \cdot D_g \cdot \nabla V_m - \frac{i_{intracell}}{c} - \frac{i_{extracell}}{c} \tag{2.13}$$

$$\nabla \cdot D_e \cdot \nabla \phi_e = -\frac{j_m}{c} - \frac{i_{extracell}}{c} \tag{2.14}$$

The familiar way to solve the bidomain equations is to integrate Eq 2.12 and then solve Eq 2.13 and 2.14 for ϕ_e. Solving for ϕ_e is computationally expensive for large domain sizes. To reduce the computational cost, an approximation of the Bidomain model is used, which involves only one partial differential equation called the monodomain model.

2.3 Monodomain model

In this section, we show how the monodomain equations can be directly obtained from the cable equations (Eq. 2.4) explained in section 2.1. Here, we look at each term of
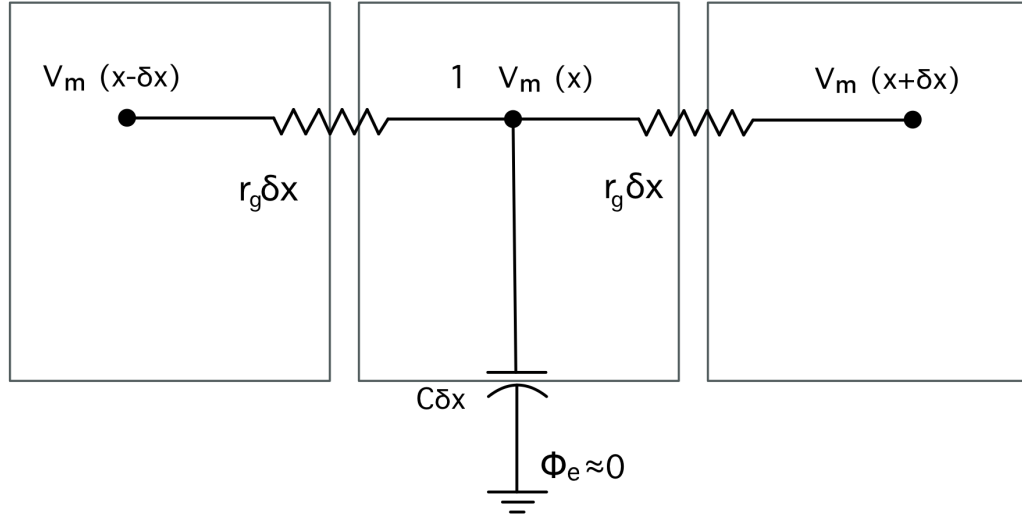
Figure 2.4: Electrical circuit diagram showing the contribution of the term $\frac{\partial V_m}{\partial t} = D_g \frac{\partial^2 V_m}{\partial x^2}$.

Eq. 2.4 separately one at a time and analyse their effects on the system. Let us consider the first term,

$$\frac{\partial V_m}{\partial t} = -\frac{i_m}{c} \tag{2.15}$$

While deriving the above equations, we assumed the cell membrane to behave as a capacitor. Therefore, Eq. 2.15 tells us that the capacitor can be charged by the current i_m flowing through the ion channels. In general terms, Eq. 2.15 is indicating how excitable the cell is. So, once the membrane potential is raised above the threshold, the term i_m activates the cell. Eq. 2.15 shows the mechanism through which this activation takes place.

Next, we focus on the other term of Eq. 2.4.

$$\frac{\partial V_m}{\partial t} = D_g \frac{\partial^2 V_m}{\partial x^2} \tag{2.16}$$

This equations arises from the resistors and membrane capacitance shown in the equivalent circuit in Fig. 2.4. The potentials on the intracellular nodes should have been $\phi_i(x - \delta x)$, $\phi_i(x)$ and $\phi_i(x + \delta x)$ respectively instead of $V_m(x - \delta x)$, $V_m(x)$ and $V_m(x + \delta x)$. The problem arises because we wanted to express the equation in terms

of ϕ_e and V_m instead of ϕ_e and ϕ_i. To circumvent this, we assume that ϕ_e is small or approximately zero. Then $V_m = \phi_i$ and the potentials shown in Fig. 2.4 are correct. The Eq. 2.16 is the heat or diffusion equation. If we put all the three terms together (i.e Eq. 2.15 and Eq. 2.16), we obtain

$$\frac{\partial V_m}{\partial t} = -\frac{i_m}{c} + D_g \frac{\partial^2 V_m}{\partial x^2} \tag{2.17}$$

Eq. 2.17 is called the Monodomain equations as it includes only the intracellular domain.

2.4   Phase Field Method

Finite difference methods are one of the widely used methods to solve partial differential equations. The simplicity of the method has led to their usage in diverse fields of science and technology such as heat conduction (Brian (1961)), diffusion (Yuste and Acedo (2005)), weather forecast (Simmons and Burridge (1981)) *etc*. However, finite difference methods have some major disadvantages. They become quite unwieldy if we have complexities such as moving boundaries or unstructured grids. The inability of finite difference methods to handle irregular geometries is one of its main disadvantages. There are workaround techniques such as finite element methods, but they come at the expense of computational power. To circumvent this problem, we use a method that automatically takes care of the no-flux boundary conditions at the irregular domain boundaries. It is called Phase Field Method. This method widely used by material scientists and engineers to solve material science problems, including dendritic solidification (Boettinger et al. (2002)), viscous fingering (Folch et al. (1999)), crack propagation (Karma et al. (2001)) *etc*.

The natural boundary conditions in mono-domain cardiac models such as Fitzhugh-Nagumo or Barkley models are no-flux. They are as given below.

$$\hat{n} \cdot \nabla u = 0 \tag{2.18}$$

where $\hat{n}$ is the unit vector normal to the boundary, and u is the transmembrane po-

tential. We use the following steps to implement Eq. 2.18 using the phase-field method at the domain boundary. First, we introduce an auxiliary field ϕ, henceforth called the phase field. It takes values $\phi = 1$ for the excitable tissue (for example, the circular domain in Fig. 2.5) and $\phi = 0$ outside with a smooth transition at the boundary. The smoothing of the values of ϕ at the interface is done by solving the partial differential Eq. 2.19 as $t \to \infty$.

$$\frac{\partial \phi}{\partial t} = (\phi_0 - \phi) + \xi^2 \nabla^2 \phi \tag{2.19}$$

Where ξ is the parameter that controls the width of the diffusive interface. The above partial differential equation maintains the values of ϕ of 1 and 0 inside and outside the excitable tissue, and the Laplacian operator smoothens out the discontinuity of ϕ at the boundary of the circular domain. In this thesis, we have used the finite difference explicit method (mentioned in section 2.6) to calculate the phase field. Fig. 2.5 shows the initial binary field ϕ_0 and the resulting equilibrium phase field ϕ.

(a) (b)
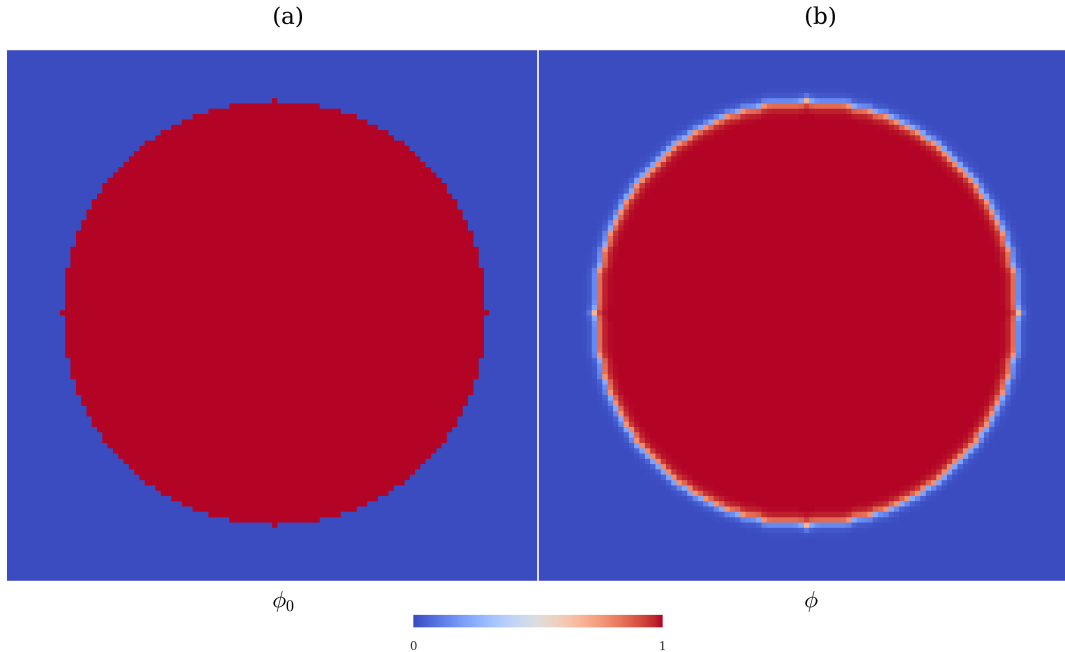
Figure 2.5: The no-flux boundary condition given in Eq. 2.18 is to be applied on the boundaries of the circular domain at the center. **(a)** Initial bipartite phase field ϕ_0. **(b)** The equilibrium solution of equation 2.19 with $\xi = 0.05$ and ϕ_0 from (a)

Once the equilibrium phase field is computed using the above mentioned method, it

is then substituted to the diffusion term as follows:

$$\nabla \cdot (D\nabla u) \rightarrow \frac{1}{\phi}\nabla \cdot (\phi D\nabla u) \tag{2.20}$$

Details about how this substitution simulates the Neumann boundary condition is given below.

Substituting Eq. 2.20 into the general reaction diffusion equation, we get,

$$\frac{\partial u}{\partial t} = f(u) + \frac{1}{\phi}\nabla \cdot (\phi D\nabla u) \tag{2.21}$$

We assume that $f(u)$ is bounded when u is bounded. We now integrate Eq. 2.21 over a small volume V (see Fig. 2.6) as follows,

$$\int_V \phi \frac{\partial u}{\partial t} dV = \int_V \phi f(u) dV + \int_V \nabla \cdot (\phi D\nabla u) dV = \int_V \phi f(u) dV + \oint \phi D\nabla u \cdot dA. \tag{2.22}$$
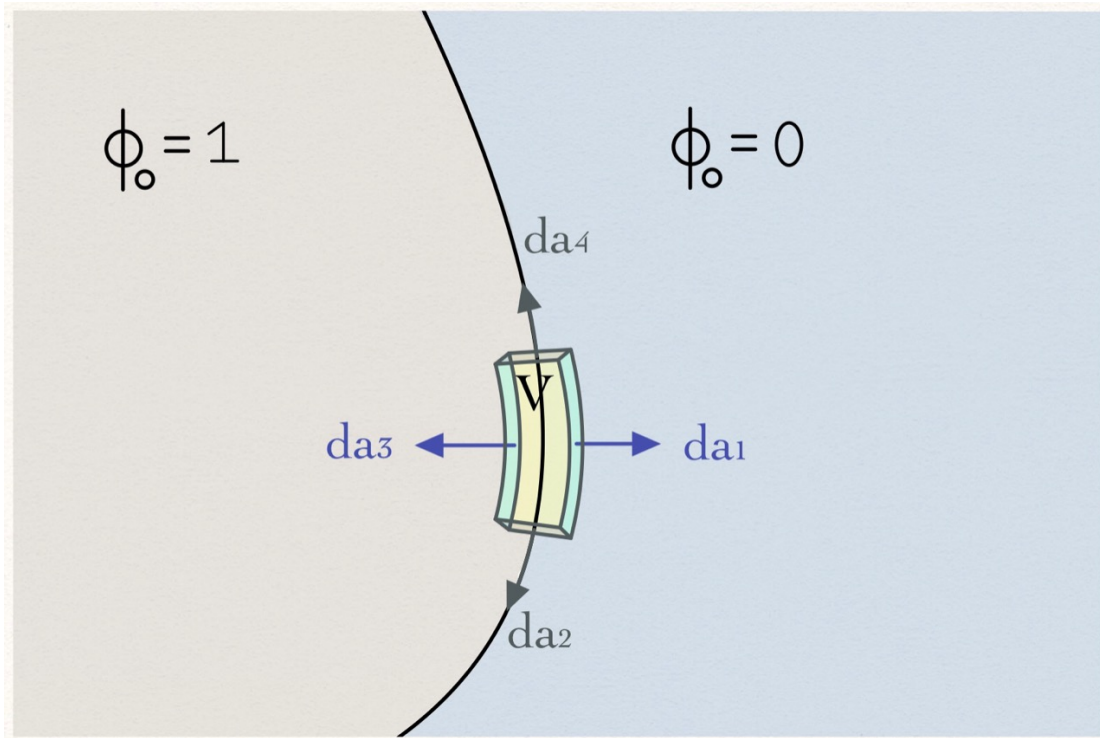
Figure 2.6: Graph showing the volume integration of equation 2.22 at the boundary between $\phi_0 = 1$ (brown) and $\phi_0 = 0$ (blue). The arrows shows the surface normal vectors to the integration volume, V.

Now, we write the contributions from individual surfaces as follows,

$$\int_V \phi \frac{\partial u}{\partial t}\, dV = \int_V \phi f(u)\, dV + \int_{a_1} \phi D\nabla u \cdot da_1 + \int_{a_2} \phi D\nabla u \cdot da_2 + \int_{a_3} \phi D\nabla u \cdot da_3 + \int_{a_4} \phi D\nabla u \cdot da_4 + \dots$$
(2.23)

The dots stand for the two surfaces of the volume V above and below the interface. For a chosen width of the interface ξ, the width of V normal to the interface is fixed so that the two surfaces parallel to the interface are having the values of $\phi = 1 - \delta$ and $\phi = \delta$ for an arbitrarily small $\delta > 0$.

If the volume we pick is sufficiently small and if the u is bounded, we can approximate the individual integrands of Eq. 2.23 by constants excluding ϕ. Now, if we let $\xi \to 0$ and reduce the width of the volume V, the tangential components a_2 and a_4 vanish as their size goes to zero. This is also true for the first term on the RHS of Eq. 2.23. Now, since we have $\phi \approx 1$ on the surface da_3 it survives. The other term on the surface da_1 vanishes as $\phi \approx 0$ there. Considering all the above arguments Eq. 2.23 can be written as,

$$0 = \int_{a_1} \phi D\nabla u \cdot dn_3 \approx \hat{n} \cdot D\nabla u$$
(2.24)

The technical details about the mechanism of boundary condition enforcement can be found in the book by Philip Bittihn (Bittihn (2014)).

2.5   Models of Excitable Media

A typical *bottom-up approach* cardiac model begins with a mathematical description of various ion species and transmembrane potentials required to describe an action potential. Several such models have been proposed for different kind of cardiac cells. An exhaustive list of physiological models for different regions of the heart using several ion species is given in (Fenton and Cherry (2008)). Ionic models can be beneficial when studying tissue-specific diseases as the model's variables are directly related to the physiological properties. But they involve a large number of parameters and the

variables, making numerical simulations expensive. In this thesis we study the propagation dynamics of the excitation waves. For this reason, we use the generic models of excitable media, constructed using the *top-down approach* like Barkley model (Barkley (1991)) and Fitzhugh-Nagumo model (see section 2.5.1). Both the models use only two variables and three parameters.

2.5.1 Fitzhugh Nagumo Model

R. Fitzhugh and J Nagumo independently published a series of papers developing a mathematical model for reproducing the current dynamics seen in excitable neuron cells (FitzHugh (1961), Nagumo et al. (1962)). This model is a simplification of the Hodgkin-Huxley model used for modelling the spiking neurons. The same set of equations can be used to model the cardiac tissue as both the neuronal and cardiac cells share excitable properties.

The model consists only two equations as given below:

$$\frac{\partial u}{\partial t} = \frac{1}{\varepsilon}(u(1-u)(u-a) - v) + D\nabla^2 u \tag{2.25}$$

$$\frac{\partial v}{\partial t} = bu - v \tag{2.26}$$

The quantity u is the transmembrane potential, and the variable v acts as the recovery variable. a, b and ε are the parameters of the model. The variable v is slower than u by the factor of $1/\varepsilon$, where $\varepsilon << 1$. The parameter a sets the threshold of excitation.

The quantity $u(1-u)(u-a)$ has a cubic non-linearity with three equilibrium points at $u = 0$, $u = a$ and $u = 1$. The points $u = 0$ and $u = 1$ represent the stable resting and excited states, respectively, while $u = a$ represents the unstable threshold. Therefore, being a bi-stable system, the quantity $u(1-u)(u-a)$ cannot model the excitable medium. We need another quantity that makes one of the stable equilibrium points gradually become unstable so that the system goes back to the resting state. This can be achieved by subtracting a time-dependent quantity v from $u(1-u)(u-a)$. So the term now becomes $(u(1-u)(u-a)) - v$. The evolution of v is given by the differential

equation 2.26.
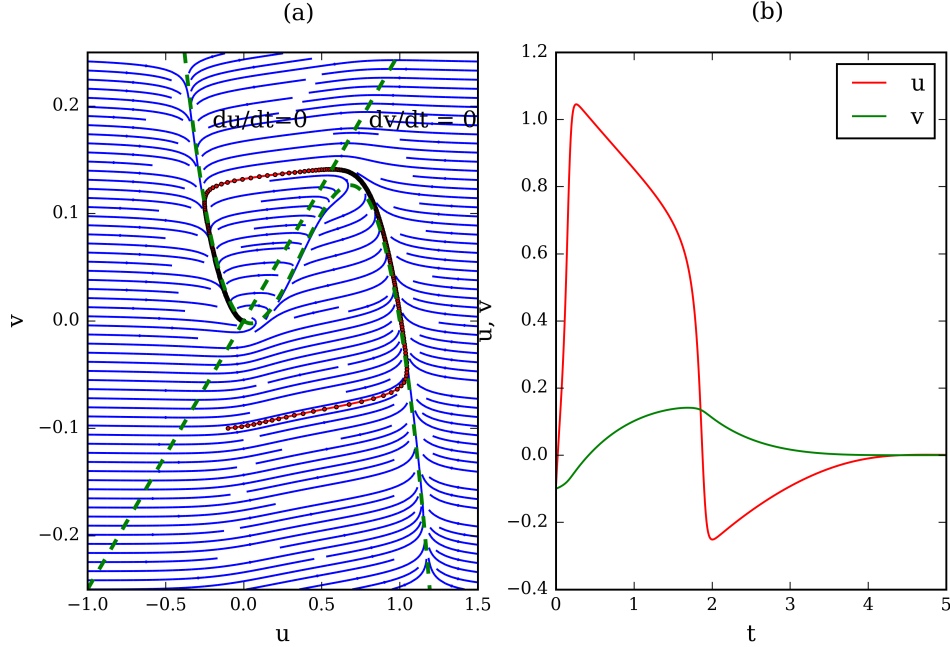
Figure 2.7: **(a)** The phase portrait of Eq. 2.25 and Eq. 2.26 with a initial condition $u = -0.1$ and $v = -0.1$. **(b)** The time evolution of u and v variables for $a = 0.1, b = 0.25$ and $\varepsilon = 0.025$.

The fixed points of the Fitzhugh Nagumo equations are the solutions of the following equations:

$$u(1-u)(u-a) - v = 0$$
$$bu - v = 0$$

(2.27)

The equations $u(1-u)(u-a) - v$ and $bu - v$ are called u-nullcline and v-nullcline respectively. Fig. 2.7 (a) shows the phase portrait of the model. The point of intersection of two nullclines denote the stable equilibrium point. For portions below (above) the u-nullcline, $du/dt > 0\ (<0)$ and for the portions to the left (right) of v-nullcline, $dv/dt < 0\ (>0)$. Therefore, if one follows the direction of flow beginning from some initial condition somewhere in the phase portrait, one can obtain the trajectory of the system. Fig. 2.7 (b) shows the time evolution of the u and v variables for a fixed values of the model parameters a and b.

When applying the phase field method, the boundary condition given in Eq. 2.18 is

incorporated into the circular boundary in Fitzhugh Nagumo model equation as follows.

$$
\frac{\partial u}{\partial t} = \frac{1}{\varepsilon} u(1-u)(u-a) - v) + \nabla \cdot (\nabla u) + \nabla(\ln \phi) \cdot (\nabla u) - (\nabla(\ln \phi) \cdot \vec{E})
$$
$$
\frac{\partial v}{\partial t} = bu - v
$$
(2.28)

In Cartesian co-ordinates, Eq. 2.28 are integrated on a gird size of 300×300 medium with no-flux boundary conditions on the domain boundaries using finite difference method. The central difference method is applied to calculate the five point Laplacian term $\nabla^2 u$ and the gradient terms. The space steps and time steps are $dx = dy = 0.1$ and $dt = 10^{-4}$ respectively. The value of ξ is taken to be 0.05.

2.5.2 Barkley Model

Barkley Model was proposed by Dwight Barkley in 1990 with an intention of performing very fast numerical simulations of spiral and scroll waves in excitable media. The dynamics of the model is similar to the Fitzhugh Nagumo model but has gained importance due to the reduced computational cost and extensions to the model proposed later (Bär and Eiswirth (1993)). The model equations are as follows:

$$
\frac{\partial u}{\partial t} = \frac{1}{\varepsilon}(u(1-u)(u - \frac{v+b}{a})) + D\nabla^2 u
$$
(2.29)

$$
\frac{\partial v}{\partial t} = u - v
$$
(2.30)

with a, b and ε as parameters of the model and D is the diffusion coefficient. The (u,v) phase space of the model is shown in Fig. 2.8. The stable fixed point of the model is at (0,0), indicating that the trajectories starting close to it will return to (0,0) immediately. This corresponds to a sub-threshold stimulation. However, the trajectories beginning to the right of the nullcline $u = u_{th} = \frac{v+b}{a}$ will make a long roundabout before settling at the fixed point. This process corresponds to a supra-threshold stimulation and the resulting action potential. The significance of the three parameters of the model can be determined directly from the phase space diagram. At rest, the ratio b/a gives

the excitation threshold. The parameter a sets the width of action potential, and the parameter ε determines the time scale between the variables u and v.
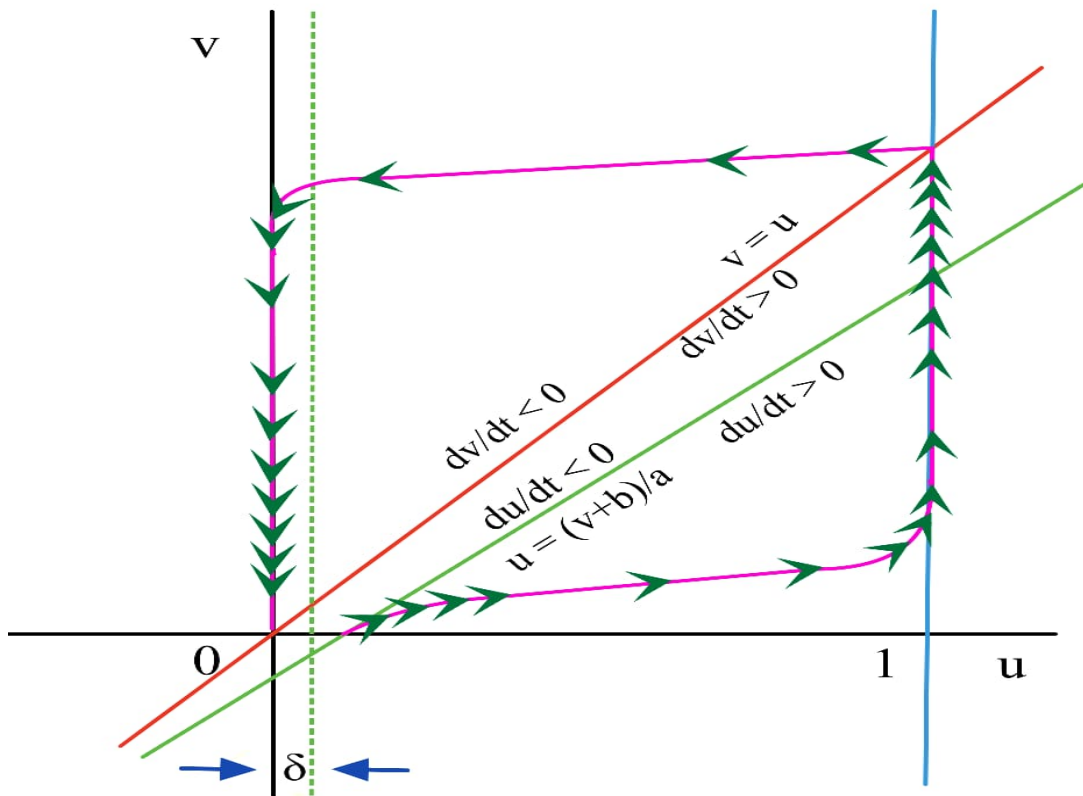
Figure 2.8: **Phase portrait of Barkley model.** Nullclines of the model are shown: The straight line $v = u$ corresponds to the v nullcline and the lines $u = 0$, $u = 1$ and $u = \frac{v+b}{a}$ corresponds to u nullclines. The point $(0,0)$ denotes an excitable fixed point. The parameter δ, introduced to speed up the computation, corresponds to a boundary layer which determines the state of the system. If the system is inside the boundary layer, its recovering and if its outside, its excited.

2.6 Time Stepping Scheme

Reaction diffusion equations most often display the change in the concentration of one or more chemical substances in space and time. Mathematically, reaction-diffusion

equations are parabolic partial differential equations which can be represented as follows,

$$\frac{\partial \mathbf{u}}{\partial t} = D\nabla^2\mathbf{u} + \mathbf{R}(\mathbf{u}) \tag{2.31}$$

where, $\mathbf{u}(\mathbf{r},\mathbf{t})$ is a vector of concentration variables, D is the matrix of diffusion coefficients and $\mathbf{R}$ describes all the local reaction kinetics. Eq. 2.31 is an initial value problem defined on a spacial domain $\mathcal{D}$. So, if the initial field, $\mathbf{u}(\mathbf{r},\mathbf{t}=\mathbf{0})$ and the appropriate boundary conditions are given, $\mathbf{u}(\mathbf{r},\mathbf{t})$ can be determined for $t \in [0,T]$. Suppose we seek the solution of $\mathbf{u}(\mathbf{r},\mathbf{t})$ for a time interval $0 < t < T$ in the domain having dimensions $[0,L_x] \times [0,L_y] \times [0,L_z]$, where L_x, L_y and L_z are the length of the domain along x, y and z directions. As a first step, we generate a mesh with discretization steps dx, dy and dz in three spatial directions and dt in time as follows;

$$
\begin{aligned}
0 &= x_0 < x_1 \cdots < x_{n_x} = L_x \\
0 &= y_0 < y_1 \cdots < y_{n_y} = L_y \\
0 &= z_0 < z_1 \cdots < z_{n_z} = L_z
\end{aligned}
\tag{2.32}
$$

The temporal domain $[0,T]$ is discretized as,

$$0 = t_0 < t_1 \cdots < t_{n_t} = T \tag{2.33}$$

The solution $u(x,y,z,t)$ is known only on the grid points (x_i, y_j, z_k) with $i = 0,\ldots,n_x$, $j = 0,\ldots,n_y$ and $k = 0,\ldots,n_z$. We approximate $u(x,y,z,t)$ by a discrete function $u_{i,j,k}^n$. At any spatial grid, the time derivative is calculated using forward Euler of forward time centered-space (FTCS) scheme as follows,

$$\frac{\partial u}{\partial t} = \frac{u_{i,j,k}^{n+1} - u_{i,j,k}^n)}{dt} \tag{2.34}$$

2.6.1 Approximation of the Laplacian

For a sufficiently smooth u we can write,

$$u(x+dx,y,z,t) = u(x,y,z,t) + dx\frac{\partial u}{\partial x} + \frac{dx^2}{2}\frac{\partial^2 u}{\partial x^2} + \mathcal{O}(dx^3) \tag{2.35}$$

$$u(x-dx,y,z,t) = u(x,y,z,t) - dx\frac{\partial u}{\partial x} + \frac{dx^2}{2}\frac{\partial^2 u}{\partial x^2} + \mathcal{O}(dx^3) \tag{2.36}$$

Adding Eqs. 2.35 and 2.36 together we get,

$$u(x+dx,y,z,t) + u(x-dx,y,z,t) = 2u(x,y,z,t) + dx^2\frac{\partial^2 u}{\partial x^2} + \mathcal{O}(dx^4 \tag{2.37}$$

Ignoring the $\mathcal{O}(dx^4)$ term and rewriting Eq. 2.37 we get the x component of the Laplacian,

$$\frac{\partial^2 u}{\partial x^2} = \frac{u(x+dx,y,z,t) - 2u(x,y,z,t) + u(x-dx,y,z,t)}{dx^2} \tag{2.38}$$

Note that one can derive the same for y and z components, which together gives the approximation for the Laplacian as follows,

$$\begin{aligned}\nabla^2 u(x,y,z,t) = {} & \frac{u(x+dx,y,z,t) - 2u(x,y,z,t) + u(x-dx,y,z,t)}{dx^2} + \\ & \frac{u(x,y+dy,z,t) - 2u(x,y,z,t) + u(x,y-dy,z,t)}{dy^2} + \\ & \frac{u(x,y,z+dz,t) - 2u(x,y,z,t) + u(x,y,z-dz,t)}{dz^2}\end{aligned} \tag{2.39}$$

This approximation for the Laplacian is handy because it contains only u at the current time step t.

Therefore, combining Eq. 2.34 and Eq. 2.39, the algebraic version of Eq. 2.31 can be written as follows,

$$\frac{u_{i,j,k}^{n+1} - u_{i,j,k}^{n})}{dt} = \frac{u(x+dx,y,z,t) - 2u(x,y,z,t) + u(x-dx,y,z,t)}{dx^2} +$$
$$\frac{u(x,y+dy,z,t) - 2u(x,y,z,t) + u(x,y-dy,z,t)}{dy^2} + \qquad (2.40)$$
$$\frac{u(x,y,z+dz,t) - 2u(x,y,z,t) + u(x,y,z-dz,t)}{dz^2} + R_{i,j,k}^n$$

2.6.2 Stability of scheme

The Barkley model and Fitzhugh Nagumo model equations used in this thesis to simulate excitable medium have a significant separation in Spatio-temporal scales. The time scale on which the transmembrane voltage u changes in Eq. 2.25 and Eq. 2.29 as the system becomes excited is several orders of magnitude faster than the v variable. In mathematics, such systems are called stiff differential equations. The numerical methods, such as the Explicit Euler method used in this thesis, to solve stiff differential equations are known to cause numerical instabilities unless the time step size is small enough to resolve the fast dynamics of excitation.

Another possibility of instability in reaction diffusion systems occurs due to the diffusion term. The condition for stability for this case is given by Von Neumann stability criterion as follows:

$$\frac{Ddt}{dx^2} \leq \frac{1}{2d} \qquad (2.41)$$

where, d is the spatial dimensions. The condition in Eq. 2.41 is not fulfilled when the phase-field method is applied. In this method, the diffusion term is multiplied by the phase-field ϕ. It decays quite quickly at the boundaries of the domain and decays exponentially far from the domain with a length scale approximately equal to ξ, comparable to the grid spacing dx. Therefore, the normal derivative of the phase-field can be written as $\frac{d\ln\phi}{dn} \lesssim \frac{1}{\xi}$. This leads to an advection-like term with a velocity given by $|v| \lesssim \frac{D}{\xi}$. The stability condition for an advection equation using an explicit time-stepping scheme is called Courant - Friedrichs - Lewy criterion. It is given as follows:

$$1 \geq \frac{|v|\Delta t}{dx} \gtrsim \frac{D\Delta t}{\xi dx} \tag{2.42}$$

The values of ξ in this thesis is restricted to $(\frac{dx}{2}, dx)$.

2.6.3 Spiral Tip Detection

The tip of the spiral wave in the Barkley and Fitzhugh Nagumo model is defined to be a point in space where $f(u = 1/2, v) = 0$. i.e. the point where $f = 0$ on the $u = 1/2$ contour of the spiral solution (Barkley (1995)). The tip condition is defined this way because it is easier to calculate it numerically from the u and v fields. According to the above definition, the tip (x, y) is defined implicitly by $f_1(x, y) = f_2(x, y) = 0$. For Barkley model $f(u, v) = u(1-u)(u - \frac{v+b}{a})$. So, the functions f_1 and f_2 are as follows: $f_1 = u(x, y) - u_{contour}$ and $f_2 = v(x, y) - v_{contour}$, where $u_{contour} = 1/2$ and $v_{contour} = a/2 - b$. For Fitzhugh Nagumo model, $f(u, v) = u(1-u)(u - a) - v$. Using the above definition for the tip, we obtain, $f_1 = u(x, y) - u_{contour}$ and $f_2 = v(x, y) - v_{contour}$ where $u_{contour} = 1/2$ and $v_{contour} = 1/8 - a/4$.
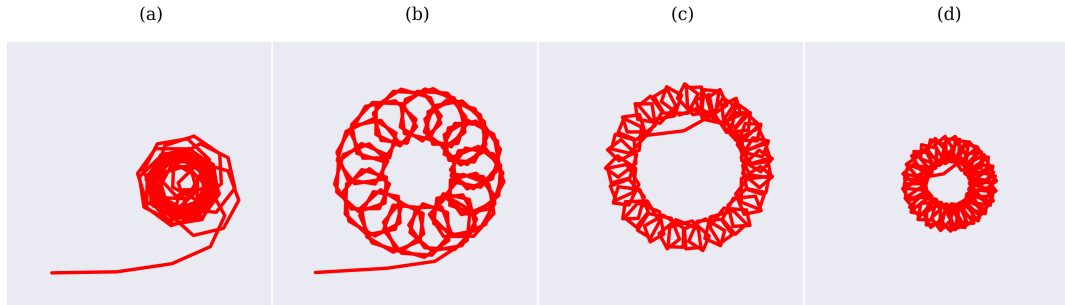
Figure 2.9: **The spiral tip trajectories in Barkley model.** The parameter values are $b = 0.05$, $\varepsilon = 0.02$ and **(a)** a = 0.56, **(b)** a = 0.58, **(c)** a = 0.69 and **(d)** a = 0.72.

The tip of the spiral is numerically determined by custom software written in dd Two-dimensional Newton's method is used to determine the root (x, y). The derivatives in newton's method are determined by the finite difference method. The u and v fields are approximated using the Lagrangian interpolation method with polynomials of order 3. The Python code used to find the spiral's tip is given in the appendix A.

2.6.4 Hardware, Software, Parallelization

The numerical simulation for this thesis was carried out on the following computers.

1. Macbook Pro (13 inch, Mid 2012), 2.5GHz dual-core Intel Core i5 processor (Turbo Boost up to 3.1GHz) with 3MB L3 cache, 8GB of 1600MHz DDR3 memory.

2. HP Z640 Workstation, Intel Xeon(R) CPU E5-2620 v3 Processor with 2.40GHz x 12, 12GB of 1600MHz DDR3 memory and GeForce GT 730/PCle/SSE2 Graphics.

3. DEL Power Edge R740 2U Rack server with Processor: 2 no's x Intel Xeon Silver 4108 1.8G, 8Core/16Tread, 9.6GT/s 2UPI, 11M Cache, Turbo, HT (85W) DDR4-2400. 384 GB RAM, 12 no's x 32GB DDR4 2400MHz (2Rx8) ECC RDIMM 2666/MT/s. SSD: 1 no x 480GB SSD SATA Read Intensive 6Gbps 512n 2.5in Hot-plug Drive, 8 no's x 600GB Hard Drive,15000RPM,2.5",SAS 12Gbps 512n (approximate 4.2TB of after RAID configured raw space).

All the computers run Unix operating system. The operating systems used are MacOS, Ubuntu and CentOs. All the codes used in this thesis are self-written in either python, C or C++ language. Post-processing is done using standard python libraries such as matplotlib and Mayavi. The parallelization was done using python's message passing interface library called mpi4py.

Chapter 3

Unpinning spiral waves anchored to two obstacles

In this chapter, the effect of the additional wave emitting site on the unpinning window of the spiral is studied for a special case where the spiral wave is pinned to both the obstacles. The study shows that the unpinning window decreases as the distance between the obstacles increases, and beyond a critical distance, the window completely vanishes.

3.1 Introduction

In many physiological systems, a wave of excitation coordinates the functioning of millions of cells that constitute the system. The excitation is produced locally within each cell, hence as long as the cells are excitable, the wave can travel without any attenuation. Waves of this type are found in a variety of systems, including in chemical reactions (Jahnke et al. (1989)), social amoebae (Gregor et al. (2010)), and in physiological tissue such as brain (Huang et al. (2004)), heart (Davidenko et al. (1992)), retina (Yu et al. (2012)), and uterus (Singh et al. (2012)). Two important properties of these waves are: (1) The conduction velocity of excitation waves depends on the curvature of the

wave, i.e., convex waves travel slower than plane waves, whereas concave waves travel faster than plane waves. (2) After excitation, the tissue remains inactive for a characteristic period called the refractory time. Because of the propagation properties, excitation waves can form a spiral shape and rotate indefinitely in the supporting medium (Karma (2013)). Such rotating waves are often associated with functional disorders in physiological tissue, such as reentrant electrical activity in the heart during cardiac arrhythmias (Tung et al. (2008)). In the heart, rotating waves of excitation are known to cause fatal cardiac arrhythmia such as Ventricular Tachycardia (VT) and Ventricular Fibrillation (VF). During tachycardia, a cardiac excitation wave rotates in the tissue overriding the natural rhythm set by the heart's pacemaking cells. During fibrillation, these rotating waves break up and form multiple wavelets, leading to irregular ECG patterns. The irregular propagation of the excitation waves causes asynchronous and irregular contraction of muscles in the heart. Hence it is important to devise methods to eliminate them.

Electrical shocks were known to terminate VF for more than 100 years (Prevost (1899)). With the advent of technology in the last half of the century, external high voltage defibrillators were made available to a greater population (Zoll et al. (1956)). The current clinical standard for the treatment of VF is to deliver biphasic shocks ($\sim$1kV, 12ms, 30A) (Otani et al. (2019)) either using the electrode panels placed on the chest (Ley (2019)) or through an implantable cardioverter-defibrillator (ICD's). The high voltage shock depolarizes the entire heart at once for a short period of time, pushing it into a refractory state and eliminating all excitation at once. Even though this technique is reliable and life-saving, the physical pain and the psychological distress caused to the patient are immense (Tung (1996)). It can also damage the tissue causing scars, leading to the dysfunction of the myocardium (Al-Khadra et al. (2000), Cook et al. (2013), Bradfield et al. (2012)). Since the demerits of high voltage shocks became known, considerable efforts have been put into developing effective defibrillation with much lower voltages. Initial studies in the field led to the elimination of monophasic waveforms and the use of biphasic waveforms (Mittal et al. (1999), Clark et al. (2002)). Recent studies using a train of low voltage pulses having millisecond (Rantner et al. (2013), Luther

et al. (2011)) and nanosecond duration (Varghese et al. (2017)) have shown promising results in achieving low voltage defibrillation.

In a method called Anti Tachycardia Pacing (ATP), low-intensity pulses are given far away from the spiral core. These pulses generate target waves emanating from the location of the stimulus electrode. If the pacing frequency is higher than the frequency of the spiral, these target waves can push the spiral wave away from the medium (Ripplinger et al. (2006)). The success rate of ATP is found to be $60 - 90\%$ (Pumir and Krinsky (1999)). While they are able to remove freely rotating spirals in a heterogeneous medium, excitation waves tend to form a stable rotating pattern around a heterogeneity in the medium. This is known as wave pinning (Davidenko et al. (1992), Valderrábano et al. (2001), Bub et al. (2002)). If not unpinned, these pinned spirals can rotate indefinitely (Luther et al. (2011)). It is therefore imperative to find optimal conditions and device efficient methods to unpin them. Further details about cardiac arrhythmia and available therapies are discussed in chapter 1, section 1.2.1.

To unpin the spiral from an obstacle, the stimulus has to be applied in the refractory tail, close to the core of the spiral wave (Bittihn et al. (2012), Shajahan et al. (2016), Takagi et al. (2004), Hörning et al. (2009), Bittihn et al. (2010)). This narrow time window, where the spiral unpins, is called the unpinning window of the spiral. The stimulus delivered in this unpinning window will nucleate a wave that can travel only in the direction opposite to the spiral due to the refractory property of the excitable media. Eventually, the wave nucleated by the stimulus and the spiral will collide head-on and annihilate each other, unpinning the spiral. To get the stimulus delivered to the core of the spiral wave, we use a technique called Far Field Pacing (FFP) (Bittihn et al. (2008)). When a low voltage global electric field is applied across a medium with obstacles, depolarization and hyperpolarisation regions form on either side of the obstacles. These regions are called Weidmann Zones (Pumir and Krinsky (1999)). Above a threshold value of the electric field, the depolarization region can nucleate an excitation wave. A stimulus delivered so that the wave it nucleates will fall into the unpinning window can unpin the spiral wave. Unpinning of a wave attached to a single obstacle has been extensively studied using FFP by (Takagi et al. (2004), Pumir et al. (2007), Bittihn

et al. (2010)). The unpinning success using velocity restitution effects in detailed cardiac models is done by (Isomura et al. (2008)). The pinned spiral waves' response to the periodic stimuli is carried out in detail by (Behrend et al. (2010), Shajahan et al. (2016)) where an alternative and robust approach to finding the pacing frequencies for unpinning is discussed.

In this chapter, we study the effect on the unpinning window by introducing a second obstacle near the central obstacle. We study the special case of unpinning where the spiral tips are attached to both the obstacles. By delivering low voltage stimulus at different phases of the spiral and systematically changing the distances between the two obstacles, we try to understand the unpinning window of the two obstacle system.

3.2 Methods

All the simulations in this chapter are carried out using the Barkley Model (Barkley (1991)), which is a modified Fitzhugh-Nagumo type model proposed by Dwight Barkley to simulate cardiac action potential efficiently. For more details, see chapter 2, section 2.5.2.

For the purpose of this study, the parameters of the model are set to $a = 0.53$, $b = 0.05$ and $\varepsilon = 0.02$ throughout the simulations. The Barkley model equations are solved in a 300×300 computational grid using forward Euler method. A five-point stencil is used to compute the Laplacian (see chapter 2, section 2.6). Neumann boundary conditions are implemented at the domain boundaries to ensure no flux escapes out of the boundary. The computation is carried out using a spatial resolution $dx = 0.1$ and Euler time step $dt = 0.001$. The Euler scheme's accuracy has been tested systematically for smaller spatial resolutions ($dx = 0.05, 0.01$), and the quantities such as action potential duration and wavelength of the spiral are found to agree with each other. The electric field is applied using no-flux boundary conditions (Pumir and Krinsky (1999)) given below

$$\hat{y} \cdot (D\nabla u - \vec{E}) = 0 \qquad (3.1)$$
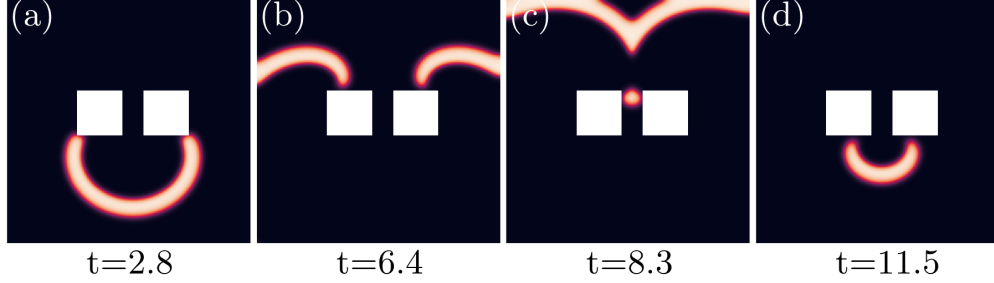
Figure 3.1: **Initial conditions.**
Spiral wave with its tip attached to both the obstacles. The obstacles are at a distance 0.625λ apart, where λ is the wavelength of the spiral wave. We treat this spiral as our initial condition for all the simulations.

$\hat{y}$ is a unit vector perpendicular to the obstacle boundary, D is the coupling constant, and $\vec{E}$ is the applied electric field. The Neumann boundary conditions in Eq. 5.1 can be implemented easily since the boundaries of the obstacle are parallel to the co-ordinate axis. In the simulations, we apply the electric field along the y-axis. Then, Eq. 5.1 becomes:

$$D\frac{\partial u}{\partial y} = E_y \tag{3.2}$$

The strength of the electric field is set to $\vec{E} = 3$ units and the pulse duration is set to 0.5. All the distances in this chapter are measured in terms of the wavelength ($\lambda = 48$) of the spiral. The the wavelength of the spiral is the number of space steps between the wavefront and the wave back.

3.3 Results and Discussions

To study unpinning in the presence of multiple obstacles, we simulated a wave attached to two obstacles in a medium as shown in Fig. 3.1. The wave rotates with a period of 10. In Fig. 3.1 the obstacles are at a distance 0.625λ apart. We define the phase as the spiral position at the time of the pulse in one complete spiral period. So, $\Phi \in [0, 1]$.

To determine the unpinning window of the above-mentioned spiral, we deliver a low
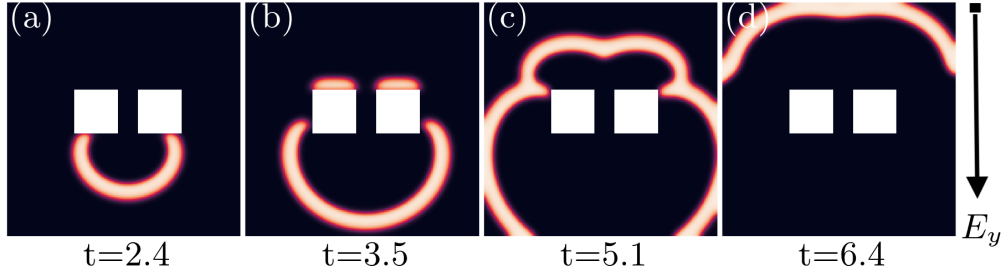
Figure 3.2: **Successful unpinning of the spiral wave attached to both the obstacles.** The FFP stimulus makes the obstacles emit secondary excitations at t=3.5. The tips of the secondary excitation and the spiral wave meet at t=5.1, which results in their annihilation. The wave is unpinned and moves away to the boundary, as shown at t=6.4.

voltage electrical stimulus along the negative y-axis (as shown in Fig. 3.2) at different phases of the spiral. After the application of the electric field, the secondary waves are nucleated at t=3.5 due to the phenomenon of Wave Emission from Heterogeneity (WEH) (Bittihn et al. (2012)). The emitted wave will then successfully unpin the spiral wave, as shown in Fig. 2 (d).

The unpinning shown in Fig. 3.2 is unique because the secondary excitation is not nucleated in the refractory tail of the spiral. Instead, the secondary excitation is nucleated from the top of the two obstacles. After the wave nucleation, there are four tips in total. The tips of the secondary excitation close to the spiral tips will collide and annihilate each other. The remaining two tips of the secondary excitation will also collide with each other at t=5.1 and move away from the obstacles, unpinning the spiral.

The unpinning mechanism mentioned above happens only in the small region in the phase window of the spiral. We call it the unpinning window of the two obstacle system. However, if the spiral tips and the tips of the secondary excitation do not meet exactly, then they do not annihilate completely. This leaves a portion of the wave which later develops and ends up pinning to one or either of the obstacles. The snapshots of failed unpinning due to the above-mentioned reason is shown in Fig. 3.3 (a-d).

In Fig. 3.3 (e-h), we show another case where the spiral fails to unpin from the obstacle. Here, the distance between the obstacles is increased to 1.014λ. As the dis-
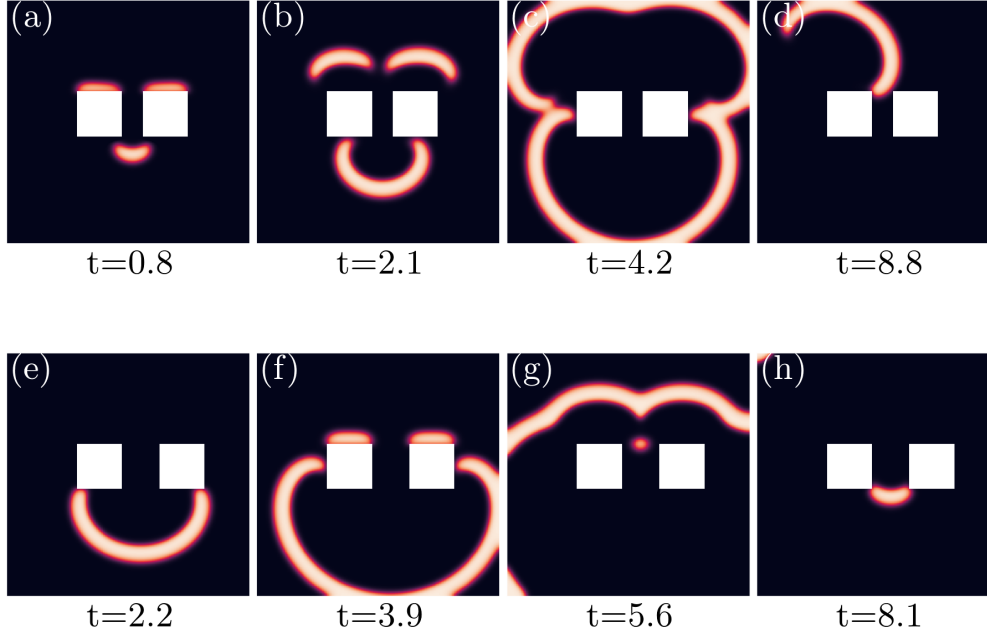
Figure 3.3: **Cases of unsuccessful unpinning.** In figure **(a - d)** the spiral tips on the left do not collide with each other perfectly. Due to imperfect collision wave which survives in the medium later develops into a pinned spiral as shown in fig **(d)**. In fig **(e - h)** the distance between the obstacles has been increased to 1.014λ. This allows the secondary excitations from the obstacles to develop more curvature which results in incomplete unpinning. The resulting wave will attach to both the obstacles as shown in Figure **(h)**.

tance between the obstacle increases, the tips generated from the secondary excitations will continue to collide and annihilate with the tips the spiral. However, the tips of the secondary excitations will have to move a more significant distance before they collide and annihilate. The increase in distance will give them more time to develop curvature so that their tips do not coincide with each other exactly. The wave left out due to inefficient collision will develop into a new pinned spiral wave as shown in Fig. 3.3 (h).

The above-mentioned unpinning mechanism shows that the spiral wave attached to both the obstacles does not have a conventional unpinning window, but it does have an unpinning window of its own. We plot a graph that indicates the unpinning window as a function of the distance between the obstacles corresponding to the electric field
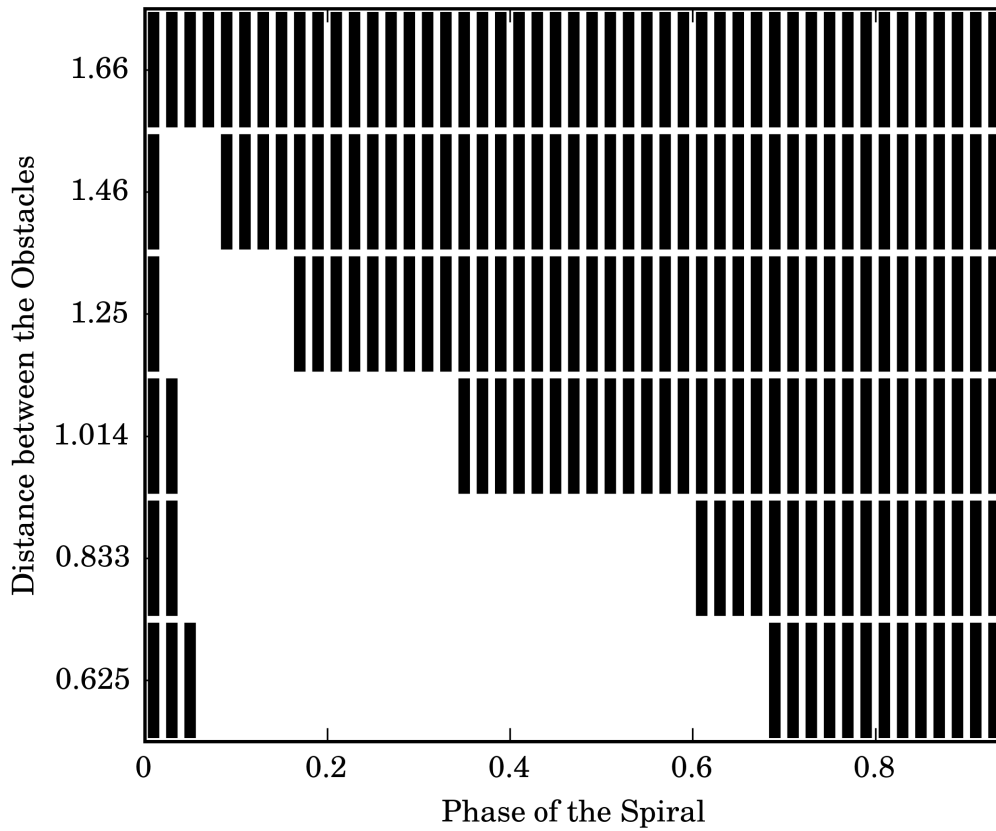
Figure 3.4: **Unpinning window of the two obstacle system.** White coloured grids indicate unpinning and black grids indicate failed unpinning. Distance between the obstacles is measured in terms of spiral wavelength. The stimulus is given every 0.2 for six different distances. The graph shows that the unpinning window decreases as the distance between the obstacles increases.

stimulus being applied at different spiral phases. From the graph, we observe a large unpinning window at lower distances between the obstacles. This success in unpinning can be attributed to the mechanism explained in Fig. 3.2. The unpinning window reduces as the distance between the obstacles increases. This is because of the unsuccessful cases mentioned in Fig. 3.3. After a certain distance, d = 1.46 λ, the window vanishes completely.

3.4   Conclusions

In this chapter, we have discussed wave unpinning from two obstacles. Here, we studied a special case of unpinning where the spiral tips are attached to both the obstacles. We have shown that the chances of unpinning, as quantified by the unpinning window, decreases as the distance between obstacles increase. After a critical distance, unpinning fails. Our results show that to unpin a spiral anchored to both the obstacles, it is not essential that the stimulus delivered falls into the spiral's refractory tail. It is sufficient if the tips of the secondary excitation will annihilate with the tips of the spiral wave.

Our results will be relevant in deciding FFP based methods for low energy fibrillation. In particular, the distribution of heterogeneities can play a critical role in deciding the unpinning window. The presence of neighbouring heterogeneities can alter the length of the unpinning window. The more general case of unpinning where the spiral is pinned to just one obstacle is considered in the next chapter (see chapter 4).

Chapter 4

Spiral wave unpinning facilitated by wave emitting sites in cardiac monolayers

---

In this chapter, the effect of the additional wave emitting site on the unpinning window of the spiral is studied for a general case where the spiral is pinned to a single obstacle. The chapter includes the numerical results and the experimental studies performed on cardiac monolayers.

The spiral waves can be unpinned from an obstacle if an electric stimulus is delivered very close to the pinning centre and within a specific time interval called the unpinning window (UW), i.e. the stimulus has to be within a narrow spatial and temporal window . As discussed in chapter 3 it is possible to generate secondary excitations from heterogeneities in the tissue using electric field pulses (Krinsky et al. (1995), Bittihn et al. (2010)). Since these excitations are generated from possible pinning centres, they can appear close to the core of the spiral and hence solve the problem of spatial location. However, the pulses still have to be generated within the unpinning window of the wave. Recently, many groups have started using periodic field pulses to increase the chances of unpinning, and these are found to be very effective in LEAP (Li et al.

(2009), Luther et al. (2011)). Studies so far have focused on unpinning a rotating wave by secondary excitations emanating from the pinning centre itself (except a paper by Tom Wörden *et al.*, which studied control of multiple pinned spirals in an excitable media (tom Wörden et al. (2019))). However, these studies show that unpinning window is quite narrow compared to the experimental studies in the intact heart. (Shajahan et al. (2016), Luther et al. (2011)). Apart from the three-dimensional nature of the heart, we hypothesized that the presence of multiple wave emitting sites in the cardiac tissue could be one of the factors affecting the width of the unpinning window. This induced us to study the role of multiple wave emitting sites in the unpinning process. Also, multiple heterogeneities in close vicinity offer the possibility of additional stimulus sites and additional anchoring sites. In such cases, one needs to examine how the distribution of heterogeneities modifies the unpinning window. Despite their critical importance in low energy antifibrillation techniques, this problem has not received much attention. In a recent paper by Tom Wörden and colleagues have looked at how multiple pinned waves can be unpinned simultaneously (tom Wörden et al. (2019)). We study how these additional obstacles can alter the unpinning of a single spiral.

This chapter shows that secondary excitations emanating from nearby heterogeneities can unpin a wave attached in the vicinity in monolayers of cardiac cells. We then undertake a detailed numerical study of the wave unpinning in the presence of two heterogeneities. We found that the unpinning window either increases or decreases in the presence of additional heterogeneity. Their influence depends on their orientation with respect to the electric field, distance from the obstacle, and the size. Along certain orientations, unpinning fails.

4.1 Methods

4.1.1 Experiments

The experiments were conducted in a monolayer of cardiac myocytes extracted from chicken embryos, prepared as described in (Borek et al. (2012), Schlemmer et al. (2015)) and plated as circular disks of 10 mm diameter.

A hole with 2 mm diameter was drilled in the middle of the glass plate, creating a central heterogeneity without any cells. Rotating waves were initiated in the monolayer by high-frequency field pacing. The excitation of the cardiac myocytes was tracked using a calcium-sensitive dye (Calcium Green, Invitrogen), and the resulting calcium waves were mapped with an Olympus MVX10 microscope and a Photometrics Cascade 512 EMCCD camera. Custom written software was used for data acquisition and further analysis.

During the experiment [1], the fluorescent signal was averaged over a small user-selected area and then it was smoothed using a bandpass filter. When this fluorescent activity from the pre-selected area of the monolayer exceeded a certain threshold, we applied electric field pulses at chosen phases of the rotating wave. The strength of the field varied from 1 V/cm to 5 V/cm and its frequency from 0.6 to 2.0 Hz and each stimulus lasted for 20 ms.
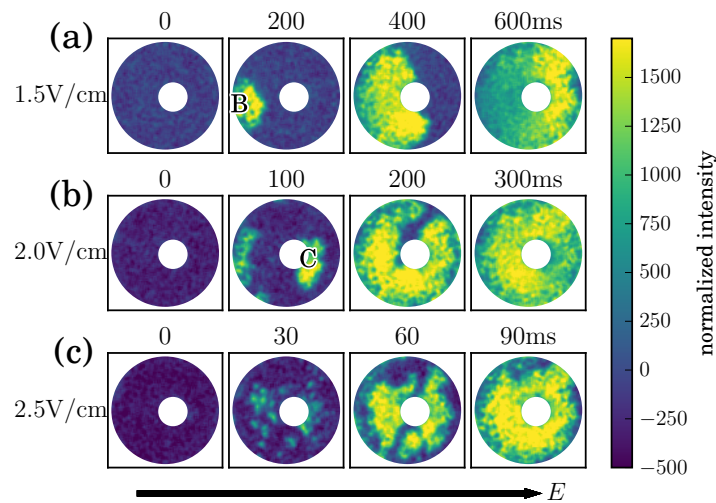
Figure 4.1: **An electric field pulse initiates multiple wave emitting sites in a cardiac cells monolayer**. The electric field $\mathbf{E}$ is applied from left to right at $t = 0$ s. **(a)** At $\mathbf{E} = 1.5$ V/cm, waves are emitted only from the monolayer outer boundary (B), see $t = 200$ ms. **(b)** At $\mathbf{E} = 2$ V/cm, the outer monolayer boundary (B) and the obstacle at the center (C) are emitting waves. **(c)** At 2.5 V/cm, excitation can also originate from smaller heterogeneities in the monolayer. Note that full excitation occurs much earlier in (c).

---

[1]The experiments are performed by Dr. T. K. Shajahan and Dr. Sebastian Berg in Max Planck Institute for Dynamics and Self-Organization, Göttingen, Germany. It is included in the thesis for the reason of continuity only.

4.1.2 Mathematical Model

We use the Fitzhugh Nagumo model (FHN) to simulate the spiral wave in a two-dimensional medium. The model equations are as follows.

$$\frac{\partial u}{\partial t} = \frac{1}{\varepsilon}(u(1-u)(u-a)-v) + D\nabla^2 u \tag{4.1}$$

$$\frac{\partial v}{\partial t} = bu - v \tag{4.2}$$

where u and v stands for transmembrane voltage and gating variable respectively. The parameter values are chosen as $a = 0.085$, $b = 0.25$ and $\varepsilon = 0.045$. The space and time coordinates are discretized for a spatial step of $\Delta x = \Delta y = 0.1$ and time step of $\Delta t = 0.0001$. We use square domain of grid size 300x300. For presentation purpose, we postulate the time units to 20 ms and space units to 1 mm. That is, 1 the time step is equivalent to 0.002 ms, and 1 grid space is equivalent to $(1/10)$ mm. The diffusion coefficient D is set to $1\text{cm}^2/\text{s}$. With this choice of spatial and temporal scales, the wavelength and conduction velocity approximately match with those observed in the experiments. These equations are solved using the explicit forward Euler method in time and the five-point finite difference method in space. The Euler scheme's accuracy has been tested systematically for smaller spatial resolutions ($dx = 0.05, 0.01$), and the quantities such as action potential duration and wavelength of the spiral are found to agree with each other.

The no flux boundary condition with an applied field E is given by,

$$\hat{y} \cdot (D\nabla u - \vec{E}) = 0 \tag{4.3}$$

where $\hat{y}$ represents the unit vector along the direction of applied electric field $\vec{E}$ (V/cm). The boundary conditions are imposed on the obstacle boundary by the phase field method Fenton et al. (2005). The phase field (ϕ) modifies the Eq. 4.1 to:

$$\frac{\partial u}{\partial t} = \frac{1}{\varepsilon}(u(1-u)(u-a)-v) + \nabla \cdot (D\nabla u) + \nabla \ln \phi \cdot (D\nabla u) - \nabla \ln \phi \cdot \vec{E} \tag{4.4}$$

A spiral wave rotating in the clockwise direction is initiated in the medium. The wavelength of the spiral is $\lambda = 3.5\,mm$. It takes 328 ms to complete one free rotation around an obstacle of radius 3 mm located at the centre. Far-Field Pacing (FFP) shock of duration 0.8 ms is applied in a horizontal direction with a weak electric field of strength E_0= 1.2 V/cm. The electric field gives rise to secondary excitations that can potentially unpin the spiral. The spiral phase at the time of the stimulus is an important parameter that determines the unpinning window (Behrend et al. (2010)).

The phase here is the location of the wavefront of the pinned spiral at the time of the stimulus, with the zero of phase being the place of wave emission from the heterogeneity. The phases of the stimuli that lead to successful unpinning are the unpinning window.

To study the effect of an additional wave emitting site on the wave unpinning, we introduced a second obstacle. We considered the unpinning to be successful only if the spiral drifted away from both the obstacles at the end of one spiral period.

4.2 Experimental Results

Field stimulus induces wave emitting sites (WES) from boundaries of heterogeneities. There were two major boundaries in our experiments: the concave boundary of the entire monolayer and the convex boundary of the circular hole within the monolayer.

Fig. 4.1 shows wave emission from these boundaries as we increase the field strength. When the field strength is low (1.5 V/cm), only the concave outer boundary of the monolayer is excited. However, at $E = 2$ V/cm, both the outer monolayer boundary and the central obstacle boundaries are excited. At higher field ($E = 2.5$ V/cm), wave emission is observed even from small scale heterogeneities such as non-excitable cells such as fibroblasts and fluctuations in cell to cell connectivity, as predicted by previous theoretical studies (Pumir and Krinsky (1999), Hörning et al. (2012), Bittihn et al. (2012)). An attached wave can be unpinned by any of these excitations.
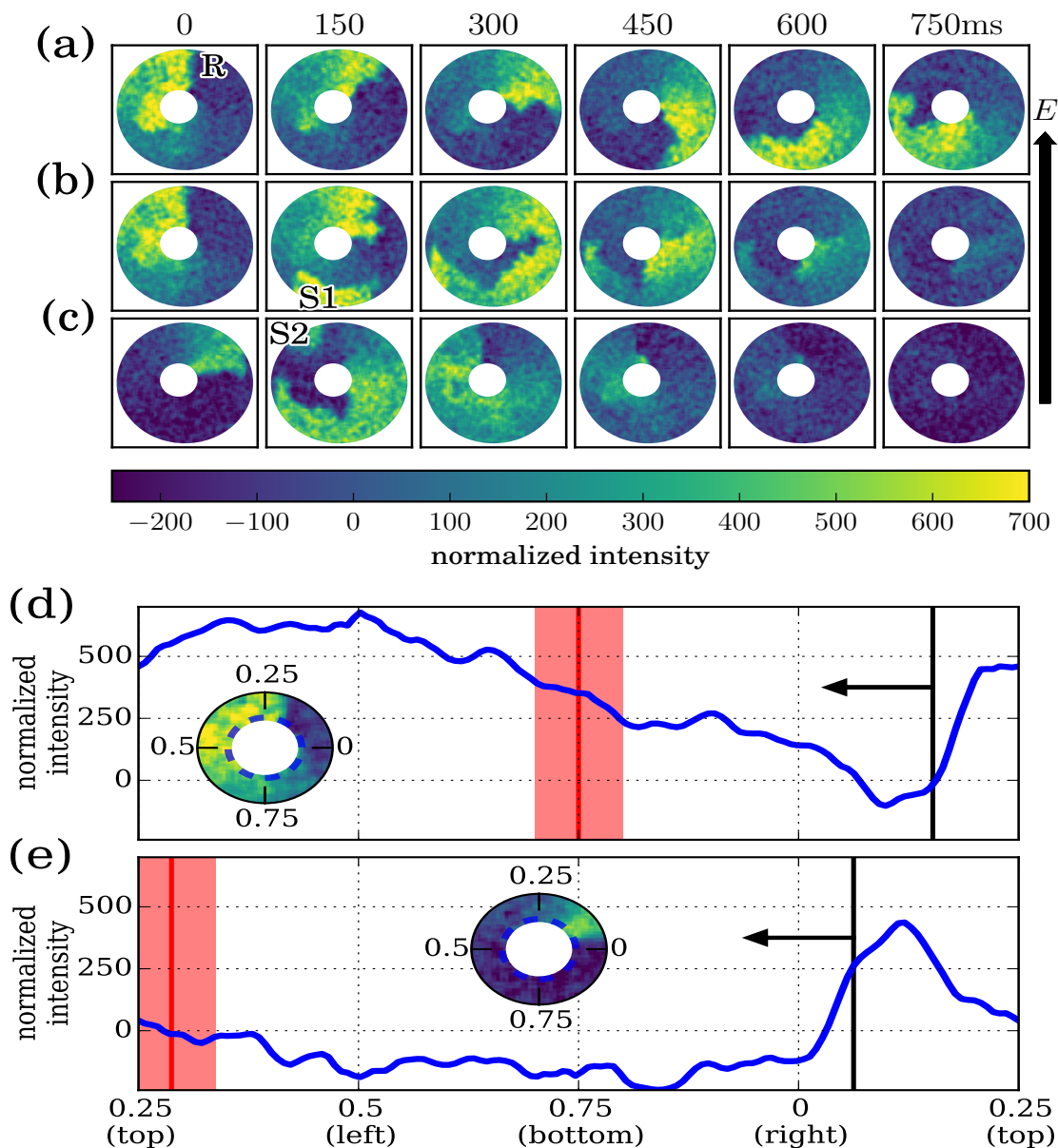
Figure 4.2: **Unpinning by two wave emitting sites in a cardiac cells monolayer.**
(a) A rotating wave R pinned to the obstacle. (b) A field stimulus is given from bottom
to top ($t = 0$). Wave emitted from the lower boundary (S1) moves opposite to wave R.
This would eventually collide and annihilate wave R. (c) The stimulus is applied when
the wave R is slightly more advanced. A second site (S2) from the top boundary also
gets excited by the stimulus ($t = 150$ ms), which terminates the rotating wave R. (d,
e) The rotating wave R along the circumference of the obstacle at the time of stimulus,
corresponding to the images in (b) and (c), respectively. The red line indicates the
location of the wave emission site (S1 or S2), and black line indicates the location of the
wavefront. The insets show the fluorescent activity directly around the heterogeneity,
indicating the corresponding phase.

However, if the medium is already excited, only some of the wave emission sites will

be active during a stimulus. For example, consider the monolayer in Fig. 4.2 (a), where an attached wave is rotating clockwise. When we apply an electric field (≈ 3 V/cm) directed vertically upwards, there can be wave emission from the lower boundary (S1, see Fig. 4.2 (b)) and the upper boundary (S2, Fig. 4.2 (c)). However, at the time of the stimulus, if any of these locations are refractory due to the passing of the rotating wave, those sites will not emit secondary excitation.

There is a short time window after the wave, such that secondary excitations in that window propagate only in the direction opposite to the rotating wave (Nomura and Glass (1996)). This is the unpinning window(UW). A stimulus within the unpinning window can unpin an attached wave. Thus, if either S1 or S2 gets activated in the rotating wave's unpinning window, the wave will be unpinned.
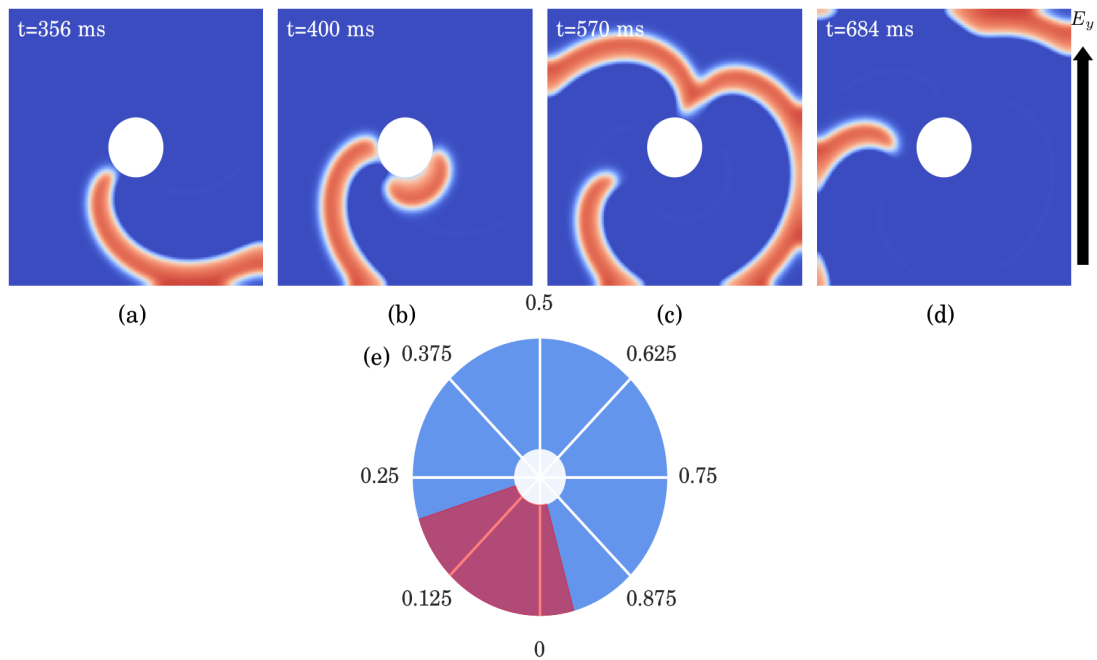
Figure 4.3: **Numerical simulations showing successful unpinning by FFP for a single obstacle.**: **(a)** A rotating spiral is pinned to an obstacle of radius 3 mm located at the centre of the domain. **(b)** Nucleation of secondary excitation from the obstacle when a pulsed stimulus is applied in a vertical direction as indicated by the black arrow on the right. **(c-d)** Detachment of pinned spiral from the obstacle. **(e)** Unpinning window of a single obstacle: Each angle inside the circle corresponds to the phase of the pinned spiral at the time of the stimulus. It is measured with respect to the point of secondary excitation represented by '0' in the figure. The red shaded sector indicates the unpinning window. All the simulations are done using Fitzhugh Nagumo model.

In Fig. 4.2 (b), the stimulus was applied when the wave is at the 12H location on the obstacle. Site S2 happened to be in the refractory tail of the wave, and S1 was activated within the unpinning window of the rotating wave, and the wave got unpinned. Another stimulus when the wavefront was at 3H (Fig. 4.2 (c)) excited both S1 and S2. Here S1 was fully excitable and could propagate both directions, but S2 was within the unpinning window and eliminated the rotating wave. Thus the UW enlarges when there are two wave emitting sites. Which of them participates in the unpinning event depends on the location of the rotating wave at the time of the stimulus.

4.3   Numerical Results

Numerical simulations are carried out to reveal the mechanisms underlying the complex interaction of excitable waves with obstacles and their effect on the unpinning window. In cardiac monolayers, the boundary of the monolayer acted as an additional wave emitting site. In the following section, we systematically study the effect of additional wave emitting sites by introducing another obstacle near the pinning centre.

In the following section, we systematically scrutinize the conditions for success and failure of unpinning by introducing an additional wave emitting site near the spiral core. Fig. 4.3 shows the unpinning of the spiral due to the secondary wave emitted from the single obstacle. We find the continuous phase window that leads to unpinning of the spiral to be 0.24.
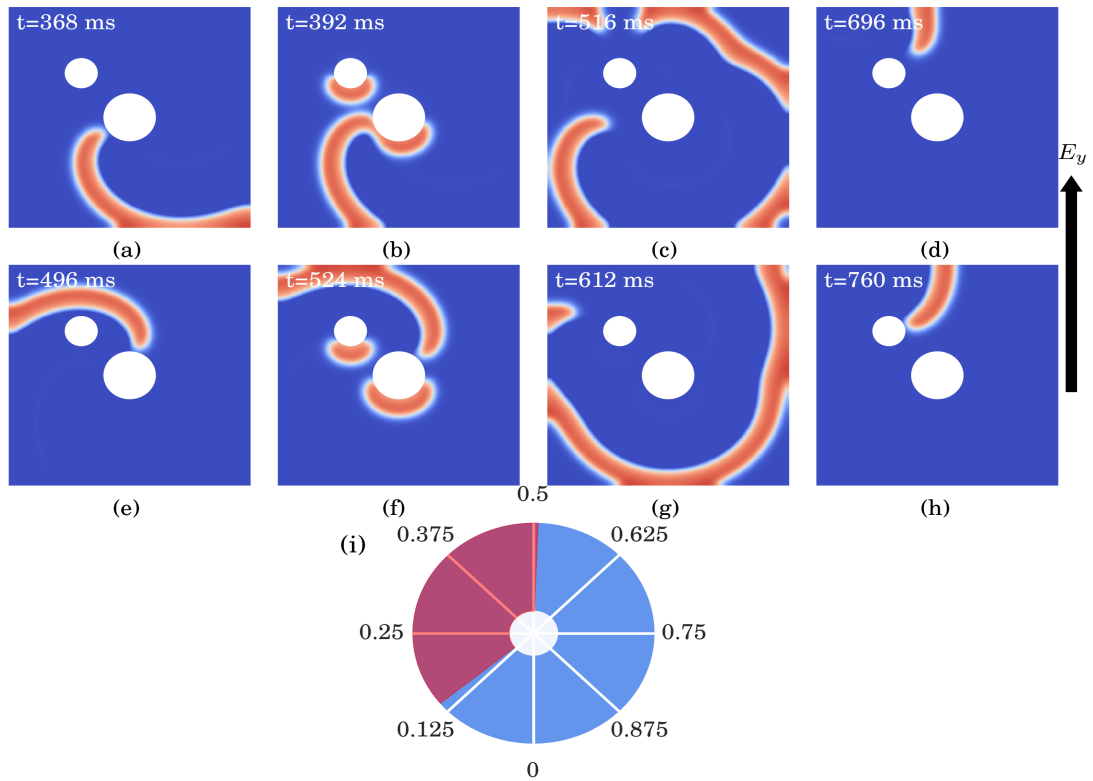
Figure 4.4: **Success and failure of unpinning of spiral pinned to an obstacle in the presence of the additional wave emitting site**: Black vertical arrow on the right indicates the direction of applied electric field of strength $E_0 = 1.2$ V/cm. **(a)** Spiral is pinned to an obstacle of radius 3 mm with second obstacle of radius 2 mm nearby. **(b)** Nucleation of secondary excitation by the application of short timed pulse. **(c-d)** Detachment of the original spiral from the obstacle resulting in successful unpinning. **(e)** Spiral wave pinned to the central obstacle at a different phase. **(h)** The spiral getting pinned back to the second obstacle leading to failure of unpinning. **(i)** The unpinning window for the above configuration of the obstacles.

To estimate the effect of the second wave emitting site on the unpinning window, we introduce a new obstacle of 2mm radius (Fig. 4.4). A global electric field now creates two excitable waves, one from each of the obstacle. Depending on the time at which the pulse is given, the spiral can (a) successfully unpin from the obstacle (Fig. 4.4 (d)) (b) detach but repin back to the second obstacle (Fig. 4.4 (g-h)) or (c) reattach to the first obstacle at a different phase. For the choice of the orientation of the obstacle considered in Fig. 4.4 the unpinning window is found to be 0.36, which is 50% more than that of the single obstacle unpinning window (Fig. 4.3 (b)).
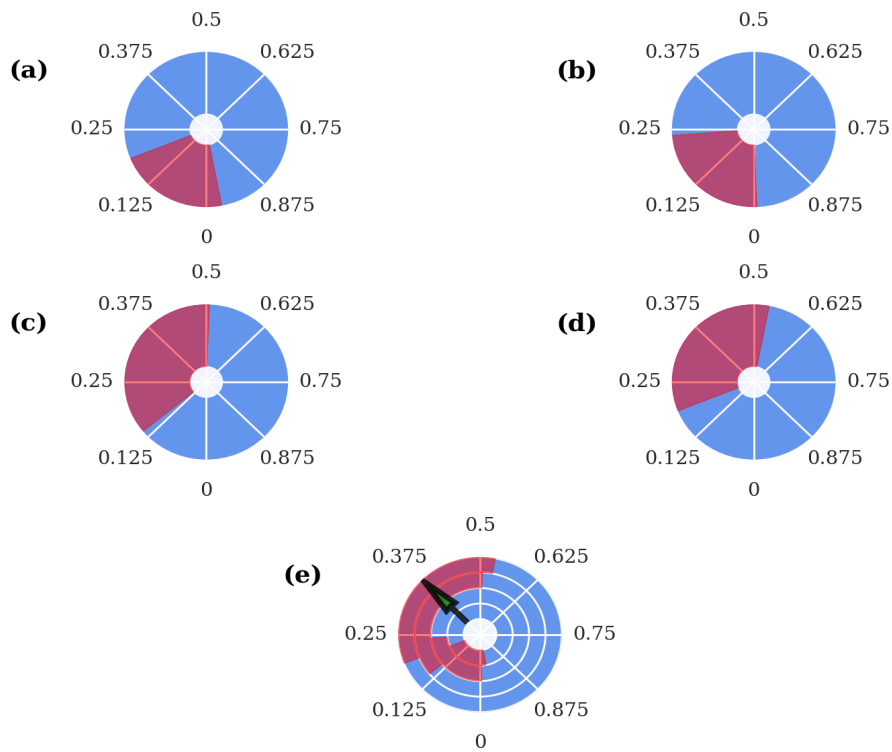
Figure 4.5: **Unpinning window for different distances of additional wave the emitting site around the central obstacle**: The orientation of the additional wave emitting site is as shown in Fig. 4.4. By keeping the radius of both the obstacle fixed, we change the second obstacle's distance from the first. The red shaded sectors in subplots **(a-d)** indicate the unpinning window for the distance between the obstacles 5.656 mm, 7.707 mm, 8.484 mm and 9.898 mm, respectively. Subplot **(e)** summarizes figures (a-d). The white shaded circular region at the centre of the obstacle indicates the central obstacle. The arrow indicates the orientation of the second obstacle. Each white concentric circle denotes the distance of the second obstacle from the central obstacle. The red shaded region corresponds to the unpinning window for a fixed distance between the two obstacles.

For a given orientation of the obstacle and fixed strength of the electric pulse, the width of the unpinning window critically depends on the distance of the second obstacle from the first. If the distance is very small, like in Fig. 4.5 (a), the unpinning window shrinks to 0.21 but widens significantly for larger distances. The variation of the unpinning window with distance is summarized in Fig. 4.5 (e). The reason for the shrinking of the unpinning window at smaller distances is because of the obstacles acting as a single entity when they are very close to each other. Owing to this merging of the obstacles, the spiral is able to sustain its pinned rotation.
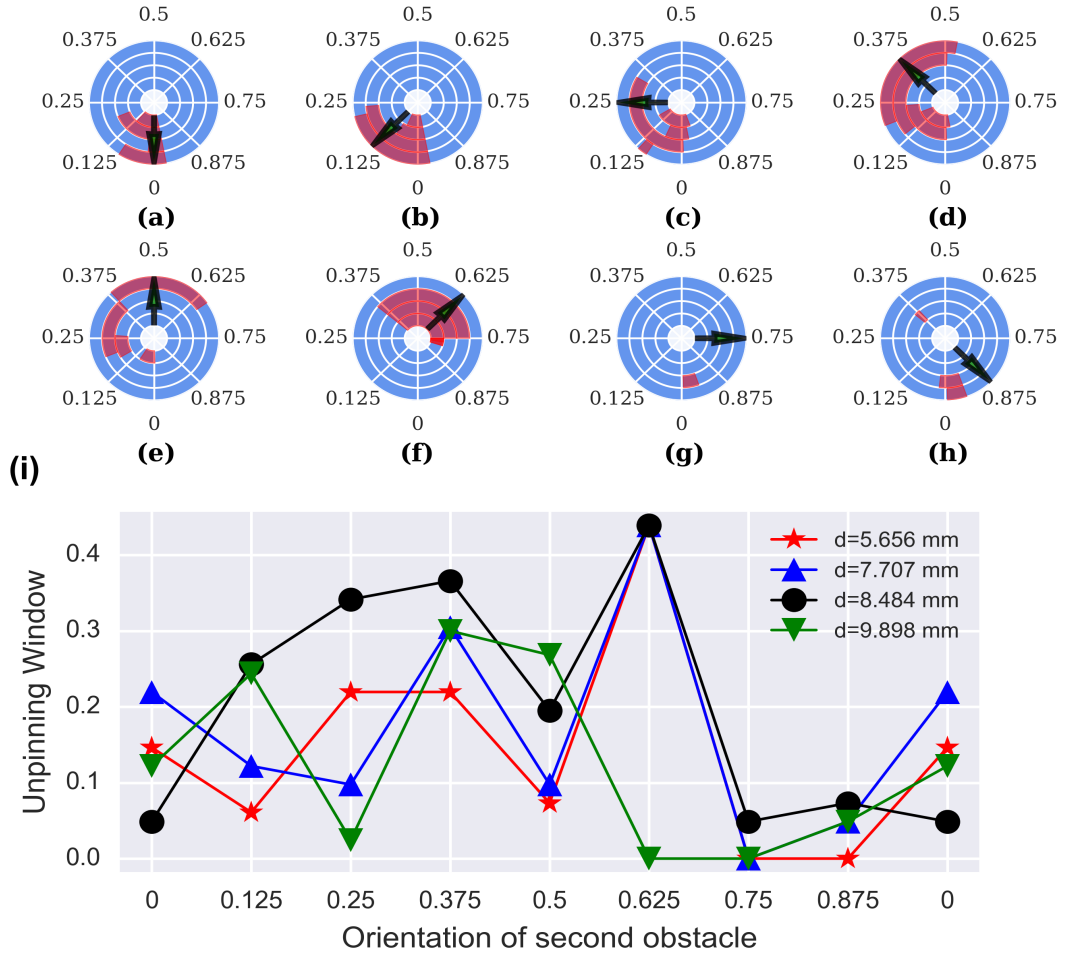
Figure 4.6: **Unpinning window for different orientation of additional wave emitting site around the central heterogeneity**: The shaded circular region at the centre of the figure represents the obstacle. The arrow indicates the angle at which the second obstacle is located. By keeping the radius of both the obstacle fixed, we change the second obstacle's distance from the first. Each white concentric circle denotes the distance of the second obstacle from the central obstacle. The red shaded region corresponds to the unpinning window for a fixed distance between the two obstacles. Figures **(a)-(h)** represents the unpinning window of 8 different orientation of the additional wave emitting site having a radius of 2 mm around the central heterogeneity. The distances between the first and second obstacles are fixed to 5.656 mm, 7.707 mm, 8.484 mm and 9.898 mm, respectively. **(i)** Plot of the orientation of the second obstacle *vs* the unpinning window for different distances between the obstacles.

Interestingly, the increase in the width of the unpinning window does not carry over uniformly across all the locations of the additional wave emitting site. To study the dependence, we place the second obstacle at eight different orientation around the central obstacle, each time shifting it by an angle of 45° (0.125 phase units) as shown in Fig. 4.6. For the majority of orientations, the unpinning window either shrieked or

vanished entirely for very small distances. From Fig. 4.6 (i), we can infer the qualitative behaviour of the unpinning window for different orientations and distances of the additional wave emitting site.
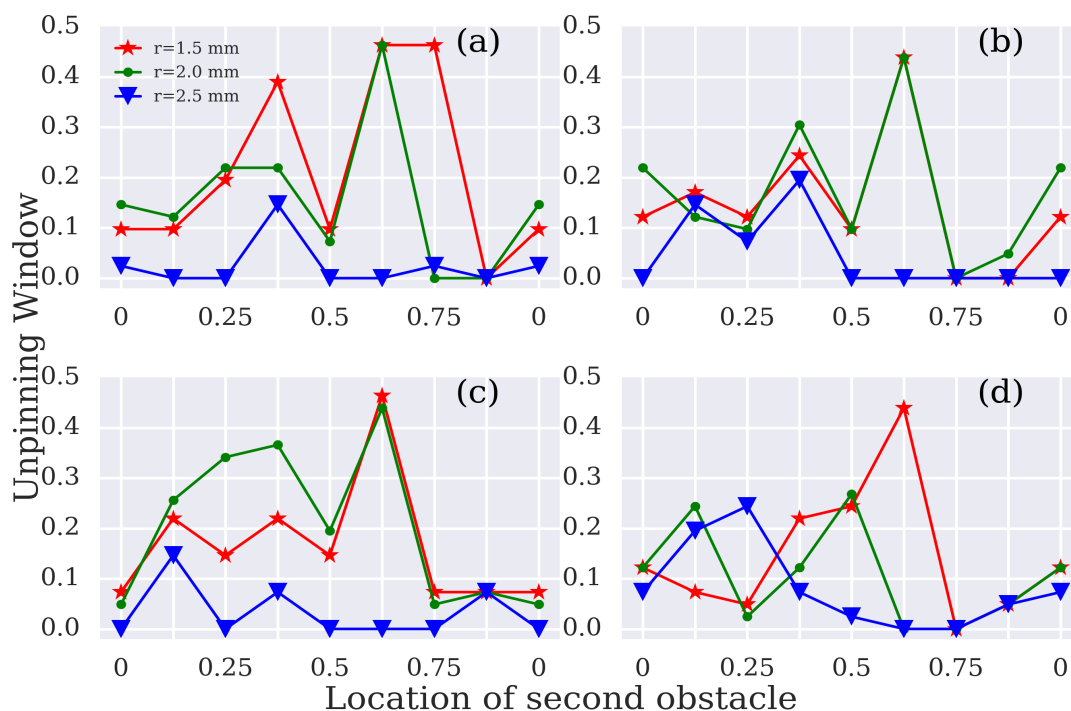
Figure 4.7: **Dependence of unpinning window with the location of second obstacle**: Figures **(a-d)** represents the unpinning window plotted for 4 different distances 5.656 mm, 7.707 mm, 8.484 mm and 9.898 mm between the centers of obstacles. 8 different location of the second obstacle varying by an angle of 45 is taken over x axis (as clock positions) and corresponding unpinning window is plotted. Inside each figure the unpinning window for three different radii of the second obstacle (denoted by 'r') corresponding to 1.5 mm, 2 mm and 2.5 mm are shown.

Then, we comprehensively study the effect of variation of the size of the second obstacle on the unpinning window. We systematically vary the radius of the second obstacle to be 1.5 mm (Fig. B.1), 2.0 mm (Fig. 4.6), and 2.5 mm (Fig. B.2). As the size of the second obstacle increases, the boundary separation between the obstacles becomes negligible. With this setting, both the central and second obstacle acts like a single entity since the excitation is unable to propagate between them (Conduction Block) (ten Tusscher and Panfilov (2005)). This increases the chances of spiral repinning to the second obstacle and hence significantly reduces the unpinning window.

Fig. 4.7 indicates the dependence of the unpinning window on the orientation of the second obstacle for 3 different sizes of the obstacle. Here, each subplot represents the unpinning window for the distance 5.656 mm, 7.707 mm, 8.484 mm, and 9.898 mm respectively. For a fixed distance between the obstacles, the unpinning window either vanishes or is very low for most orientations when the obstacle size is large. Unpinning will be easier if the additional wave emitting site is small. This is because smaller obstacles reduce the chances of spiral repinning to the obstacle. This explains the large unpinning window for smaller sized obstacles shown in Fig. 4.7.

4.4 Discussion

In this chapter, we study how introducing an additional wave emitting site modifies the unpinning window of a pinned spiral wave. In the experiments using cardiac monolayers, we found that a wave pinned to an obstacle can be unpinned by a secondary wave initiated from another nearby obstacle. We then systematically investigated unpinning in the presence of two heterogeneities and found that the second obstacle can significantly alter the unpinning window of a pinned spiral wave. The unpinning window alters depending on how the second obstacle is placed with respect to the pinning centre.

Our experiments show that a higher number of wave emitting sites can be recruited in a heterogeneous medium simply by increasing the strength of the applied electric field. Extra obstacles in proximity act as extra wave emitting sites that can help in unpinning, but they can also act as additional pinning sites. We have chosen the size of the secondary obstacle so that it is possible to have stable pinned spirals (that is, the diameter is more than the spiral core). Such large obstacles are also more likely to act as virtual electrodes than smaller obstacles for the field strengths we use.

We observed widening of the unpinning window for certain orientations and distances of additional wave emitting site. Unpinning window is seen to decrease or sometimes vanish altogether for smaller distances due to repinning. Unpinning fails if the separation between the obstacle boundary is too small compared to the spiral wavelength. This is due to the obstacles acting like a single entity, and the wave is unable to

propagate between them. We also observe that unpinning success rate decreases for a configuration containing a large secondary obstacle than that of a small one, as a large obstacle can contribute to the maximum probability of repinning.

Though these studies are conducted in a two-dimensional model, the phenomenon such as pinning, unpinning and secondary excitations described in the paper were observed in previous detailed studies carried on ionic models such as Luo-Rudy I (Pumir and Krinsky (1999)) and Beeler Reuter (Pumir et al. (2010)). Hence we expect the qualitative features of our study to be valid even in realistic ionic models. However, the quantitative details such as the width of the unpinning window are model dependent.

Studies of unpinning using two-dimensional experimental and numerical models show that the unpinning window in such cases are very narrow (Shajahan et al. (2016), Luther et al. (2011)). However, multiple field pulses are much more efficient *in vivo* experiments. We suspect several factors, including multiple heterogeneities, and the three-dimensional structure of the heart, could be assisting the unpinning. Our study using two obstacles point in this direction. Further investigations are required to understand how multiple waves finally alter the unpinning. In the next chapter (see chapter 5), we discuss the mechanism of unpinning spiral waves using circularly polarized electric fields.

Chapter 5

Spiral Wave Unpinning Using Circularly Polarized Electric Fields

In this chapter, we present a mechanism of unpinning of the spiral waves using a circularly polarized electric field. We present the simulation and theoretical results which are consistent with each other.

With the pulsed electric fields considered in the previous chapters, the stimulus needs to be carefully timed to unpin the spiral. To time the pulses, we need to know the phase of the pinned spiral. In the cardiac setting, the phase of the spiral is not always known. Therefore, we fire multiple pulses hoping that one of the pulses falls into the unpinning window of the spiral. Although this method has a much higher success rate compared to a single pulse, it can fail if the unpinning window is narrow or if the pacing frequency is not optimized. This chapter provides an alternative to pulsed electric fields using rotating circularly polarized electric fields.

Jiang-Xing Chen et al. were the first to introduce the circularly polarized electric field (CPEF) to study its influence on the drift of the spiral waves (Chen et al. (2006)). They noted that the spiral waves possess rotational symmetry and tried to exploit it by using a circularly polarised electric field with a similar symmetry. Later, Feng et al. used it to terminate the pinned spiral waves (Feng et al. (2014)). In a simulation study,

they compared the circularly polarized electric field's efficiency with that of the pulsed electric field and found a significant increase in the success rate with much lower voltage strength than pulsed electric fields. The subsequent study showed that the higher frequency circular wave trains generated by the CPEF could successfully terminate spiral turbulence (Feng et al. (2015)). Recently, the effect of a circularly polarized electric field on an irregularly shaped obstacle was also performed (Feng and Gao (2019)). Besides these studies, the ability of CPEF to control the turbulence has been shown experimentally in the Belousov-Zhabotinsky reaction (Ji et al. (2013)).

In this chapter, we present a mechanism for unpinning the spiral waves using circularly polarized electric fields. We show that for a given obstacle size, there exists a time period of the CPEF below which spiral can always be unpinned. We call it the cut-off time period. We also show that the termination always happens within the first period of the CPEF. In the following sections, first, we summarise the observations made in the simulations. Later, based on these observations, we derive a robust and generalized analytical formulation that explains the findings of the simulations. Our theory accurately predicts the cut-off time period of CPEF. In particular, we show that unpinning is always successful if the period of the CPEF is below the cut-off period. We also show that the cut-off period depends linearly on the radius of the obstacle. We find that there is no traditional unpinning window with a circularly polarized electric field.

5.1 Mathematical model

To simulate CPEF, we use a generic model of excitation waves, namely the Fitzhugh-Nagumo model given in section 2.5.1.

The equations are solved using the forward Euler scheme in time and five-point finite difference stencil on a 2D square grid as described in section 2.6. The domain boundaries are modelled using no-flux boundary conditions. In monodomain models, an additional no-flux boundary condition is applied on the boundary of the obstacle to simulate the wave emission from heterogeneity. It is given by (Pumir et al. (2007), Pan et al. (2016), Bittihn et al. (2012)),

$$\hat{n}.(D\nabla u - \boldsymbol{E}) = 0. \tag{5.1}$$

Here $\boldsymbol{E}$ is the applied electric field. The boundary conditions are imposed on the obstacle using phase field method as given in section 2.4 (Bittihn et al. (2012), Fenton et al. (2005)). For $\boldsymbol{E}$, we used a anti-clockwise rotating circularly polarized electric field of the form $\boldsymbol{E} = E_0\sin(2\pi t/T_{cp})\hat{x} + E_0(\cos(2\pi t/T_{cp})\hat{y}$, where E_0 is the strength of the field and T_{cp} is its period.

The parameter values are chosen as $a = 0.1$, $b = 0.25$, $\varepsilon = 0.025$, $D = 1$ and $E_0 = 0.1$. We used dimensionless space step $dx = 0.1$ and time step $dt = 0.0001$. Spiral waves of desired chirality were initiated in the system with their tips pinned to the obstacles. First, we consider an anticlockwise rotating spiral and then move on to the case of the clockwise rotating spiral in the next section. We define the phase difference α as the angular difference between the spiral and the initial direction of the $\boldsymbol{E}$ field. The waves were allowed to perform at least four rotations before the delivery of $\boldsymbol{E}$ field.

5.2 Results and discussion

5.2.1 Numerical studies of unpinning an anticlockwise rotating spiral with circularly polarized electric field

Fig. 5.1 shows the unpinning of the anticlockwise rotating spiral by a circularly polarized electric field. The spiral is pinned to an obstacle of fixed radius, $r = 4$. The period of the spiral, T_s around this obstacle is 12.5. In Fig. 5.1 (a)-(d) CPEF having a period $T_{cp} = 10.4166$ is used. Fig. 5.1(a) shows the spiral, S with $\alpha = 0$. When $\boldsymbol{E}$ field is applied, the wave emission happens from those points on the obstacle boundary where the field density is sufficient to nucleate a new wave. This gives rise to symmetrical crescent-shaped depolarisation, which can be divided into head, H, and tail, T. The head, H, follows the electric field vector along the boundary of the obstacle. When T collides with S, H lags behind S by a phase angle of ϕ. Due to this, H continues to stay pinned to the obstacle. In Fig. 5.1(e)-(f) $\boldsymbol{E}$ field having a period $T_{cp} = 3.6764$ is used.

Since the radius of the obstacle is fixed, and T_{cp} is shorter than in the case of Fig. 5.1 (a)-(d), H moves faster on the boundary and reaches the wave back of S when T and S collide. This makes the phase width $\phi = 0$ and causes a successful unpinning of the spiral.
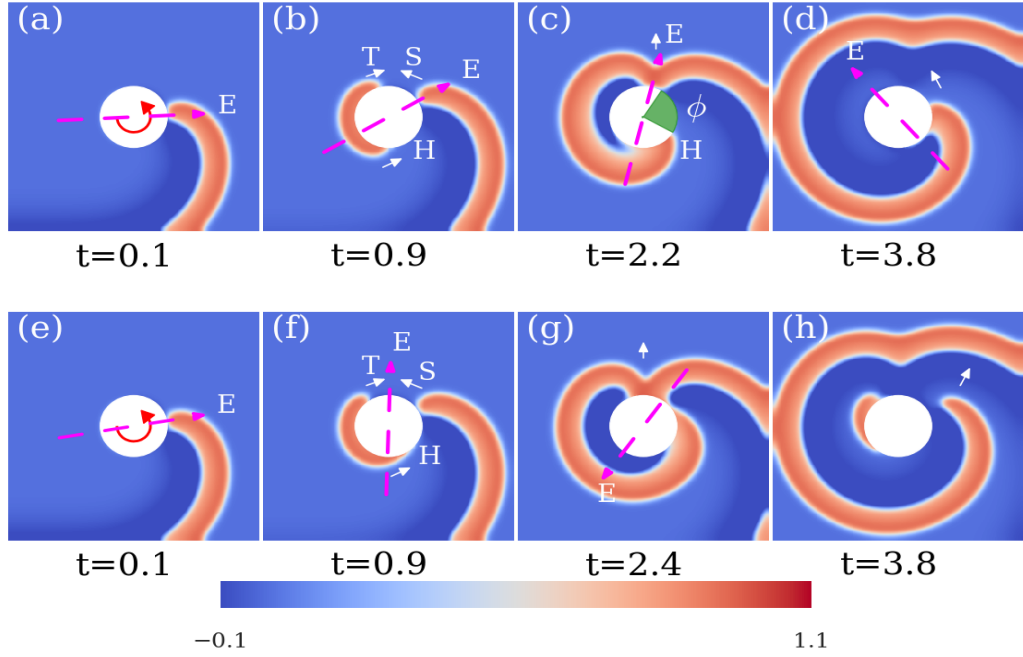
Figure 5.1: **Unpinning of anticlockwise rotating spiral.** The radius of the obstacle (white circular patch), $r = 4$ and the phase difference $\alpha = 0$. **(a)-(d)** Unsuccessful case, period of the CPEF $T_{cp} = 10.4166$. **(a)** An anticlockwise rotating pinned spiral wave, S. **(b)** Excitation is emitted from the obstacle. The leading end, labelled as head, H, follows the electric field. The trailing end is labelled as the tail, T. **(c)** T collides with S. The excitable gap $\phi > 0$ (shaded in green) between H and the wave back of S do not facilitate unpinning. **(e)-(h)** Successful case. The electric field now has a smaller period $T_{cp} = 3.6764$. **(g)** When T collides with S, H reaches the wave back of S. The excitable gap is zero, and this leads to successful unpinning **(h)**. Notations: Magenta dashed arrows show the instantaneous direction, and red circular arrows within the obstacle show the direction of rotation of the electric field.

Since we have kept the radius of the obstacle and phase difference, α fixed, if we keep on reducing the time period T_{cp}, we must reach a point where the excitable gap $\phi = 0$. This is the cut-off time period T_{cp}^* of the **E** field. Below this, ϕ is always zero, and therefore there is always unpinning.

What happens if we continue to apply the **E** field in the unsuccessful case of Fig. 5.1

(a-d)? Will the spiral unpin if we apply multiple rotations of E field by keeping the value of T_{cp} fixed? In Fig. 5.1(a-d) $T_{cp} < T_s$. So, the head, H, is being dragged along by the electric field vector along the boundary of the obstacle. Due to this, the tail of the electric field vector, around which the wave nucleation happens, always stays behind H (see Fig. 5.1(d)). Since H leaves a refractory tail behind it as it moves, the electric field cannot nucleate any waves there. So, when $T_{cp} < T_s$, applying multiple rotations of E field do not unpin the spiral wave.
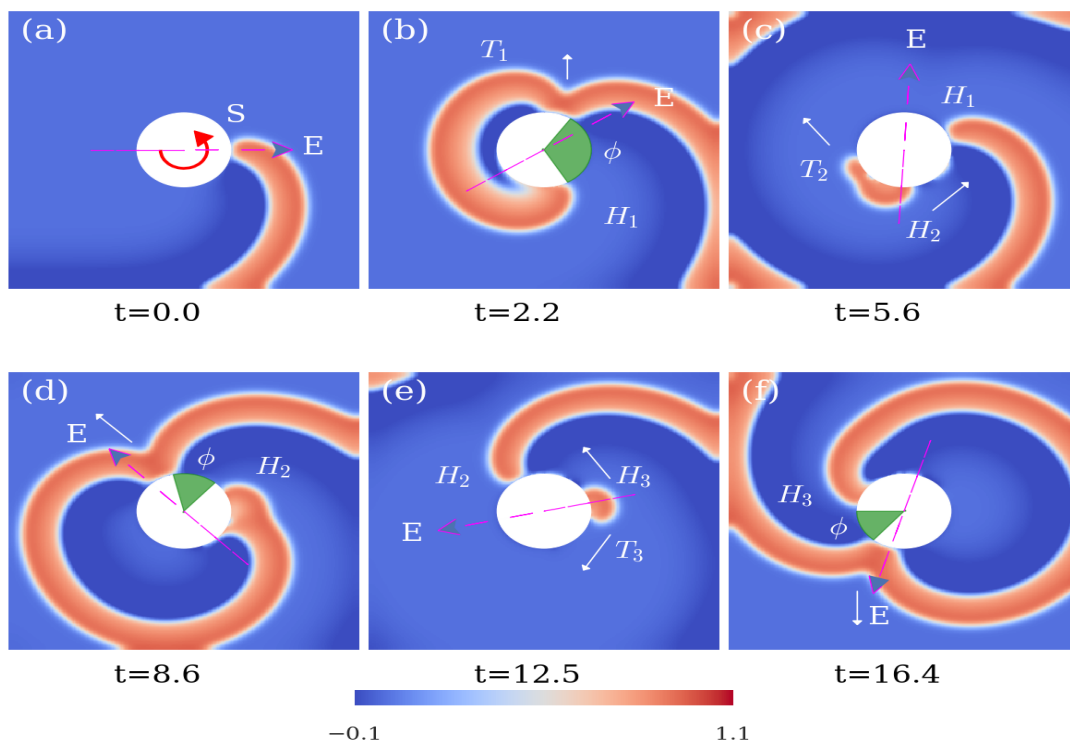
Figure 5.2: Unpinning failure when $T_{cp} > T_s$. The radius of the obstacle is $r = 4$ and the phase difference $\alpha = 0$. The period of the E field is $T_{cp} = 23.22$ and the period of the spiral $T_s = 12.5$. Here, the newly nucleated heads H_1, H_2 and H_3 move with the same period as that of the spiral. **(a)** A pinned anticlockwise spiral S. **(b)** When S and T_1 collide, the excitable gap ϕ (shaded in green) is non-zero. This leads to failure of unpinning. **(c)** The E field falls behind the refractory tail of H_1 and nucleates a new wave with head H_2 and tail, T_2. **(d)** When T_2 collides with H_1 the non-zero ϕ leads to failure of unpinning. **(e)** The E field lags once again and nucleates a new head H_3 and tail T_3. **(f)** The unpinning fails in a similar fashion, as shown in **(d)**.

The case with $T_{cp} > T_s$ is shown in Fig. 5.2. Here, every time the E field nucleates a new wave, the head H of the newly nucleated wave moves with the same speed as that

of the spiral instead of the speed dictated by the applied $\boldsymbol{E}$ field. Since the period of the $\boldsymbol{E}$ field is high compared to the period of the spiral, the electric field keeps lagging behind the spiral. As the $\boldsymbol{E}$ field lags and falls out of the refractory tail of H, it nucleates a new wave there. Because all the pinned waves now move with the same velocity on the boundary of the obstacle, the head, H of the newly nucleated wave cannot catch up with the previous one. Therefore, the excitable gap ϕ can never vanish (Fig. 5.2(d) and (f)). So, if the unpinning fails within the first rotation of the $\boldsymbol{E}$ field, then it keeps failing irrespective of whether T_{cp} is lesser or greater than T_s.

5.2.2 Theory of unpinning of anticlockwise rotating spiral with circularly polarized electric field

To provide validation for the unpinning mechanisms observed in the simulations, we derive analytical formulas based on the following assumptions. Fig. 5.3 shows the schematic diagram of the anticlockwise spiral unpinning. On the application of the $\boldsymbol{E}$ field at $t = 0$, the wave nucleates from an extended region rather than a point. At time t_0, just after the wave emerges and before it starts moving, it subtends an symmetric angle of $2\theta_0$. In the time it takes for the wave to emerge from the obstacle, the spiral S would move a distance of $r\alpha + v_s t_0$ in the anticlockwise direction. Here, $v_s = (2\pi r/T_s)$ is the velocity of S. Eventually, T and S collide. The expression for the collision time t between T and S can be obtained as follows. The angular distance covered by S in anticlockwise direction in time t can be expressed as $\alpha + (v_s t)/r$. At the same instant, T collides with S travelling clockwise and covering an angle $\theta_1 = \theta_0 + (v_T(t - t_0))/r$, where, v_T is the velocity of T. But, we have $(\theta_1 + \alpha + (v_s t)/r) = \pi$. So, we can write the expression for t as follows,

$$t = \frac{r}{v_s + v_T} \left(\pi - \alpha - \theta_0 + \frac{v_T t_0}{r} \right). \tag{5.2}$$

Meanwhile, H moves an angle of $\theta_2 = \theta_0 + (2\pi/T_{cp})(t - t_0)$ in anticlockwise direction. But, the total angle is $\theta_1 + \theta_2 + \phi = 2\pi$. Therefore, the final expression for the

Figure 5.3: **Schematic diagram of anticlockwise spiral unpinning. (a)** Pinned spiral wave, S time $t = 0$. α is the angular difference between the E field and the spiral wavefront at time $t = 0$. **(b)** At $t = t_0$, excitation emerges out symmetrically making an angle θ_0. Meanwhile, S covers a distance of $v_s t_0$. **(c)** S and T collide at time, t. θ_1 and θ_2 are the angle covered by T and H. The excitable gap, $\phi = 2\pi - (\theta_1 + \theta_2)$.

excitable gap ϕ can be written as,

$$\phi = \pi + \alpha + \frac{v_s t}{r} - \theta_0 - \frac{2\pi}{T_{cp}}(t - t_0) - \theta_{sw}. \tag{5.3}$$

In Fig. 5.3(c), we considered ϕ as the angle between the wavefront of H and the waveback of S. However, on deriving the equation, we found that the value of ϕ measured in simulations and the one obtained through the equations differed by an angle corresponding to the width of the spiral on the obstacle boundary. To compensate for this, we add θ_{sw} to ϕ, which is the width of S on the obstacle boundary. In Eq. 5.3 we have taken the quantity to the RHS.

Eq. 5.3 is plotted as a function of T_{cp} for an obstacle of radius $r = 4$ for three different phase differences $\alpha = 0, \pi/4$ and $-\pi/4$ in Fig. 5.4 (a). The curve predicted by Eq. 5.3 agrees with the one obtained through simulations.

What happens when the initial phase difference α is varied? Consider a case with $\alpha = \pi/4$. Then, S is much closer to T at $t = 0$. If H has to meet the collision point of T and S simultaneously and unpin the spiral, then the E field should move much faster on the boundary of the obstacle. So it should have a shorter time period. i.e the cut-off period $T_{cp}^*(\alpha = \pi/4) < T_{cp}^*(\alpha = 0)$. If $\alpha = -\pi/4$ is the initial phase difference; then, S is closer to H than T at $t = 0$. So, S has more distance to cover on the boundary

of the obstacle to reach T. So, $\boldsymbol{E}$ should have a longer time period ($T^*_{cp}(\alpha = -\pi/4) > T^*_{cp}(\alpha = 0)$) such that H reaches collision point of T and S only when those two collide. So, depending upon how the initial phase difference α is varied, the period of the $\boldsymbol{E}$ field should be timed so that H, S, and T meet together and unpins the spiral. This confirms that in this mechanism of unpinning, we do not have an unpinning window. However, for a given phase difference α, we only have a threshold value for T_{cp} below which there is always unpinning.
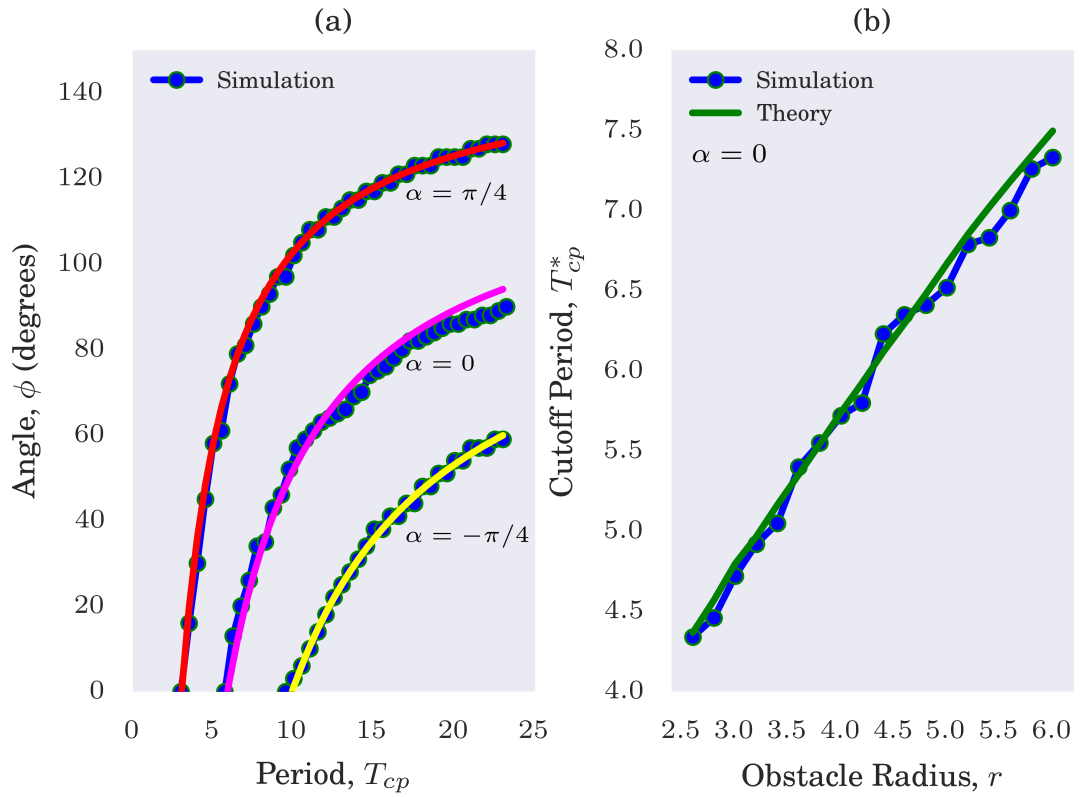
Figure 5.4: **(a)** Graph of the excitable gap ϕ as a function of period of the circularly polarized electric field T_{cp} for anticlockwise rotating spiral. The radius of the obstacle $r = 4$. α's denote the phase difference between the spiral and the initial direction of the electric field. The solid lines represent the theoretical curves. **(b)** Graph of cut-off period T^*_{cp} as a function of obstacle radius r for anticlockwise rotating spiral. The value of $\alpha = 0$.

The variation of the excitable gap ϕ as a function of T_{cp} for different phase differences (α's) are shown in Fig. 5.4 (a). The x-intercept of each curve gives the cut-off period T^*_{cp}. Once the cut-off period T^*_{cp} is determined for an obstacle of radius r and phase difference α, the unpinning is guaranteed for all the time periods lower than T^*_{cp}.

If we set the left-hand side of Eq. 5.3 to zero, we can write T_{cp}^* as a function of the phase difference α and the obstacle radius r. To test our theory, we performed simulations for obstacles of different radius and a fixed phase difference of $\alpha = 0$. The curve obtained through simulation study matches the theoretical predictions. The results are shown in Fig. 5.4 (b).
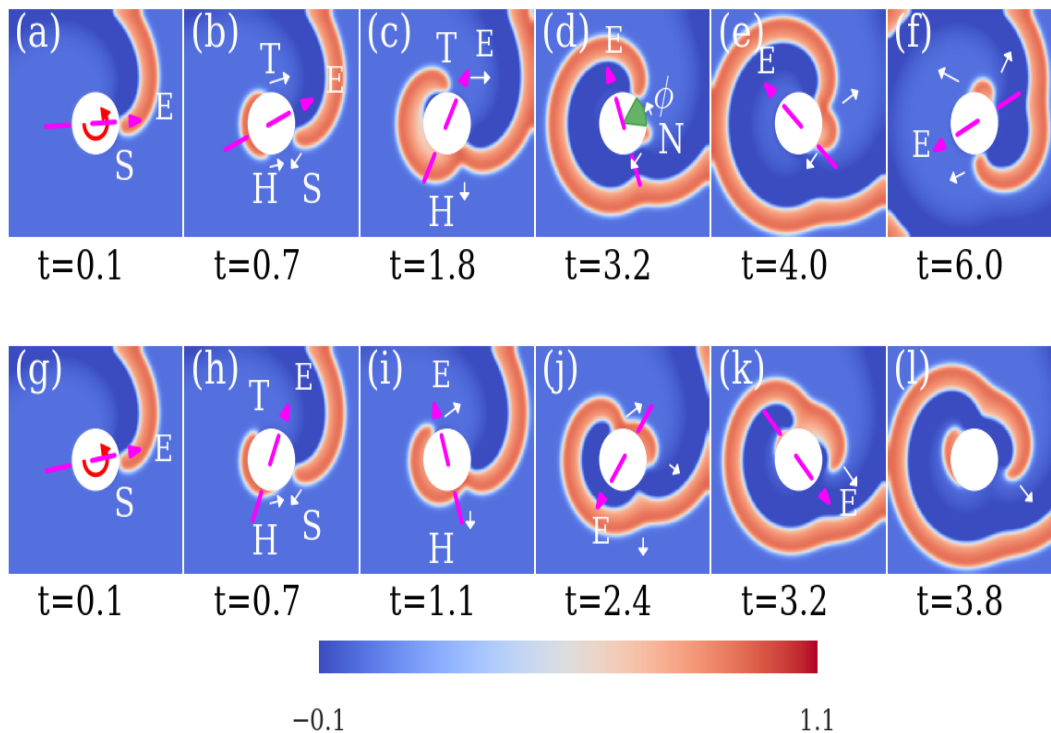
Figure 5.5: **Unpinning of a clockwise rotating spiral.** The radius of the obstacle, $r = 4$ and the phase difference $\alpha = 0$. **(a)-(d)** Unsuccessful case, period of the rotating field $T_{cp} = 10.4166$. **(a)** A clockwise rotating pinned spiral wave, S. **(b)** Excitation is emitted from the obstacle. **(c)** H and S collide. **(d)** When H and S fuse together and detach from the obstacle, the electric field nucleates a new wave, N. The excitable gap $\phi > 0$ (shaded in green) between N and T keeps the spiral pinned to the obstacle **(f)**. **(g)-(l)** Successful case, period of the rotating field, $T_{cp} = 3.6764$. **(j)** When N collides with T, the excitable gap is zero, and this leads to successful unpinning **(l)**.

5.2.3 Numerical studies of unpinning a clockwise rotating spiral with circularly polarized electric field

The unpinning of a clockwise rotating spiral by E field is shown in Fig. 5.5. After the E field induces the depolarization, H and S start moving towards each other. They eventually collide and start detaching from the obstacle as the excitation cannot go past the refractory tail left behind by the other (Fig. 5.5 (c)). Since the E field is rotating, it induces a new excitation head, N, once it crosses the refractory tail of S. The non-zero excitable gap ϕ from the wavefront of N to the wavefront of T when H and S just detach from the obstacle, prevents unpinning. In Fig. 5.5 (g)-(l) E field having smaller rotation period ($T_{cp} = 3.6764$) is used. Now, when H and S fuse and detach from the obstacle, the new head, N, already collides with T. So, there is no excitable gap. This leads to the successful unpinning of the spiral (see Fig. 5.5 (l)). Since we have kept the radius of the obstacle and phase difference fixed, similar to the anticlockwise case, if we keep on reducing the time period T_{cp}, we will reach a point where the excitable gap $\phi = 0$. This is the cut-off time period T_{cp}^* of the E field. Below this, ϕ is always zero, and therefore there is always unpinning.

5.2.4 Theory of unpinning of clockwise rotating spiral with circularly polarized electric field

The schematic diagram of the clockwise spiral unpinning is shown in Fig. 5.6. α is the phase difference between the E field and the spiral wavefront at time $t = 0$. At the time t_0, the nucleated wave subtends a symmetric angle of $2\theta_0$. When the depolarization emerges from the obstacle, S moves clockwise towards H, covering a distance of $v_s t_0$. Later, H and S collide at time $t = t_1$.

The angle covered by H before collision with S can be given as $\theta_2 = \theta_0 + (2\pi/T_{cp})(t_1 - t_0)$. In the meantime, S travels clockwise and covers an angular distance of $(v_s t_1)/r$. But, we have $\theta_2 + (v_s t_1)/r = \pi + \alpha$. We use these conditions to obtain a formula for t_1.

$$t_1 = \left(\pi + \alpha - \theta_0 + \frac{2\pi t_0}{T_{cp}}\right)\left(\frac{rT_{cp}}{2\pi r + T_{cp}v_s}\right). \tag{5.4}$$
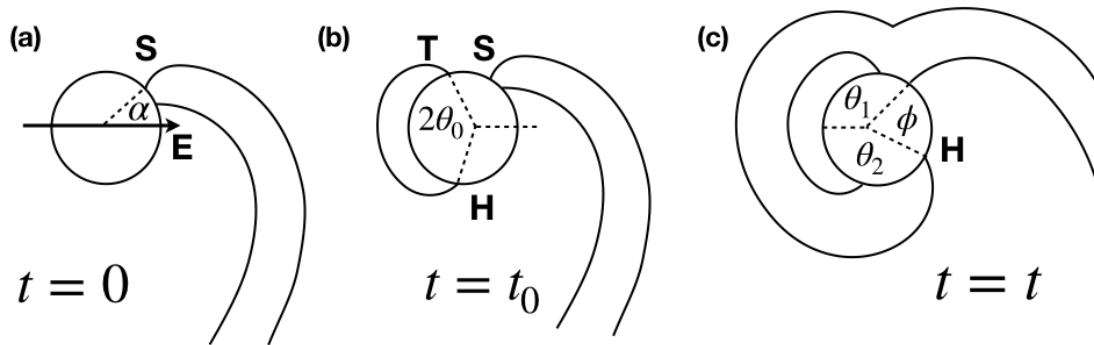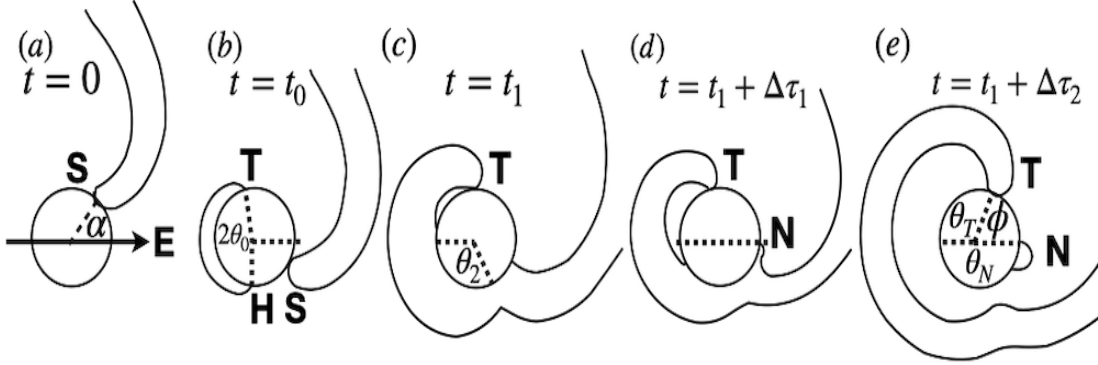

Figure 5.6: **Schematic diagram of clockwise spiral unpinning.** (a) Pinned spiral wave, S. α is the phase difference between the $\boldsymbol{E}$ field and the spiral wavefront at time $t = 0$. (b) At $t = t_0$, excitation emerges out symmetrically making an angle θ_0. Meanwhile, S covers a distance of $v_s t_0$ moving clockwise. (c) S and H collide at time, t_1. θ_1 and θ_2 are the angle covered by S and H. Meanwhile, T covers a distance of $v_T t_1$. (d) At time $t_1 + \Delta\tau_1$, the rotating electric field nucleates a new wave, N after crossing the refractory tail of S. (e) At $t = t_1 + \Delta\tau_2$, H and S detach from the obstacle. The excitable gap $\phi = 2\pi - (\theta_N + \theta_T)$.

Once H and S collide, they begin to detach from the obstacle. As the detachment is in progress, the anticlockwise rotating $\boldsymbol{E}$ field nucleates a new head, N once it crosses the refractory tail of S. For an obstacle of a given radius, how fast the $\boldsymbol{E}$ field crosses the refractory tail depends on how small its time period T_{cp} is. Let us denote the time taken by the $\boldsymbol{E}$ field to cross the refractory tail of S and nucleate N as $\Delta\tau_1$. Once the detachment of H and S from the obstacle is complete at time $t = t_1 + \Delta\tau_2$, we measure the excitable gap $\phi = 2\pi - (\theta_N + \theta_T)$. Here, $\Delta\tau_2$ is the time taken by H and S to detach from the obstacle after their collision at $t = t_1$. The angle covered by T can be written as $\theta_T = \theta_0 + (t_1 - t_0 + \Delta\tau_2)(v_T/r)$ whereas the total angle covered by the head (H and N included) is, $\theta_N = \theta_0 + (2\pi/T_{cp})(t_1 - t_0) + (2\pi/T_{cp})(\Delta\tau_2 - \Delta\tau_1)$.

We can identify two cases depending on whether the term $(\Delta\tau_2 - \Delta\tau_1)$ in θ_N is positive or negative. The first case is $\Delta\tau_2 > \Delta\tau_1$. Here, T_{cp} is fast enough so that the new head, N is nucleated before H and S detaches from the obstacle. Then the excitable

gap ϕ can be given as,
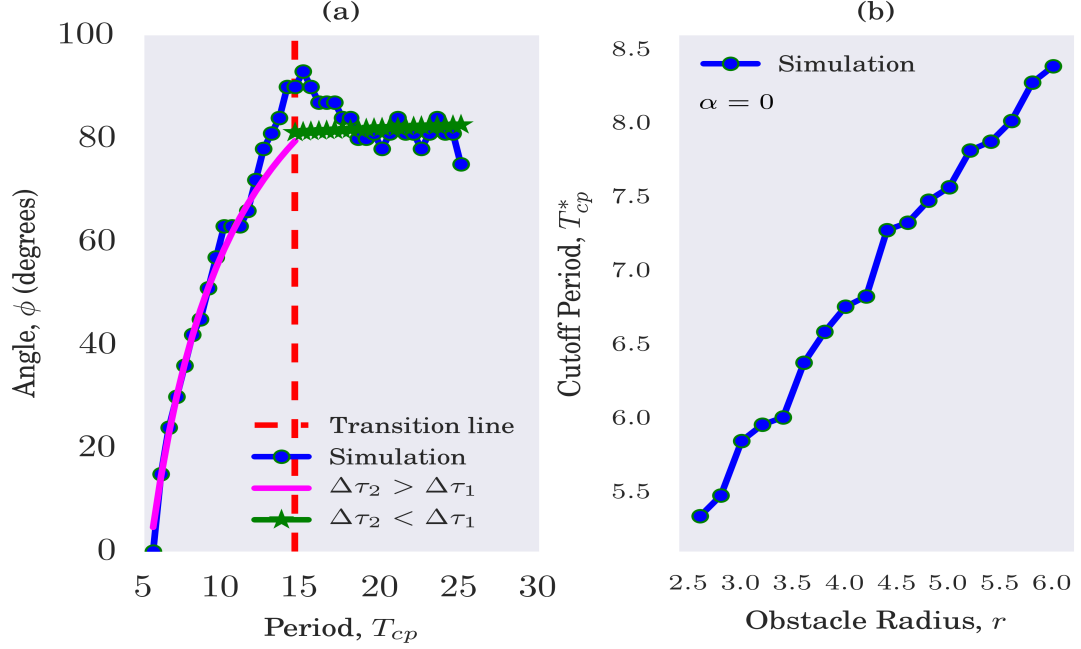
Figure 5.7: **(a)** Graph of the excitable gap ϕ as a function of period of the rotating electric field T_{cp} for a clockwise rotating spiral. The radius of the obstacle $r = 4$ and the phase difference $\alpha = 0$. **(b)** Graph of cut-off period T_{cp}^* as a function of obstacle radius r for clockwise rotating spiral.

$$\phi = 2(\pi - \theta_0) - \left(\frac{2\pi}{T_{cp}} + \frac{v_T}{r}\right)(t_1 - t_0 + \Delta\tau_2) + \frac{2\pi\Delta\tau_1}{T_{cp}} - \theta_{sw}. \qquad (5.5)$$

In theory, the angular distance ϕ is calculated between the collision point of H and S and the wavefront of T. But, in simulations, it is measured between the wavefronts of N and T. To compensate for this, we subtract θ_{sw} from Eq. 5.5. Here, θ_{sw} is the width of the newly nucleated head, N on the boundary of the obstacle.

In the second case (i.e $\Delta\tau_2 < \Delta\tau_1$), T_{cp} is so slow that it cannot cross refractory tail of S until H and S detaches from the obstacle. So, N does not reappear at all and $\Delta\tau_1 = 0$. So, $\theta_N = \theta_0 + (2\pi/T_{cp})(t_1 - t_0)$. Then, the excitable gap ϕ can be written as,

$$\phi = 2(\pi - \theta_0) - \left(\frac{2\pi}{T_{cp}} + \frac{v_T}{r}\right)(t_1 - t_0) - \frac{v_T\Delta\tau_2}{r}. \qquad (5.6)$$

In the second case, ϕ is measured from the point of collision between the H and S.

The parameters $\Delta\tau_1$ and $\Delta\tau_2$ are measured directly from the simulations. As mentioned above, $\Delta\tau_1$ varies with the period of the applied E field. For an obstacle of radius r and phase difference α, we measured $\Delta\tau_1$ as a function of T_{cp}. For the measured values, we obtain a straight line fit ($\Delta\tau_1 = mT_{cp} + c$) where m and c are the slope and intercept of the straight line. Both the parameters m and c are the functions of radius r and the spiral phase α. The measured values of the parameter $\Delta\tau_2$ is found to be a constant.

Somewhere in between the two cases, $\Delta\tau_2 = \Delta\tau_1$. We call the corresponding T_{cp} as T_{cp} transition. Since $\Delta\tau_2$ is a known constant, the value of T_{cp} transition can be calculated from the straight-line fit of $\Delta\tau_1$. The results are summarised in Fig. 5.7. Similar to the anticlockwise mechanism, the unpinning happens within one rotation of the E field, and if we vary the phase difference α, we find that there is no unpinning window for this mechanism.

5.3 Summary

This chapter has identified a robust mechanism for unpinning the spiral waves using a circularly polarized electric field. We show that for an obstacle of a given radius and fixed phase difference of the spiral, it is always possible to time the period of the electric field so that unpinning is guaranteed. This period is called the cut-off period of the electric field. When the electric field period is below the cut-off, the spiral is unpinned before it finished one full rotation around the obstacle and within the first rotation of the electric field. Our theory accurately predicts this cut-off period and is also quantitatively consistent with all the simulation results. Since arguments used in deriving the theory are based only on fundamental properties of the excitable media, we expect these results to be valid in more general settings.

Typical unpinning studies with field stimulus identify an unpinning window, which is a phase window of the spiral during which it can be unpinned using a field pulse. However, in our mechanism with the circularly polarized electric field, there is no unpinning window. All rotating fields below the cut-off frequency can result in unpinning.

Yet, it must be noted that we use a simple monodomain model for simulating the effect of the electric field near the obstacle. A Bidomain model, which is the more accurate cardiac tissue model, predicts a complicated distribution of polarization around an obstacle, and it could affect the mechanism of unpinning (Takagi et al. (2004)).

Our results can be tested in experiments that show two-dimensional excitation waves, including cardiac monolayers and excitable chemical media. Specifically, experimental verification of the results showed in Fig. 2 would serve as a qualitative test for our mechanism. The circularly polarized electric field can be obtained using two perpendicular AC electric fields with a phase difference of $\pi/2$ generated with a pair of electrodes kept mutually perpendicular to each other. We hope that our analytical results of the spiral wave unpinning using a circularly polarized electric field will stimulate further studies in this direction.

Chapter 6

Conclusion

In this chapter, we present a brief summary of the work carried out in this thesis. We also discuss the possibility of experimental verification of the results and scope for future research in related areas.

The project aimed to study the dynamics and control of rotating excitation waves via electric field pulses in excitable media. This problem had a wide range of application since such rotating waves are seen in many physiological systems and are the leading cause of cardiac arrhythmias such as ventricular tachycardia and fibrillation. We proposed studying the effect of multiple heterogeneities and different types of electric fields to control such waves. We have made significant progress in all these objectives, the results of which are published in two international journals and a conference proceeding. The work presented in this thesis is summarised below.

We have investigated the detailed mechanism of unpinning when there are multiple heterogeneities. First, we investigated a special case of a rotating wave pinned to two nearby heterogeneities and studied it's unpinning using an electric field pulse (Punacha et al. (2019a)). We have shown that the chances of unpinning, as quantified by the unpinning window, decreases as the distance between obstacles increase. After a critical distance, unpinning fails. For this special case, our results show that to unpin a spiral anchored to both the obstacles, it is not essential that the stimulus delivered falls into

the spiral's refractory tail.

We then systematically investigated unpinning of the spiral for a more general case in the presence of two obstacles and found that the second obstacle can significantly alter the unpinning window of a pinned spiral wave (Punacha et al. (2019b)). The unpinning window alters depending on how the second obstacle is placed with respect to the pinning centre. We observed widening of the unpinning window for certain orientations and distances between two obstacles. The unpinning window either decreases or vanishes altogether for smaller distances due to repinning. We also observe that unpinning success rate decreases for a configuration containing a large secondary obstacle than that of the small one, as a large obstacle can contribute to the maximum probability of repinning.

We then studied unpinning by circularly polarized electric fields (CPEF) (Punacha et al. (2020)). We have identified two separate mechanisms for unpinning the spiral waves using a circularly polarized electric field based on their chirality. We show that for an obstacle of a given radius and fixed phase of the spiral, it is always possible to time the period of the CPEF so that unpinning is guaranteed. This is called the cut-off period of the electric field. Once the cut-off period is determined, unpinning occurs for all the periods of the CPEF below the cut-off period. Our theory accurately predicts this cut-off period in simulations. We also provide a robust explanation of why this unpinning mechanism does not have an unpinning window.

Thus we have made considerable progress in our understanding of the control rotating waves. We are hopeful that our work will lead to developing optimized control strategies for situations such as cardiac arrhythmias. In all the chapters, homogeneous 2D excitable media having rectangular geometries were considered to study the dynamics and assess the complexity in controlling them. The theoretical and simulation study is completely based on simplified models of cardiac tissue called mono-domain description. To model the application of external defibrilating electric field, boundary conditions mimicking the bi-domain effect are used. During the modelling, we have ignored several important aspects of the cardiac muscle, such as the heart's electrical conduction system, the Purkinje fibers in the ventricles, the repercussion of muscle

contraction, and the fluid dynamics of the blood flow *etc*. We believe that considering the minimal working model that displays the crucial dynamics of the medium makes it easier to understand the underlying mechanisms ~~involved~~. We hope that the knowledge obtained from these minimalistic studies will help better understand the mechanisms involved in more realistic studies in the future. Even though these studies are conducted in a generic, two-variable model of an excitable media, the phenomenon such as pinning, unpinning and secondary excitations described here were observed in previous studies carried on in detailed models of cardiac cells, such as Luo-Rudy I (Pumir and Krinsky (1999)) and Beeler Reuter (Pumir et al. (2010)), that take into account the transport of various ions across the cell membrane. Hence we expect the qualitative features of our study to be valid even in realistic ionic models. However, the quantitative details, such as the width of the unpinning window, are model-dependent—this need to be explored in further work.

In this project, we have also exclusively focused on the two-dimensional dynamics on the surface. The physiological tissues such as atria can be treated as two-dimensional, but many physiological systems are three dimensional. In three dimensions, the rotating waves take a more complicated structure of a scroll wave. However, initial studies show that their unpinning is easier. Experiments in intact hearts also point to a broader unpinning window in three dimensions. There have not been many studies in three-dimensions; we believe this need to be explored further.

Appendices

Appendix A

Codes to study the dynamics of spiral waves in excitable media

A.1   Code to trace the tip trajectory of the spiral wave

```
from __future__ import print_function

"""
This import is required to write the print output to a file in
Newton().
Please do not put any other print statements in this file before
disabling this import.

"""

""" **************************************

Author   : Shreyas Punacha
Filename : Plotting_And_TipTracking.py
Date     : 18 February 2020

****************************************** """

""" *********************************************************

* This program can be used to locate multiple spiral tips.

* The Tip Definition:
    The tip (x,y) is defined as the intersection of two countors f1(x,y) = f2(x,y) = 0.
    In Barkley Model the countors are u = 1/2 and f(u,v) = u * (1-u) * (u - uth), with
    uth = (v+b)/a. The functions f1 and f2 are defined below in the body of the program.
    The tip definition is taken from Dwight Barkley's paper "A model for fast computer
    simulation of waves in excitable media."

* Newtons Method (2D):
    2D Newtons iterations are used to find the roots (x,y). The partial derivatives in the
    Jacobian matrix are calculated using finite difference method.
```

```
    # The Dx and Dy required for finite differencing are fixed (don't change them) and are
      defined below.

    # The TOOBIG variable is defined to prevent blowup.

    # The MXNWT variable is an upper limit on maximum number of newton iterations to be performed.

    # TOL2 is the tolerence, used for limiting the accuracy of the method.

* Eval_func and hh:
    These are used to interpolate (2D Lagrange interpolation is used) u and v fields
    with polynomials of order N_ORDER. Testing shows N_ORDER = 3 gives most accurate
    results. N_ORDER must always be odd.

* Find_tips(t):
    Every time this function is called, the entire 2D grid is searched for possible tips
    (Except the points that are too close to the boundaries).
    The first two if statements are used to determine the square within which the tip is
    located. Once located, the tip is approximated to be at the center of this square. i.e
    x = i + 0.5 and y = j + 0.5. This is the initial guess for Newton's method.

******************************************************************** """

import numpy as np
import matplotlib.pyplot as plt
import os

def f1(i, j):
    return udata[i,j] - U_CONT

def f2(i, j):
    return vdata[i,j] - V_CONT

def Newton(t, px, py, pz):
    nwt = 0
    new = 1
    old = 0
    x = px
    y = py

    while (nwt<MXNWT):

        f1_val = Eval_func(f1,x,y,new)
        f2_val = Eval_func(f2,x,y,old)
        nrm2 = (f1_val*f1_val) + (f2_val*f2_val)

        if (nrm2>TOOBIG):
            # print("nrm2 greater than TOOBIG")
            return False

        if (nrm2<TOL2):
            px = x
            py = y
            #print("Sucess!")
            print("%d        %0.5f        %0.5f        %0.5f"%(t, x-1.,y-1., pz), file=TipFile)
            #print("%d        %0.5f        %0.5f        %0.5f"%(t, x-1.,y-1., pz))
            return True


        df1dx = (Eval_func(f1,x+DX,y,new) - f1_val)/DX
        df2dx = (Eval_func(f2,x+DX,y,old) - f2_val)/DX
        df1dy = (Eval_func(f1,x,y+DY,new) - f1_val)/DY
```

```
        df2dy = (Eval_func(f2,x,y+DY,old) − f2_val)/DY
        jac   = df1dx*df2dy − df1dy*df2dx
        x −= ( (df2dy*f1_val) − (df1dy*f2_val))/jac
        y −= ((−df2dx*f1_val) + (df1dx*f2_val))/jac
        nwt += 1
    # print("Warning: nwt > MXNWT in Newton()")
    #return None


def Eval_func(f, x, y, new):

    hx = np.zeros([NORDER+1], dtype="float32")
    hy = np.zeros([NORDER+1], dtype="float32")
    ix_0 = 0
    iy_0 = 0

    sum = 0.

    if (True):
        ix_0 = np.int32(x) − ((NORDER+1)/2 −1) # int(x) − 1.
        iy_0 = np.int32(y) − ((NORDER+1)/2 −1) # int(y) − 1.
        x_local = x − ix_0
        y_local = y − iy_0
        for i in range(0,(NORDER+1),1):
            hx[i] = hh(x_local,i)
            hy[i] = hh(y_local,i)

    if((ix_0 < 1) or (ix_0 > NX−NORDER) or (iy_0 < 1) or (iy_0 > NY−NORDER)):
        # print("Warning: (x,y) out of range in Eval_func()")
        return(TOOBIG+1.)

    for i in range(0,(NORDER+1),1):
        for j in range(0,(NORDER+1),1):
            sum += hx[i]*hy[j]*f(ix_0+i,iy_0+j)
    return sum




def hh(x_local, i):
    product = 1.

    for j in range(0, NORDER+1, 1):
        if (j != i):
            product *= (x_local − float(j))/float(i−j)
    return product

def Find_tips(t,z):

    x = 0.
    y = 0.
    count = 0
    ntips = 0
    tip_x = np.zeros([MAX_TIPS], dtype="float32")
    tip_y = np.zeros([MAX_TIPS], dtype="float32")


    for i in range(2, NX−1, 1):
        for j in range(2, NY−1, 1):
            index = ((f1(i  ,j  ) >= 0.)      ) | ((f1(i+1,j  ) >= 0.) <<1) | ((f1(i  ,j+1) >= 0.) <<2) | ((f1(i+1,j
                +1) >= 0.) <<3)

            if ((index != 0) and (index != 15)):
```

```python
                index = ((f2(i  ,j   ) >= 0.)      ) | ((f2(i+1,j   ) >= 0.) <<1) | ((f2(i   ,j+1) >= 0.) <<2) | ((f2(i
                    +1,j+1) >= 0.) <<3)

                if ((index != 0) and (index != 15)):
                    x = float(i) + 0.5
                    y = float(j) + 0.5
                    #print("t=%d x=%f, y=%f"%(t, x,y))

                    if( (ntips==0) or (count==0) or ((x-tip_x[ntips-1])*(x-tip_x[ntips-1]) +  (y-tip_y[ntips-1])*(y
                        -tip_y[ntips-1])) > 4 ):
                        if ( Newton(t, x, y, z) ):
                            tip_x[ntips] = x
                            tip_y[ntips] = y
                            ntips += 1
                            count += 1
    #print("number of tips in one field = %d"%count)
    return None


if __name__ == "__main__":

    #import pdb; pdb.set_trace()

    a, b, epsilon = 0.8, 0.05, 0.02
    NX = 61
    NY = 61
    NZ = 61


    ###################################################################

    nt = 147000 # This is the only thing need to be changed.

    ###################################################################

    StartTime = 100000
    SavingInterval = 500

    # ==============================
    #       DO NOT CHANGE THESE.
    # ==============================

    U_CONT = 0.5
    V_CONT = (0.5*a - b)
    ntips = 0
    NORDER = 3
    DX = 0.05
    DY = 0.05
    TOL2 = 1.E-10
    TOOBIG = 10.
    MXNWT = 8
    MAX_TIPS = 100000

    # If file exists then append the subsequent data,
    # else open a new one

    if os.path.isfile("TipFile.txt"):
        TipFile = open("TipFile.txt", "a")
    else:
        TipFile = open("TipFile.txt", "w")


    # ==============================
    for t in range(StartTime, StartTime+nt+SavingInterval, SavingInterval):
```

```python
    u_data_1D = np.loadtxt("u_%0.7d.txt"%t)
    v_data_1D = np.loadtxt("v_%0.7d.txt"%t)

    udata = np.zeros([NX+2, NY+2])
    udata[1:NX+1, 1:NY+1] = u_data_1D.reshape(NX,NY).T
    vdata = np.zeros([NX+2, NY+2])
    vdata[1:NX+1, 1:NY+1] = v_data_1D.reshape(NX,NY).T
    Find_tips(t)


TipFile.close()


# ==============================
```

A.2 Code to generate the phase field

```c
#include <stdio.h>
#include "HeaderFiles.h"

double PhaseFieldTimeEvolution(int nx, int ny, int nt, double dx, double dy, double dt, double zi)
{
    /* Define */
    double c1 = (dt*(zi*zi))/(dx*dx);
    double c2 = (dt*(zi*zi))/(dy*dy);


    /* Define arrays */
    double Phi_0[nx+2][ny+2];
    double Phi[nx+2][ny+2];
    double PhiBackup[nx+2][ny+2];

    /* Load the initial conditions from Phi_0.txt file into Phi_0 and Phi arrays. */

    FILE *f1, *f2;
    double buffer;

    f1 = fopen("Phi_0.txt", "r");

    for(int i=1;i<=nx;i++)
    {
        for(int j=1;j<=ny;j++)
        {
            fscanf(f1, "%lf", &buffer);
            Phi_0[i][j] = buffer;
            PhiBackup[i][j] = buffer;
        }
    }
    fclose(f1);

    /* Time Loop */

    for(int t=0;t<=nt;t++)
    {
        /* Array Exchange */

        for(int i=1;i<=nx;i++)
        {
```

```
                        for(int j=1;j<=ny;j++)
                        {
                                Phi[i][j] = PhiBackup[i][j];
                        }
                }

        /* Neumann Boundary Conditions */

        for(int i=1;i<=nx;i++)
        {
                Phi[i][0] = Phi[i][2];
                Phi[i][ny+1] = Phi[i][ny-1];
        }

        for(int j=1;j<=ny;j++)
        {
                Phi[0][j] = Phi[2][j];
                Phi[nx+1][j] = Phi[nx-1][j];
        }

        for(int i=1;i<=nx;i++)
        {
                for(int j=1;j<=ny;j++)
                {
                        PhiBackup[i][j] = Phi[i][j] + ( dt * (Phi_0[i][j] - Phi[i][j]) ) + ( (c1)*(Phi[i
                                +1][j] - 2.*Phi[i][j] + Phi[i-1][j]) ) + ( (c2)*(Phi[i][j+1] - 2.*Phi[i][j] +
                                Phi[i][j-1]) );
                }
        }
        }

        /* Saving the last value of Phi, i.e Phi_Equilibrium into a file */

        f2 = fopen("Phi_Equilibrium.txt", "w");

        for(int i=1;i<=nx;i++)
        {
                for(int j=1;j<=ny;j++)
                {
                        fprintf(f2, "%lf\n", PhiBackup[i][j]);
                }
        }
        fclose(f2);

        return(0);
}
```

A.3   Code to study the dynamics of spiral wave in Barkley model

```
#include <stdio.h>
#include <math.h>
#include "HeaderFiles.h"
```

```
double BarkleyTimeEvolution(int nx, int ny, double dx, double dy, double dt, int nt, double a, double b, double
    epsilon, double DELTA, int StartTime, double Ex, double Ey, int PulseStartTime, int savingInterval, int
    centre_x, int centre_y, int obstacle_radius, double A)
{

    double u_th;
    double f;
    double c1 = (dt)/(dx*dx);
    double c2 = (dt)/(dy*dy);
    double c3 = (c1/4.0);
    double c4 = (c2/4.0);
    double c5 = (dt/(2.0*dx));
    double c6 = (dt/(2.0*dy));
    double c7 = (-A*c5);
    double c8 = (-A*c6);


    printf("c1 = %lf\n",c1);
    printf("c2 = %lf\n",c2);
    printf("c3 = %lf\n",c3);
    printf("c4 = %lf\n",c4);
    printf("c5 = %lf\n",c5);
    printf("c6 = %lf\n",c6);



    /* Memory Allocation */
    double u[nx+2][ny+2];
    double v[nx+2][ny+2];
    double ubackup[nx+2][ny+2];
    double vbackup[nx+2][ny+2];

    double PhiEquilibrium[nx+2][ny+2];
    double Ln_PhiEquilibrium[nx+2][ny+2];
    double D[nx+2][ny+2];


    /* Load phi equilibrium file */

    FILE *f1;
    double buffer;
    f1 = fopen("Phi_Equilibrium.txt", "r");

    printf("Loading Phi_Equilibrium file\n");

    for(int i=1;i<=nx;i++)
    {
            for(int j=1;j<=ny;j++)
            {
                    fscanf(f1, "%lf", &buffer);
                    PhiEquilibrium[i][j] = buffer;
                    // printf("%lf\t",PhiEquilibrium[i][j]);
            }
    }
    fclose(f1);

    printf("Done\n");


    /* Calculate the log of PhiEquilibrium array */
    // In c log is natural logarithm, i.e ln.

    printf("Calculating log(Phi_Equilibrium) \n");
```

```
for(int i=1;i<=nx;i++)
{
        for(int j=1;j<=ny;j++)
        {
                Ln_PhiEquilibrium[i][j] = log(PhiEquilibrium[i][j]);
                //printf("%lf\t",Ln_PhiEquilibrium[i][j]);
        }
}

printf("Done\n");
/* Load the obstacle array here */


/* Files for saving u and v data */
FILE *fu;
FILE *fv;


/* Replacing all the garbage values of the arrays with zeros. */

for(int i=0;i<=nx+1;i++)
{
        for(int j=0;j<=ny+1;j++)
        {
                ubackup[i][j] = 0.0;
                vbackup[i][j] = 0.0;
        }
}

for(int i=0; i<nx+2; i++)
{
        for(int j=0; j<ny+2; j++)
                {
                        D[i][j] = 1.0; // Initialising all entries to 1
                }
}

for(int i=centre_x-obstacle_radius; i<centre_x+obstacle_radius+1; i++)
{
        for(int j=centre_y-obstacle_radius; j<centre_y+obstacle_radius+1; j++)
        {
                        if(((i-centre_x)*(i-centre_x) + (j-centre_y)*(j-centre_y)) <= obstacle_radius*
                                obstacle_radius)
                        {
                                D[i][j] = 0.00001;
                        }
        }
}

if (StartTime == 0) /* Load Initial Conditions */
{

        printf("Loading Initial Conditions\n");

        for(int i=((nx/2)-5);i<=((nx/2)+5);i++)
        {
                // printf("i = %d\n",i);
                for(int j=1;j<=(ny/2);j++)
                {
                        ubackup[i][j] = 1.0;
                }
        }
```

```
                    for(int i=(nx/2)+10;i<=nx;i++)
                    {
                            for(int j=1;j<=ny;j++)
                            {
                                    vbackup[i][j] = 0.5;
                            }
                    }
            }
            printf("Done\n");
if (StartTime != 0)
            {
                    FILE *f3;
                    double ubuffer;
                    double vbuffer;

                    char file[32];
                    sprintf(file, "data_%.7d.txt",StartTime);

                    f3 = fopen(file, "r");

                    for(int i=1;i<=nx;i++)
                    {
                            for(int j=1;j<=ny;j++)
                            {
                                    fscanf(f3, "%lf \t %lf\n", &ubuffer,&vbuffer);
                                    ubackup[i][j] = ubuffer;
                                    vbackup[i][j] = vbuffer;
                            }
                    }

                    fclose(f3);
            }


        /* if (StartTime != 0)   Load the StartTime'th iteration file
         {

                    printf("Loading file %d\n",StartTime);
                    FILE *f3, *f4;
                    double ubuffer;
                    double vbuffer;

                    char ufile[32];
                    char vfile[32];
                    sprintf(ufile, "u_%.7d.txt",StartTime);
                    sprintf(vfile, "v_%.7d.txt",StartTime);

                    f3 = fopen(ufile, "r");
                    f4 = fopen(vfile, "r");

                    for(int i=1;i<=nx;i++)
                    {
                            for(int j=1;j<=ny;j++)
                            {
                                    fscanf(f3, "%lf", &ubuffer);
                                    ubackup[i][j] = ubuffer;
                                    fscanf(f4, "%lf", &vbuffer);
                                    vbackup[i][j] = vbuffer;
                            }
                    }
                    fclose(f3);
                    fclose(f4);
```

```c
       } */
       printf("Done\n");



       printf("Entering  time  evolution  loop\n");
       /* Time Loop */

       for(int  t=0;t<=nt;t++)
       {
               /* Array Exchange */

               for(int  i=1;i<=nx;i++)
               {
                       for(int  j=1;j<=ny;j++)
                       {
                               u[i][j] = ubackup[i][j];
                               v[i][j] = vbackup[i][j];
                       }
               }


               /* Neumann Boundary Conditions */

               for(int  i=1;i<=nx;i++)
               {
                       u[i][0] = u[i][2];
                       u[i][ny+1] = u[i][ny-1];
                       v[i][0] = v[i][2];
                       v[i][ny+1] = v[i][ny-1];
               }

               for(int  j=1;j<=ny;j++)
               {
                       u[0][j] = u[2][j];
                       u[nx+1][j] = u[nx-1][j];
                       v[0][j] = v[2][j];
                       v[nx+1][j] = v[nx-1][j];
               }

               if ( ( t >= PulseStartTime) && (t <= PulseStartTime+1000) )
               {
                       /* Solving PDE inside the grid */
                       /* printf("Applying E field %d\n",t); */

                       for(int  i=1;i<=nx;i++)
                       {
                               for(int  j=1;j<=ny;j++)
                               {
                                       if (u[i][j] < DELTA)
                                       {
                                               ubackup[i][j] =
                                                       ( (D[i][j]  * c1) * (u[i+1][j] - 2.0*u[i][j] + u[i
                                                           -1][j]) ) +
                                                       ( (D[i][j]  * c2) * (u[i][j+1] - 2.0*u[i][j] + u[i
                                                           ][j-1]) ) +
                                                       ( (D[i][j]  * c3) * (Ln_PhiEquilibrium[i+1][j] -
                                                           Ln_PhiEquilibrium[i-1][j]) * (u[i+1][j] - u[i
                                                           -1][j]) ) +
                                                       ( (D[i][j]  * c4) * (Ln_PhiEquilibrium[i][j+1] -
                                                           Ln_PhiEquilibrium[i][j-1]) * (u[i][j+1] - u[i
                                                           ][j-1]) ) -
```

```
                                                                                ( (D[ i ] [ j ]   *  c5   * Ex) * ( Ln_PhiEquilibrium [ i +1][ j
                                                                                    ] − Ln_PhiEquilibrium [ i −1][ j ] ) )  −
                                                                                ( (D[ i ] [ j ]   *  c6   * Ey) * ( Ln_PhiEquilibrium [ i ] [ j
                                                                                    +1] − Ln_PhiEquilibrium [ i ] [ j −1]) )+
                                                                                (( c7 ) *( u [ i +1][ j]−u [ i −1][ j ] ) ) +(( c8 ) *( u [ i ] [ j +1]−u [ i ] [
                                                                                    j −1]) ) ;

                                                       vbackup [ i ] [ j ] = (  (1.  −  dt ) *  v [ i ] [ j ]  ) ;
                                               }

                                               e l s e
                                               {
                                                       u_th  =  ( v [ i ] [ j ]  +  b ) / ( a ) ;
                                                       f  = (  (1./ epsilon )  *  ( ( u [ i ] [ j ] ) * ( 1.0  − u [ i ] [ j ] ) * ( u [ i ] [ j ] −
                                                               u_th )  )  ) ;
                                                       ubackup [ i ] [ j ] =   u [ i ] [ j ] + ( dt  *  f ) +
                                                                               ( (D[ i ] [ j ]   *  c1 )  * ( u [ i +1][ j ]  − 2.0* u [ i ] [ j ] + u [ i
                                                                                   −1][ j ] )  ) +
                                                                               ( (D[ i ] [ j ]   *  c2 )  * ( u [ i ] [ j +1] − 2.0* u [ i ] [ j ] + u [ i
                                                                                   ] [ j −1])  ) +
                                                                               ( (D[ i ] [ j ]   *  c3 )  * ( Ln_PhiEquilibrium [ i +1][ j ] −
                                                                                   Ln_PhiEquilibrium [ i −1][ j ] ) * ( u [ i +1][ j ]  − u [ i
                                                                                   −1][ j ] )  ) +
                                                                               ( (D[ i ] [ j ]   *  c4 )  * ( Ln_PhiEquilibrium [ i ] [ j +1] −
                                                                                   Ln_PhiEquilibrium [ i ] [ j −1]) * ( u [ i ] [ j +1]  − u [ i
                                                                                   ] [ j −1])  )  −
                                                                               ( (D[ i ] [ j ]   *  c5   * Ex) * ( Ln_PhiEquilibrium [ i +1][ j
                                                                                   ] − Ln_PhiEquilibrium [ i −1][ j ] ) )  −
                                                                               ( (D[ i ] [ j ]   *  c6   * Ey) * ( Ln_PhiEquilibrium [ i ] [ j
                                                                                   +1] − Ln_PhiEquilibrium [ i ] [ j−i ]  ))+
                                                                               (( c7 ) *( u [ i +1][ j]−u [ i −1][ j ] ) ) +(( c8 ) *( u [ i ] [ j +1]−u [ i
                                                                                   ] [ j −1]) ) ;
                                                       vbackup [ i ] [ j ] = v [ i ] [ j ] + (  ( dt )  *  ( u [ i ] [ j ]  − v [ i ] [ j ] )  )  +(( c7 ) *( v [
                                                               i +1][ j]−v [ i −1][ j ] ) ) +(( c8 ) *( v [ i ] [ j +1]−v [ i ] [ j −1]) )  ;
                                               }
                                       }
                               }
                       }

                       e l s e
                       {

                               /* Solving PDE inside the grid with no electric field applied . */
                               /* printf (" Inside  else  loop  %d\n" , t ) ; */

                               for ( int  i =1; i <=nx ; i ++)
                               {
                                       for ( int  j =1; j <=ny ; j ++)
                                       {
                                               if  ( u [ i ] [ j ] < DELTA)
                                               {
                                                       ubackup [ i ] [ j ] =
                                                               ( (D[ i ] [ j ]   *  c1 ) * ( u [ i +1][ j ]  − 2.0* u [ i ] [ j ] + u [ i −1][ j ] ) )
                                                                       +
                                                               ( (D[ i ] [ j ]   *  c2 ) * ( u [ i ] [ j +1]  − 2.0* u [ i ] [ j ] + u [ i ] [ j −1]) )
                                                                       +
                                                               ( (D[ i ] [ j ]   *  c3 ) * ( Ln_PhiEquilibrium [ i +1][ j ] −
                                                                   Ln_PhiEquilibrium [ i −1][ j ] ) * ( u [ i +1][ j ]  − u [ i −1][ j ] ) )
                                                                       +
                                                               ( (D[ i ] [ j ]   *  c4 ) * ( Ln_PhiEquilibrium [ i ] [ j +1] −
                                                                   Ln_PhiEquilibrium [ i ] [ j −1]) * ( u [ i ] [ j +1]  − u [ i ] [ j −1]) )
                                                                       +
                                                               (( c7 ) *( u [ i +1][ j]−u [ i −1][ j ] ) ) +(( c8 ) *( u [ i ] [ j +1]−u [ i ] [ j −1]) ) ;
```

```c
                                        vbackup[i][j] = ( (1. - dt) * v[i][j] )+((c7)*(v[i+1][j]-v[i-1][j
                                            ]))+((c8)*(v[i][j+1]-v[i][j-1]));
                                }

                                else
                                {
                                        u_th = (v[i][j] + b)/(a);
                                        f = ( (1./epsilon) * ( (u[i][j]) * (1.0 - u[i][j]) * (u[i][j] -
                                            u_th) ) );
                                        ubackup[i][j] =    u[i][j] + (dt * f) +
                                                                ( (D[i][j]   * c1) * (u[i+1][j] - 2.0*u[i][j] + u[i
                                                                    -1][j]) ) +
                                                                ( (D[i][j]   * c2) * (u[i][j+1] - 2.0*u[i][j] + u[i
                                                                    ][j-1]) ) +
                                                                ( (D[i][j]   * c3) * (Ln_PhiEquilibrium[i+1][j] -
                                                                    Ln_PhiEquilibrium[i-1][j]) * (u[i+1][j] - u[i
                                                                    -1][j]) ) +
                                                                ( (D[i][j]   * c4) * (Ln_PhiEquilibrium[i][j+1] -
                                                                    Ln_PhiEquilibrium[i][j-1]) * (u[i][j+1] - u[i
                                                                    ][j-1]) )+
                                                                ((c7)*(u[i+1][j]-u[i-1][j]))+((c8)*(u[i][j+1]-u[i][
                                                                    j-1]));
                                                                // - ( (c5 * Ex) * (Ln_PhiEquilibrium[i+1][j] -
                                                                    Ln_PhiEquilibrium[i-1][j]) ) -
                                                                //( (c6 * Ey) * (Ln_PhiEquilibrium[i][j+1] -
                                                                    Ln_PhiEquilibrium[i][j-1]) );
                                        vbackup[i][j] = v[i][j] + ( (dt) * (u[i][j] - v[i][j]) )+((c7)*(v[i
                                            +1][j]-v[i-1][j]))+((c8)*(v[i][j+1]-v[i][j-1]));
                                }
                        }
                }

        }

        /* Saving Data into files */

FILE *Values;
if((t%savingInterval) == 0)
        {
                char file[32];
                sprintf(file, "data_%.7d.txt",t+StartTime);

                Values = fopen(file, "w");

                for(int i=1;i<=nx;i++)
                {
                        for(int j=1;j<=ny;j++)
                        {
                                fprintf(Values, "%lf \t %lf\n", u[i][j], v[i][j]);
                        }
                }
                fclose(Values);
        }

}
return(0);
}
```
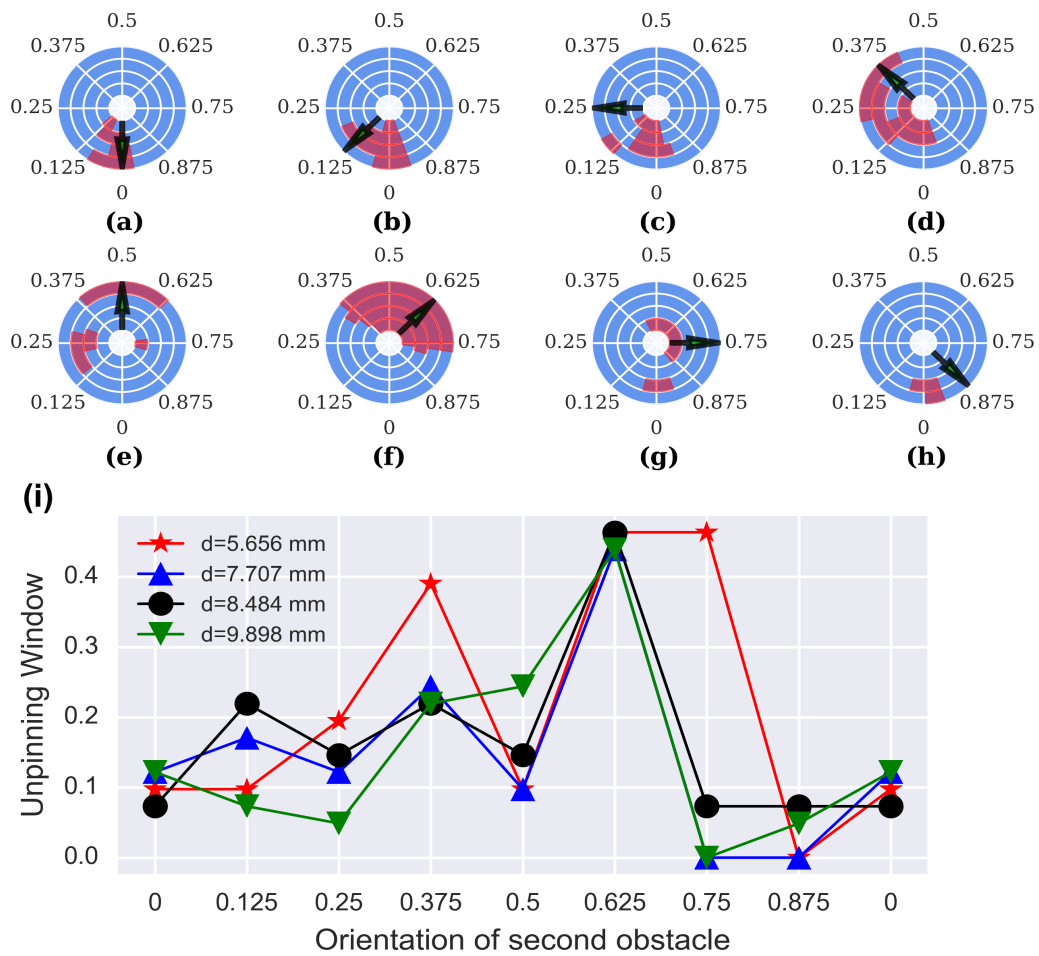
Appendix B

Supplementary Data

Figure B.1: **Unpinning window for different orientation of additional wave emitting site around the central heterogeneity.** The figure is same as in Fig. 4.6 (chapter 4) but with additional wave emitting site having a radius of 1.5 mm.
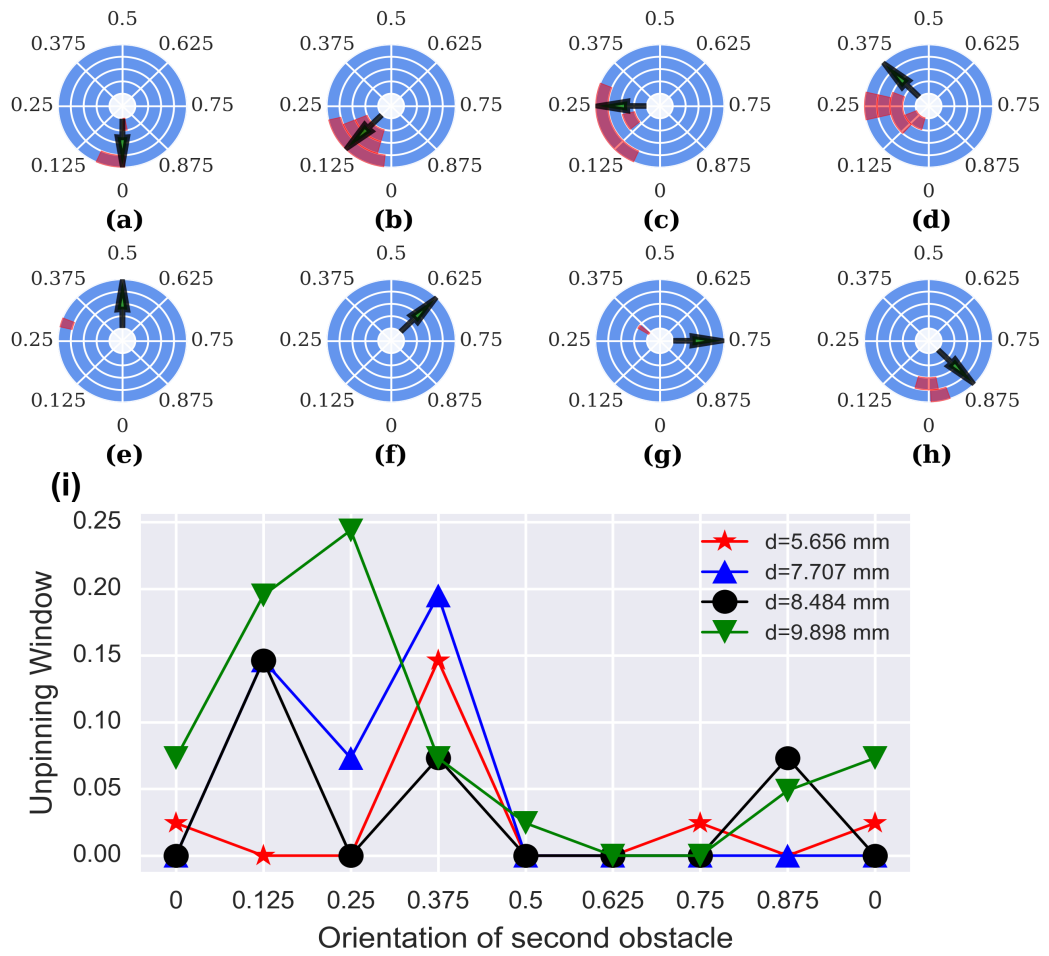
Figure B.2: **Unpinning window for different orientation of additional wave emitting site around the central heterogeneity.** The figure is same as Fig. 4.6 (chapter 4) but with additional wave emitting site having a radius of 2.5 mm.

Appendix C

Modelling Details

Model	Parameter Set	Parameter Values
Barkley Model (see Chapter 3)	a	0.53
	b	0.05
	ε	0.02
Fitzhugh-Nagumo Model (see Chapter 4)	a	0.085
	b	0.25
	ε	0.045
Fitzhugh Nagumo Model (see Chapter 5)	a	0.1
	b	0.25
	ε	0.025

Table C.1: The model parameters used for Barkley model and Fitzhugh-Nagumo models in respective chapters.

Bibliography

Al-Khadra, A., Nikolski, V., and Efimov, I. R. (2000). The role of electroporation in defibrillation. *Circ. Res.*, 87(9):797–804.

Alcantara, F. and Monk, M. (1974). Signal propagation during aggregation in the slime mould dictyostelium discoideum. *Microbiology*, 85(2):321–334.

Bär, M. and Eiswirth, M. (1993). Turbulence due to spiral breakup in a continuous excitable medium. *Phys. Rev. E*, 48(3):R1635.

Barkley, D. (1991). A model for fast computer simulation of waves in excitable media. *Physica D*, 49(1-2):61–70.

Barkley, D. (1995). Spiral meandering. In *Chemical waves and patterns*, pages 163–189. Kluwer Academic Publishers, Dordrecht.

Behrend, A., Bittihn, P., and Luther, S. (2010). Predicting unpinning success rates for a pinned spiral in an excitable medium. In *Computing in Cardiology, 2010*, pages 345–348. IEEE.

Biktashev, V. and Holden, A. (1998). Reentrant waves and their elimination in a model of mammalian ventricular tissue. *Chaos*, 8(1):48–56.

Bittihn, P. (2014). *Complex structure and dynamics of the heart*. Springer.

Bittihn, P., Hörning, M., and Luther, S. (2012). Negative curvature boundaries as wave emitting sites for the control of biological excitable media. *Phys. Rev. Lett.*, 109(11):118106.

Bittihn, P., Luther, G., Bodenschatz, E., Krinsky, V., Parlitz, U., and Luther, S. (2008). Far field pacing supersedes anti-tachycardia pacing in a generic model of excitable media. *New J. Phys.*, 10(10):103012.

Bittihn, P., Squires, A., Luther, G., Bodenschatz, E., Krinsky, V., Parlitz, U., and Luther, S. (2010). Phase-resolved analysis of the susceptibility of pinned spiral waves to far-field pacing in a two-dimensional model of excitable media. *Philos. Trans. R. Soc. A*, 368(1918):2221–2236.

Boettinger, W. J., Warren, J. A., Beckermann, C., and Karma, A. (2002). Phase-field simulation of solidification. *Annu. Rev. Mater. Res.*, 32(1):163–194.

Borek, B., Shajahan, T., Gabriels, J., Hodge, A., Glass, L., and Shrier, A. (2012). Pacemaker interactions induce reentrant wave dynamics in engineered cardiac culture. *Chaos*, 22(3):033132.

Bradfield, J. S., Buch, E., and Shivkumar, K. (2012). Interventions to decrease the morbidity and mortality associated with implantable cardioverter-defibrillator shocks. *Curr Opin Crit Care*, 18(5):432–437.

Brian, P. L. T. (1961). A finite-difference method of high-order accuracy for the solution of three-dimensional transient heat conduction problems. *AIChE Journal*, 7(3):367–370.

Bub, G., Glass, L., Publicover, N. G., and Shrier, A. (1998). Bursting calcium rotors in cultured cardiac myocyte monolayers. *Proc. Nat. Acad. Sc.*, 95(17):10283–10287.

Bub, G., Shrier, A., and Glass, L. (2002). Spiral wave generation in heterogeneous excitable media. *Phys. Rev. Lett.*, 88(5):058101.

Bub, G., Shrier, A., and Glass, L. (2005). Global organization of dynamics in oscillatory heterogeneous excitable media. *Phys. Rev. Lett.*, 94(2):028105.

Chang, M. G., Chang, C. Y., De Lange, E., Xu, L., O'Rourke, B., Karagueuzian, H. S., Tung, L., Marbán, E., Garfinkel, A., Weiss, J. N., et al. (2012). Dynamics of early

afterdepolarization-mediated triggered activity in cardiac monolayers. *Biophys. J.*, 102(12):2706–2714.

Chen, J.-X., Zhang, H., and Li, Y.-Q. (2006). *J. Chem. Phys.*, 124(1):014505.

Clark, C. B., Zhang, Y., Davies, L. R., Karlsson, G., and Kerber, R. E. (2002). Transthoracic biphasic waveform defibrillation at very high and very low energies: a comparison with monophasic waveforms in an animal model of ventricular fibrillation. *Resuscitation*, 54(2):183–186.

Cook, S. C., Valente, A. M., Maul, T. M., Dew, M. A., Hickey, J., Burger, P. J., Harmon, A., Clair, M., Webster, G., Cecchin, F., et al. (2013). Shock-related anxiety and sexual function in adults with congenital heart disease and implantable cardioverter-defibrillators. *Heart Rhythm*, 10(6):805–810.

Courtemanche, M. and Winfree, A. T. (1991). Re-entrant rotating waves in a beeler–reuter based model of two-dimensional cardiac electrical activity. *International Journal of Bifurcation and Chaos*, 1(02):431–444.

Davidenko, J. M., Pertsov, A. V., Salomonsz, R., Baxter, W., and Jalife, J. (1992). Stationary and drifting spiral waves of excitation in isolated cardiac muscle. *Nature*, 355(6358):349.

DeHaan, R. L. and Gottlieb, S. H. (1968). The electrical activity of embryonic chick heart cells isolated in tissue culture singly or in interconnected cell sheets. *J. Gen. Physiol.*, 52(4):643–665.

Feng, X. and Gao, X. (2019). *Nonlinear Dyn.*, 98(3):1919–1927.

Feng, X., Gao, X., Pan, D.-B., Li, B.-W., and Zhang, H. (2014). Unpinning of rotating spiral waves in cardiac tissues by circularly polarized electric fields. *Sci. Rep.*, 4:4831.

Feng, X., Gao, X., Tang, J.-M., Pan, J.-T., and Zhang, H. (2015). *Sci. Rep.*, 5(1):1–9.

Fenton, F. H. and Cherry, E. M. (2008). Models of cardiac cell. *Scholarpedia*, 3(8):1868.

Fenton, F. H., Cherry, E. M., Hastings, H. M., and Evans, S. J. (2002). Multiple mechanisms of spiral wave breakup in a model of cardiac electrical activity. *Chaos*, 12(3):852–892.

Fenton, F. H., Cherry, E. M., Karma, A., and Rappel, W.-J. (2005). Modeling wave propagation in realistic heart geometries using the phase-field method. *Chaos*, 15(1):013502.

FitzHugh, R. (1961). Impulses and physiological states in theoretical models of nerve membrane. *Biophys. J.*, 1(6):445–466.

Folch, R., Casademunt, J., Hernández-Machado, A., and Ramirez-Piscina, L. (1999). Phase-field model for hele-shaw flows with arbitrary viscosity contrast. i. theoretical approach. *Phys. Rev. E*, 60(2):1724.

Frommeyer, G. and Eckardt, L. (2016). Drug-induced proarrhythmia: risk factors and electrophysiological mechanisms. *Nat. Rev. Cardiol.*, 13(1):36–47.

Galvani, L. (1792). *De viribus electricitatis in motu musculari comentarius cum joannis aldini dissertatione et notis; accesserunt epistolae ad animalis electricitatis theoriam pertinentes*. Apud Societatem Typographicam.

Glass, L. (1996). Dynamics of cardiac arrhythmias. *Phys. Today*, 49(8):40–45.

Godemann, F., Butter, C., Lampe, F., Linden, M., Schlegl, M., Schultheiss, H.-P., and Behrens, S. (2004). Panic disorders and agoraphobia: side effects of treatment with an implantable cardioverter/defibrillator. *Clin. Cardiol.*, 27(6):321–326.

Gray, R. A., Pertsov, A. M., and Jalife, J. (1998). Spatial and temporal organization during cardiac fibrillation. *Nature*, 392(6671):75–78.

Gregor, T., Fujimoto, K., Masaki, N., and Sawai, S. (2010). The onset of collective behavior in social amoebae. *Science*, 328(5981):1021–1025.

Guyton, A. C. and Hall, J. E. (2006). Medical physiology. *Gökhan N, Çavuşoğlu H (Çeviren)*, 3.

Hodgkin, A. L. and Huxley, A. F. (1952a). The components of membrane conductance in the giant axon of loligo. *J. Physiol. (Lond.)*, 116(4):473–496.

Hodgkin, A. L. and Huxley, A. F. (1952b). Currents carried by sodium and potassium ions through the membrane of the giant axon of loligo. *J. Physiol. (Lond.)*, 116(4):449–472.

Hodgkin, A. L. and Huxley, A. F. (1952c). The dual effect of membrane potential on sodium conductance in the giant axon of loligo. *J. Physiol. (Lond.)*, 116(4):497–506.

Hodgkin, A. L. and Huxley, A. F. (1952d). A quantitative description of membrane current and its application to conduction and excitation in nerve. *J. Physiol. (Lond.)*, 117(4):500–544.

Hodgkin, A. L., Huxley, A. F., and Katz, B. (1952). Measurement of current-voltage relations in the membrane of the giant axon of loligo. *J. Physiol. (Lond.)*, 116(4):424–448.

Hörning, M., Isomura, A., Agladze, K., and Yoshikawa, K. (2009). Liberation of a pinned spiral wave by a single stimulus in excitable media. *Phys. Rev. E*, 79(2):026218.

Hörning, M., Takagi, S., and Yoshikawa, K. (2012). Controlling activation site density by low-energy far-field stimulation in cardiac tissue. *Phy. Rev. E*, 85(6):061906.

Huang, X., Troy, W. C., Yang, Q., Ma, H., Laing, C. R., Schiff, S. J., and Wu, J.-Y. (2004). Spiral waves in disinhibited mammalian neocortex. *J. Neurosci.*, 24(44):9897–9902.

Huxley, A. (1996). Kenneth stewart cole, 1900-1984, a biographical memoir. *Biogr. Mem. Natl. Acad. Sci.*, pages 23–45.

Isomura, A., Hörning, M., Agladze, K., and Yoshikawa, K. (2008). Eliminating spiral waves pinned to an anatomical obstacle in cardiac myocytes by high-frequency stimuli. *Phys. Rev. E*, 78(6):066216.

Jahnke, W., Skaggs, W., and Winfree, A. T. (1989). Chemical vortex dynamics in the belousov-zhabotinskii reaction and in the two-variable oregonator model. *J. Phys. Chem.*, 93(2):740–749.

Ji, L., Zhou, Y., Li, Q., Qiao, C., and Ouyang, Q. (2013). *Phys. Rev. E*, 88(4):042919.

Kakkar, R. and Lee, R. T. (2010). Intramyocardial fibroblast myocyte communication. *Circ. Res.*, 106(1):47–57.

Karma, A. (2013). Physics of cardiac arrhythmogenesis. *Annu. Rev. Condens. Matter Phys.*, 4(1):313–337.

Karma, A., Kessler, D. A., and Levine, H. (2001). Phase-field model of mode iii dynamic fracture. *Phys. Rev. Lett.*, 87(4):045501.

Krinskii, V. (1966). Spread of excitation in an inhomogeneous medium (state shviilar to cardiac fibrillation).

Krinsky, V. and Agladze, K. (1983). Interaction of rotating waves in an active chemical medium. *Physica D*, 8(1-2):50–56.

Krinsky, V., Plaza, F., and Voignier, V. (1995). Quenching a rotating vortex in an excitable medium. *Phys. Rev. E*, 52(3):2458.

Lei, M., Wu, L., Terrar, D. A., and Huang, C. L.-H. (2018). Modernized classification of cardiac antiarrhythmic drugs. *Circulation*, 138(17):1879–1896.

Ley, S. J. (2019). Cardiac surgical resuscitation: State of the science. *Crit. Care Clin.*, 31(3):437–452.

Li, W., Ripplinger, C. M., Lou, Q., and Efimov, I. R. (2009). Multiple monophasic shocks improve electrotherapy of ventricular tachycardia in a rabbit model of chronic infarction. *Heart Rhythm*, 6(7):1020–1027.

Luther, S., Fenton, F. H., Kornreich, B. G., Squires, A., Bittihn, P., Hornung, D., Zabel, M., Flanders, J., Gladuli, A., Campoy, L., et al. (2011). Low-energy control of electrical turbulence in the heart. *Nature*, 475(7355):235.

Matchett, M., Sears, S. F., Hazelton, G., Kirian, K., Wilson, E., and Nekkanti, R. (2009). The implantable cardioverter defibrillator: its history, current psychological impact and future. *Expert Rev. Med. Devices*, 6(1):43–50.

Mittal, S., Ayati, S., Stein, K. M., Knight, B. P., Morady, F., Schwartzman, D., Cavlovich, D., Platia, E. V., Calkins, H., Tchou, P. J., et al. (1999). Comparison of a novel rectilinear biphasic waveform with a damped sine wave monophasic waveform for transthoracic ventricular defibrillation. *J. Am. Coll. Cardiol.*, 34(5):1595–1601.

Moe, G. K., Rheinboldt, W. C., and Abildskov, J. (1964). A computer model of atrial fibrillation. *Am. Heart J.*, 67(2):200–220.

Nagumo, J., Arimoto, S., and Yoshizawa, S. (1962). An active pulse transmission line simulating nerve axon. *Proceedings of the IRE*, 50(10):2061–2070.

Noble, D. (1962). A modification of the hodgkin—huxley equations applicable to purkinje fibre action and pacemaker potentials. *J. Physiol.*, 160(2):317.

Nomura, T. and Glass, L. (1996). Entrainment and termination of reentrant wave propagation in a periodically stimulated ring of excitable media. *Phys. Rev. E*, 53(6):6353.

Otani, N. F., Wheeler, K., Krinsky, V., and Luther, S. (2019). Termination of scroll waves by surface impacts. *Phys. Rev. Lett.*, 123(6):068102.

Pan, D.-B., Gao, X., Feng, X., Pan, J.-T., and Zhang, H. (2016). *Sci. Rep.*, 6(1):1–8.

Prevost, J.-L. (1899). Sur quel ques effets des dechanges electriques sur le coer mammifres. *C. R. Acad. Sci.*, 129:1267.

Pumir, A. and Krinsky, V. (1999). Unpinning of a rotating wave in cardiac muscle by an electric field. *J. Theor. Biol.*, 199(3):311–319.

Pumir, A., Nikolski, V., Hörning, M., Isomura, A., Agladze, K., Yoshikawa, K., Gilmour, R., Bodenschatz, E., and Krinsky, V. (2007). Wave emission from heterogeneities opens a way to controlling chaos in the heart. *Phys. Rev. Lett.*, 99(20):208101.

Pumir, A., Sinha, S., Sridhar, S., Argentina, M., Hörning, M., Filippi, S., Cherubini, C., Luther, S., and Krinsky, V. (2010). Wave-train-induced termination of weakly anchored vortices in excitable media. *Phys. Rev. E*, 81(1):010901.

Punacha, S., Abhishek, M., and Shajahan, T. (2019a). Unpinning spiral wave anchored to two obstacles. *Indian Academy of Sciences Conference Series*, 2.

Punacha, S., Berg, S., Sebastian, A., Krinski, V., Luther, S., and Shajahan, T. (2019b). *Proc. R. Soc. A*, 475(2230):20190420.

Punacha, S., Shajahan, T., et al. (2020). Theory of unpinning of spiral waves using circularly polarized electric fields in mathematical models of excitable media. *Phys. Rev. E*, 102(3):032411.

Rantner, L. J., Tice, B. M., and Trayanova, N. A. (2013). Terminating ventricular tachyarrhythmias using far-field low-voltage stimuli: mechanisms and delivery protocols. *Heart Rhythm*, 10(8):1209–1217.

Rappel, W.-J., Fenton, F., and Karma, A. (1999). Spatiotemporal control of wave instabilities in cardiac tissue. *Phys. Rev. Lett.*, 83(2):456.

Ripplinger, C. M., Krinsky, V. I., Nikolski, V. P., and Efimov, I. R. (2006). Mechanisms of unpinning and termination of ventricular tachycardia. *Am. J. Physiol.*, 291(1):H184–H192.

Roden, D. M. (1998). Mechanisms and management of proarrhythmia. *Am. J. Cardiol.*, 82(4):49I–57I.

Rohr, S., Kucera, J. P., Fast, V. G., and Kléber, A. G. (1997). Paradoxical improvement of impulse conduction in cardiac tissue by partial cellular uncoupling. *Science*, 275(5301):841–844.

Rosen, M. R. and hoffman, b. f. (1973). Mechanisms of action of antiarrhythmic drugs. *Circ. Res.*, 32(1):1–8.

Schlemmer, A., Berg, S., Shajahan, T., Luther, S., and Parlitz, U. (2015). Entropy rate maps of complex excitable dynamics in cardiac monolayers. *Entropy*, 17(3):950–967.

Seiden, G. and Curland, S. (2015). The tongue as an excitable medium. *New J.Phys.*, 17(3):033049.

Shajahan, T., Berg, S., Luther, S., Krinski, V., and Bittihn, P. (2016). Scanning and resetting the phase of a pinned spiral wave using periodic far field pulses. *New J. Phys.*, 18(4):043012.

Shajahan, T., Sinha, S., and Pandit, R. (2007). Spiral-wave dynamics depend sensitively on inhomogeneities in mathematical models of ventricular tissue. *Phys. Rev. E*, 75(1):011929.

Simmons, A. J. and Burridge, D. M. (1981). An energy and angular-momentum conserving vertical finite-difference scheme and hybrid vertical coordinates. *Mon. Weather Rev.*, 109(4):758–766.

Singh, R., Xu, J., Garnier, N. G., Pumir, A., and Sinha, S. (2012). Self-organized transition to coherent activity in disordered media. *Phys. Rev. Lett.*, 108(6):068102.

Sinha, S., Pande, A., and Pandit, R. (2001). Defibrillation via the elimination of spiral turbulence in a model for ventricular fibrillation. *Phys. Rev. Lett.*, 86(16):3678.

Szentadrassy, N., Banyasz, T., Biro, T., Szabo, G., Toth, B. I., Magyar, J., Lazar, J., Varro, A., Kovacs, L., and Nanasi, P. P. (2005). Apico–basal inhomogeneity in distribution of ion channels in canine and human ventricular myocardium. *Cardiovascular research*, 65(4):851–860.

Takagi, S., Pumir, A., Pazo, D., Efimov, I., Nikolski, V., and Krinsky, V. (2004). Unpinning and removal of a rotating wave in cardiac muscle. *Phys. Rev. Lett.*, 93(5):058101.

Ten Tusscher, K. and Panfilov, A. V. (2003). Reentry in heterogeneous cardiac tissue described by the luo-rudy ventricular action potential model. *Am. J Physio. Heart Circ. Physiol.*, 284(2):H542–H548.

ten Tusscher, K. H. and Panfilov, A. V. (2005). Wave propagation in excitable media with randomly distributed obstacles. *Multiscale Modeling & Simulation*, 3(2):265–282.

Terasawa, T., Balk, E. M., Chung, M., Garlitski, A. C., Alsheikh-Ali, A. A., Lau, J., and Ip, S. (2009). Systematic review: comparative effectiveness of radiofrequency catheter ablation for atrial fibrillation. *Ann. Intern. Med.*, 151(3):191–202.

tom Wörden, H., Parlitz, U., and Luther, S. (2019). Simultaneous unpinning of multiple vortices in two-dimensional excitable media. *Phys. Rev. E*, 99(4):042216.

Tung, L. (1996). Detrimental effects of electrical fields on cardiac muscle. *Proc. IEEE*, 84(3):366–378.

Tung, L. and Zhang, Y. (2006). Optical imaging of arrhythmias in tissue culture. *J. Electrocardiol.*, 39(4):S2–S6.

Tung, R., Zimetbaum, P., and Josephson, M. E. (2008). A critical appraisal of implantable cardioverter-defibrillator therapy for the prevention of sudden cardiac death. *J. Am. Coll. Cardiol.*, 52(14):1111–1121.

Valderrábano, M., Lee, M.-H., Ohara, T., Lai, A. C., Fishbein, M. C., Lin, S.-F., Karagueuzian, H. S., and Chen, P.-S. (2001). Dynamics of intramural and transmural reentry during ventricular fibrillation in isolated swine ventricles. *Circ. Res.*, 88(8):839–848.

Varghese, F., Neuber, J. U., Xie, F., Philpott, J. M., Pakhomov, A. G., and Zemlin, C. W. (2017). Low-energy defibrillation with nanosecond electric shocks. *Cardiovasc. Res.*, 113(14):1789–1797.

Weiner, N. and Rosenblunth, A. (1946). The mathematical formulation of the problem of conduction of impulses in a network of connected excitable elements specifically in cardiac muscle.

Weiss, J. N., Qu, Z., Chen, P.-S., Lin, S.-F., Karagueuzian, H. S., Hayashi, H., Garfinkel, A., and Karma, A. (2005). The dynamics of cardiac fibrillation. *Circulation*, 112(8):1232–1240.

Winfree, A. T. (1972). Spiral waves of chemical activity. *Science*, 175(4022):634–636.

Winfree, A. T. (1989). Electrical instability in cardiac muscle: phase singularities and rotors. *J. Theor. Biol.*, 138(3):353–405.

Winfree, A. T. (1992). Erratum: Varieties of spiral wave behavior: An experimentalist's approach to the theory of excitable media [chaos 1, 303–334 (1991)]. *Chaos: An Interdisciplinary Journal of Nonlinear Science*, 2(2):273–273.

Yu, Y., Santos, L. M., Mattiace, L. A., Costa, M. L., Ferreira, L. C., Benabou, K., Kim, A. H., Abrahams, J., Bennett, M. V., and Rozental, R. (2012). Reentrant spiral waves of spreading depression cause macular degeneration in hypoglycemic chicken retina. *Proc. Natl. Acad. Sci.*, 109(7):2585–2589.

Yuste, S. B. and Acedo, L. (2005). An explicit finite difference method and a new von neumann-type stability analysis for fractional diffusion equations. *SIAM J. Numer. Anal.*, 42(5):1862–1874.

Zlochiver, S., Munoz, V., Vikstrom, K. L., Taffet, S. M., Berenfeld, O., and Jalife, J. (2008). Electrotonic myofibroblast-to-myocyte coupling increases propensity to reentrant arrhythmias in two-dimensional cardiac monolayers. *Biophys. J.*, 95(9):4469–4480.

Zoll, P. M., Linenthal, A. J., Gibson, W., Paul, M. H., and Norman, L. R. (1956). Termination of ventricular fibrillation in man by externally applied electric countershock. *N. Engl. J. Med.*, 254(16):727–732.

LIST OF PUBLICATIONS

Journal publications

1. **Shreyas Punacha**, Sebastian Berg, Anupama Sebastian, Valentin I Krinski, Stefan Luther and T. K. Shajahan (2019). " Spiral wave unpinning facilitated by wave emitting sites in cardiac monolayers". *Proceedings of Royal Society A, 475 (2230) : 20190420, 2019.*
   DOI:10.1098/rspa.2019.0420.

2. **Shreyas Punacha**, Naveena Kumara A and T. K. Shajahan (2020). " A theory of unpinning of spiral waves using circularly polarized electric fields in mathematical models of excitable media." *Physical Review E, 102(3), 032411. 2020.*
   DOI:10.1103/PhysRevE.102.032411.

3. Naveena Kumara A, Ahmed Rizwan C. L., **Shreyas Punacha**, Ajith K. M and Md Sabir Ali (2020). " Photon Orbits and Thermodynamic Phase Transtion of Regular Ads Black Holes." *Physical Review D, 102, 084059, 2020.*
   DOI:10.1103/PhysRevD.102.084059.

Conference proceedings

1. **Shreyas Punacha**, M. Abhishek and T. K. Shajahan. (2019). " Unpinning spiral wave anchored to two obstacle". *Indian Academy of Sciences Conference Series, 2, 2019.*
   DOI:10.29195/iascs.02.01.0001.

Shreyas Punacha

Personal Data

Residential Address :	#3/1418, Mandara House, Haleyangadi,
	Karnataka, 574146, India.
Marital Status :	Married
Date of Birth:	22-07-1991
Citizenship :	Indian
email :	shreyasp444@gmail.com
Sex :	Male
ID :	ORCID

Education

2021   Ph.D. in Physics, **National Institute of Technology Karnataka**, Surathkal
Thesis: "Excitation wave dynamics and their interaction with external fields"
Advisor: Dr. T K Shajahan

2014   Master of Science in Physics, **Mangalore University**, Mangalore, Karnataka.

2012   Bachelor of Science in Physics, **Vivekananda College**, Puttur, Karnataka.

Computational Skills

Numerical Solutions to PDEs | Finite difference method | Phase Field Method
Parallel Programming | Mathematica | Message Passing Interface | Version Control
Programming Languages: Python | C | C++ | Shell Scripting | R
Markup Languages: Latex | HTML

Research Intrests

Pattern formation in Excitable Media | Computational Biology | Cardiac Arrhythmias
Low Voltage Defibrillation | Spiral Waves

Experience

2016-2020	Mentored five Masters student projects with two leading to publications during the course of the Ph.D.
2017-2019	Teaching Assistant for M.Sc. Computational Physics course at NITK Surathkal.
2015-2017	Teaching Assistant for B.Tec. Physics Course at NITK Surathkal.
2015-2016	Laboratory Teaching Assistant for M.Sc. Physics Laboratory at NITK Surathkal.
2015-2020	Laboratory Teaching Assistant for B.Tec. Physics Laboratory at NITK Surathkal.

Publications

1. **Shreyas Punacha**, Naveena Kumara A and T. K. Shajahan (2020). " A theory of unpinning of spiral waves using circularly polarized electric fields in mathematical models of excitable media." *Physical Review E, 102(3), 032411.*

2. Naveena Kumara A, Ahmed Rizwan C. L., **Shreyas Punacha**, Ajith K. M and Md Sabir Ali (2020). " Photon Orbits and Thermodynamic Phase Transtion of Regular Ads Black Holes." *Physical Review D, 102, 084059.*

3. **Shreyas Punacha**, Sebastian Berg, Anupama Sebastian, Valentin I Krinski, Stefan Luther and T. K. Shajahan (2019). " Spiral wave unpinning facilitated by wave emitting sites in cardiac monolayers". *Proceedings of Royal Society A, 475 (2230) : 20190420.*

4. **Shreyas Punacha**, M. Abhishek and T. K. Shajahan. (2019). " Unpinning spiral wave anchored to two obstacle". *Indian Academy of Sciences Conference Series, 2.*

Preprints

1. A. Naveena Kumara, **Shreyas Punacha**, Karteek Hegde, C. L. A. Rizwan, M. S. Ali and K. M. Ajith. (2021) "Dynamics and kinetics of phase transition for regular AdS black holes in general relativity coupled to non-linear electrodynamics". *Submitted to Physical Review D.*
[arXiv:2106.11095]

Manuscript Under Preparation

1. A. Naveena Kumara, **Shreyas Punacha**, Karteek Hegde, C. L. A. Rizwan, M. S. Ali and K. M. Ajith. (2021) "Dynamic phase transition for regular black holes in massive gravity". *To be submitted to Physical Review D.*

2. Amrutha S V, Sibeesh P P, Anupama Sebastian, **Shreyas Punacha** and T K Shajahan. (2021) "Unpinning Of Spiral Waves Using Advective Fields In Chemical Excitable Media". *To be submitted to Journal of Chemical Physics.*

Scholarships

Schools and Conferences

2018	Conference on Nonlinear Systems and Dynamics
	Jawaharlal Nehru University, New Mehrauli Road, Delhi.
2018	IFCAM Summer School on Mathematical and Computational Biology
	Indo-French Centre for Applied Mathematics,
	Indian Institute of Science, Bangalore.
2016	4th Winter School on Nonlinear Dynamics
	PSG college Coimbatore, Tamilnadu, India.
2013	Workshop on Quantum Mechanics and Applications
	National Institute of Technology Surathkal, Karnataka, India.
2011	National Conference in Physics (CAPSRAA)
	Govinda Dasa First Grade College, Surathkal, Karnataka, India.

Languages

Konkani:	Mothertongue
Kannada:	Native
Tulu:	Native
Hindi:	Fluent
English:	Fluent
German:	A1 Level

Extras

Setup a 28 core DELL Server in the physics laboratory.

Coordinated a science outreach initiative "The Principia" for high school students in Karnataka and Kerala States of India.

Amateur bird photographer.

Ebirder - An active participant in eBird, a citizen science project for bird observation from Cornell Lab of Ornithology.

References

1. Dr. T. K Shajahan
   Assistant Professor
   Department of Physics
   National Institute of Technology Karnataka (NITK), Surathkal
   Mangalore - 575025, Karnataka, India.
   email : shajahan@nitk.edu.in

2. Dr. Ajith K M
   Associate professor
   Department of Physics
   National Institute of Technology Karnataka (NITK), Surathkal
   Mangalore - 575 025, Karnataka, India.
   email : ajith@nitk.ac.in

3. Dr. Deepu Vijayasenan
   Associate professor
   Department of Electronics and Communication Engineering
   National Institute of Technology Karnataka (NITK), Surathkal
   Mangalore - 575 025, Karnataka, India.
   email : deepu.senan @gmail.com